Signal Processing Design of
Low Probability of Intercept Waveforms
Via Intersymbol Dither

THESIS

Nathaniel Christian Liefer, Captain, USAF

AFIT/GE/ENG/08-18

DEPARTMENT OF THE AIR FORCE
AIR UNIVERSITY

AIR FORCE INSTITUTE OF TECHNOLOGY

Wright-Patterson Air Force Base, Ohio

AFIT/GE/ENG/08-18

Signal Processing Design of
Low Probability of Intercept Waveforms
Via Intersymbol Dither

THESIS

Presented to the Faculty

Department of Electrical and Computer Engineering

Graduate School of Engineering and Management

Air Force Institute of Technology

Air University

Air Education and Training Command

In Partial Fulfillment of the Requirements for the

Degree of Master of Science in Electrical Engineering
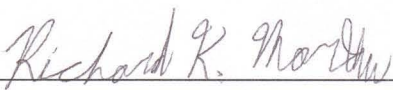
Nathaniel Christian Liefer, B.S.E.E.
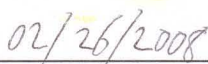
Captain, USAF

March 2008

SIGNAL PROCESSING DESIGN OF
LOW PROBABILITY OF INTERCEPT WAVEFORMS
VIA INTERSYMBOL DITHER

Nathaniel Christian Liefer, B.S.E.E.

Captain, USAF

Approved:

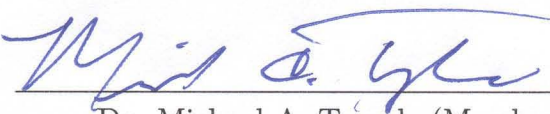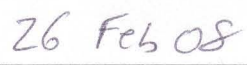|	
Richard K. Martin	_02/26/2008_
Dr. Richard K. Martin (Chairman)	date
[signature]	_26 Feb 08_
Dr. Michael A. Temple (Member)	date
[signature]	_26 Feb 08_
Dr. Robert F. Mills (Member)	date

AFIT/GE/ENG/08-18

Abstract

This thesis investigates a modification to Differential Phase Shift Keyed (DPSK) modulation to create a Low Probability of Interception/Exploitation (LPI/LPE) communications signal. A pseudorandom timing offset is applied to each symbol in the communications stream to intentionally create intersymbol interference (ISI) that hinders accurate symbol estimation and bit sequence recovery by a non-cooperative receiver. Two cooperative receiver strategies are proposed to mitigate the ISI due to symbol timing offset: a modified minimum Mean Square Error (MMSE) equalization algorithm and a multiplexed bank of equalizer filters determined by an adaptive Least Mean Square (LMS) algorithm. Both cooperative receivers require some knowledge of the pseudorandom symbol timing dither to successfully demodulate the communications waveform.

Numerical `Matlab`® simulation is used to demonstrate the bit error rate performance of cooperative receivers and notional non-cooperative receivers for binary, 4-ary, and 8-ary DPSK waveforms transmitted through a line-of-sight, additive white Gaussian noise channel. Simulation results suggest that proper selection of pulse shape and probability distribution of symbol timing offsets produces a waveform that is accurately demodulated by the proposed cooperative receivers and significantly degrades non-cooperative receiver symbol estimation accuracy. In typical simulations, non-cooperative receivers required 2-8 dB more signal power than cooperative receivers to achieve a bit error rate of 1.0%. For nearly all reasonable parameter selections, non-cooperative receivers produced bit error rates in excess of 0.1%, even when signal power is unconstrained.

Acknowledgements

Table of Contents

List of Figures

ix

List of Tables

List of Symbols

List of Abbreviations

Signal Processing Design of
Low Probability of Intercept Waveforms
Via Intersymbol Dither

I. Introduction

Secure communications have proven to be vital to successful military operations across all levels of warfare [9]. With the advent of wireless technology, distributed communication has become a military staple [17]. The advantage of wireless communications is not without risks. In particular, the broadcast nature of wireless transmissions makes this form of communication highly susceptible to eavesdropping by third parties utilizing non-cooperative receiver devices. This vulnerability has led to an ever-evolving challenge to develop and field wireless communications systems that hinder or preclude detection, interception, and exploitation by non-cooperative receivers [12].

A multitude of strategies have been employed to prevent the exploitation of communication signals. Perhaps the most common approach is data encryption which involves coding of the information bits prior to transmission. Successful encryption prevents a third party from extracting information from the intercepted and demodulated communications waveform [21:463].

Another way to approach wireless communications security is to prevent the adversary from intercepting the waveform in a meaningful way. Spread spectrum and frequency hopping techniques, for example, enhance wireless communications security by making the signal difficult to detect and intercept [21:95]. This thesis investigates a strategy that manipulates the transmitted waveform to inject self-inflicted interference between communications symbols such that a non-cooperative receiver cannot resolve

the transmitted communications symbols. Two cooperative receivers are proposed that mitigate this self-interference using signal processing techniques.

1.1 Problem Statement

Because many types of wireless communications are broadcast over a large area, the signals are highly vulnerable to third-party interception and monitoring. Protection strategies at both the bit and waveform level are desirable to prevent eavesdropping. This can be achieved by applying techniques to obstruct non-cooperative parties from detecting, intercepting, and/or exploiting the communications signal. The goal of a Low Probability of Detection (LPD) signal is to prevent other parties from being aware that the signal is present. For the purposes of this thesis, Low Probability of Interception (LPI) refers to difficulty in identifying and extracting the symbols from the waveform. Finally, Low Probability of Exploitation (LPE) describes methods that prevent recovery of the signal's information at the bit level.

1.2 Research Focus

This thesis develops a modification to Differential Phase Shift Keyed (DPSK) modulation to achieve a waveform with LPI characteristics. This is achieved by inserting controlled intersymbol interference (ISI) in the transmitted waveform that inhibits accurate symbol estimation in non-cooperative receivers. Additional signal processing in the cooperative receiver must be designed to mitigate the injected ISI. Symbol estimation accuracy of the cooperative receiver for the LPI signalling scheme should be similar to the optimal DPSK signalling performance. The additional costs of computational complexity in the cooperative receiver and potential bandwidth expansion of the waveform are considered.

1.3 Implications

The LPI signalling strategy proposed in this thesis potentially provides an additional layer of information security for wireless communications that can be used in

concert with existing LPD/LPI/LPE protection schemes. The concept presented in this research is applicable to common modulation techniques such as Pulse Amplitude Modulation, Quadrature Amplitude Modulation, and Phase Shift Keyed Modulation.

1.4   Preview

Chapter II contains background information, outlining existing physical layer strategies for LPI communications, develops a model framework for multipath channel effects and equalization, and surveys blind equalization techniques. Proposed signal processing techniques for generating low-probability of intercept waveforms are developed in Chapter III. Chapter IV develops a numerical simulation of these signal processing techniques, simulation results are presented in Chapter V, and conclusions are summarized in Chapter VI.

II. Background and Literature Review

This chapter begins by reviewing several common existing strategies for creating secure wireless communications signals. LPE signalling via encryption, LPD through spread spectrum, and LPI via frequency hopping are presented. The remainder of the chapter discusses ISI in the context of wireless communications. The LPI signalling scheme developed in this thesis uses ISI to degrade non-cooperative receiver performance. Significant research exists concerning the mitigation of ISI caused by multipath channels. These techniques are applicable to the signal processing design of a cooperative receiver for the LPI scheme developed in Chapter III. Blind equalization methods, which mitigate ISI due to multipath with minimal *a-priori* knowledge of the signal, are also reviewed for potential application to non-cooperative receivers attempting to demodulate the proposed LPI technique.

2.1 Existing Secure Communications Strategies

Encryption is perhaps the most widely implemented form of digital communications protection in both the wireless and wired environments. Encryption techniques are widely studied, and a survey of encryption is beyond the scope of this document. It is sufficient to state that the goal of encryption is to prevent a third party from extracting information from an intercepted bit stream. In other words, encryption protects the information in the event that the transmitted bits are intercepted. A cooperative receiver relies on *a-priori* knowledge of the decryption key to extract the message from the received bit stream. The security of encryption relies on the inability of a third party to determine the key, even if the encryption technique is known [21:463]

Spread spectrum, on the other hand, makes it difficult for a third party to recognize that a communications signal is being transmitted. The modulated signal is spread over a large bandwidth by mixing with a high rate pseudorandom sequence. By dispersing the signal power over a large bandwidth, a non-cooperative receiver is less likely to discern the presence of a transmitted signal from the channel noise [21:95].

The pseudorandom code used to create a spread spectrum waveform must be known by the receiver to recover (despread) the waveform to achieve to original modulated communications signal. In many cases, a non-cooperative receiver will not have access to this code, making demodulation difficult even if the signal of interest is known to be present [15].

Frequency hopping involves adjusting the carrier frequency of the modulated signal according to a pseudorandom sequence. A cooperative receiver uses knowledge of the pseudorandom sequence of carrier frequencies to locate and demodulate the signal. Presumably, a non-cooperative receiver lacks access to the hopping sequence and must detect each successive carrier frequency and match the frequency in order to demodulate the signal. To prevent signal interception, the hop rate must be sufficiently fast enough to prevent the non-cooperative receiver from adjusting to and extracting information at any carrier frequency [21:199].

2.2   *Intersymbol Interference and Equalization*

Direct sequence digital communications signals transmit information as a series of consecutive symbols representing binary data. In a basic signalling scheme, symbols are transmitted in succession, with the end of the current symbol coinciding exactly with the beginning of the next symbol. The bandlimited nature of physical channels, however, limits the speed at which the communications waveform can be changed. This temporal spreading of the signal blurs the boundaries between communications symbols, creating ISI [4, 16]. In wireless communications, ISI is exacerbated by the multiple paths a transmitted signal may take to reach a receiver, with each path inducing different amplitude and phase (time delay) distortions on the signal. At any single instant, the composite signal measured at the receiver is the result of multiple symbols that have travelled over multiple routes [16:771].

The composite effect of these distortions can be modeled as a linear time-invariant system characterized by the overall channel impulse response $h(t)$ which
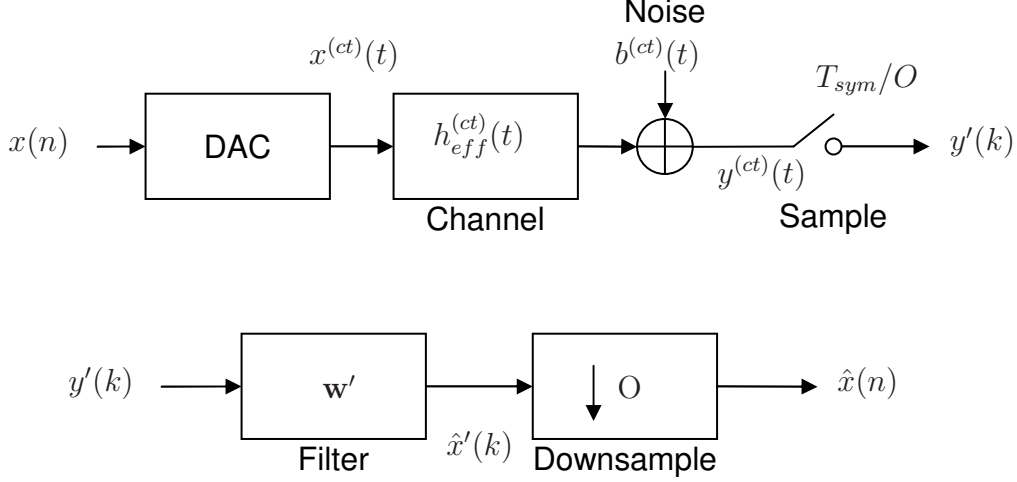
Figure 2.1:   Baseband communications model

maps the transmitted signal $x(t)$ to the received signal $y(t)$ according to (2.1) [6:70].

$$y(t) = \int_{-\infty}^{\infty} x(\lambda) h(t - \lambda) d\lambda \qquad (2.1)$$

This chapter considers the baseband communications model shown in Figure 2.1. The transmitted symbol sequence is represented by a series of discrete, complex symbols denoted $x(n)$. The digital to analog converter (DAC) block converts the discrete series to a *continuous time (ct)* impulse train with symbol impulses occurring every T_{sym} seconds. The transmitted signal is subject to the effective channel impulse response $h_{eff}^{(ct)}(t)$, which may introduce ISI, and additive noise $b^{(ct)}(t)$. The effective channel impulse response represents pulse shaping in the transmitter $f^{(ct)}(t)$, the physical channel impulse response $h_{phys}^{(ct)}(t)$, and a matched filter in the receiver $f^{(ct)*}(-t)$. The superscript (ct) denotes *continuous time* signals in this thesis. The received signal after matched filtering is $y^{(ct)}(t)$ and is sampled an integer number of times O per symbol period T_{sym}.

The goal of equalization is to mitigate or even remove the ISI via signal processing within the communications receiver. Filtering, a common approach to equalization, attempts to modify the received signal in a manner that isolates the individual symbols, essentially inverting the effect of the channel [16:150]. The digital transverse

2-3

filter is a linear time-invariant system defined by its discrete impulse response $\mathbf{w'}$ which acts on the received signal samples $y'(k)$ to produce an estimate of the transmitted signal $(\hat{x}(n) \approx x(n - \delta))$ as shown in Figure 2.1. The "prime" designation denotes oversampled signals with T_{sym}/O seconds between samples. The transverse filtering operation is described mathematically by the discrete convolution sum:

$$x'(k) = w'(k) * y'(k) = \sum_{m=0}^{M-1} w'(m)y'(k-m) . \tag{2.2}$$

The above model assumes the channel response is static. In many physical systems, however, the channel impulse response varies over time [16:946]. For static channels, preset equalization in which the filter taps are constant is sufficient. For slowly time-varying channels, an adaptive equalizer is required. An adaptive equalizer may update the filter taps continuously or periodically. In either case, an adaptive filter is characterized by a convergence rate. When the channel variation rate exceeds the convergence rate of the filter, symbol recovery is degraded [16:158]. The LPI signal design in Chapter III attempts to vary the effective channel impulse response beyond the filter convergence rate to prevent eavesdropping.

Of particular interest to non-cooperative receiver design are blind, adaptive equalization methods. These methods are designed to undo the effects of the linear, time-invariant channel using only limited knowledge of the channel and the statistics of the source signal [4:684]. A successful blind equalizer allows a non-cooperative receiver to minimize ISI and extract communications signals with little or no prior knowledge of the information content.

2.3 Single/Multichannel Communications Model Equivalence

When the sampling period is an integer multiple of the symbol period in the single channel model (Figure 2.1), the system can be equivalently represented as a multiple channel system with discrete signals and impulse responses at a sampling frequency of $1/T_{sym}$ as shown in Figure 2.2. This section derives the equivalent multi-
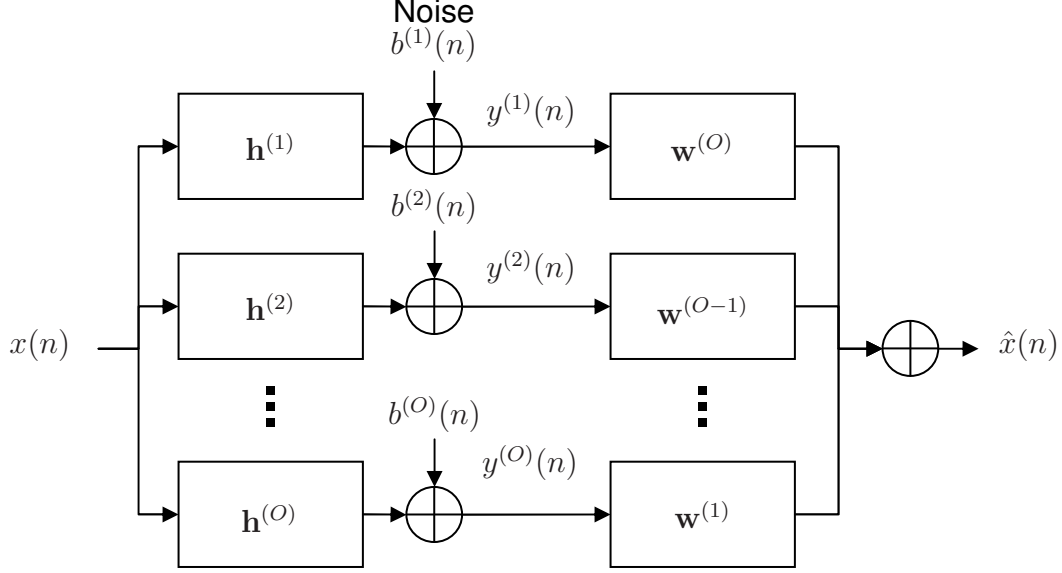
Figure 2.2:   Multichannel communications model

channel model and presents a block matrix notation for the system. The equivalence derivation is based on [5].

2.3.1 Model Equivalence. In this thesis, the effective channel impulse response is a combination of the transmitter pulse shape, the physical channel model, and the receiver matched filter. The continuous time effective channel impulse response $h_{eff}^{(ct)}(t)$ can be expressed as

$$h_{eff}^{(ct)}(t) = f^{(ct)}(t) \star h_{phys}^{(ct)}(t) * f^{(ct)*}(-t) \ , \tag{2.3}$$

where

$$f^{(ct)}(t) = \text{Pulse shape (and matched filter)} \ ,$$

$$h_{phys}^{(ct)}(t) = \text{Physical channel impulse response.}$$

All pulse shapes considered in this thesis are real and symmetric, so the pulse shape and matched filter are identical ($f^{(ct)}(t) = f^{(ct)*}(-t)$). Note that *continuous time* signals are explicitly denoted by the superscript (*ct*).

2-5

In the baseband communications model, the N transmitted symbols are represented by a series of complex, discrete terms $x(n)$. The continuous time signal after matched filtering in the receiver can be written as

$$y^{ct}(t) = \sum_{n=0}^{N-1} x(n) h_{eff}^{(ct)}(t - nT_{sym} - t_o) + b^{(ct)}(t) \ . \tag{2.4}$$

The additive noise signal $b^{(ct)}(t)$ is the channel noise passed through the matched filter. Unless otherwise stated, the channel noise is assumed to be additive white Gaussian noise $\nu^{(ct)}(t)$. It follows that the resulting noise signal is described by

$$b^{(ct)}(t) = \int_{-\infty}^{\infty} f^{(ct)}(\tau) \nu^{(ct)}(t - \tau) d\tau \ . \tag{2.5}$$

The oversampling factor O defines the number of samples per symbol period T_{sym}, resulting in a sampling rate of O/T_{sym} samples per second. In this way, the sampled matched filter output can be written as

$$y^{(ct)}\left(\frac{kT_{sym}}{O}\right) = \sum_{n=0}^{N-1} x(n) h_{eff}^{(ct)}\left(\frac{kT_{sym}}{O} - nT_{sym} - t_o\right) + b^{(ct)}\left(\frac{kT_{sym}}{O}\right) \ . \tag{2.6}$$

The synchronization of the sampling is determined by t_0. The sampled signals in (2.6) have obvious discrete analogs defined in (2.7). The "prime" designation is used to indicate an oversampled discrete series with T_{sym}/O seconds between samples.

$$y'(k) = y^{(ct)}\left(\frac{kT_{sym}}{O}\right)$$
$$h'(k) = h_{eff}^{(ct)}\left(\frac{kT_{sym}}{O} - t_o\right)$$
$$b'(k) = b^{(ct)}\left(\frac{kT_{sym}}{O}\right) \tag{2.7}$$

After sampling the matched filter output in the baseband model, the equalization filter with M taps spaced T_{sym}/O seconds apart is applied. The resulting signal $\hat{x}'(k)$ is given by

$$\hat{x}'(k) = \sum_{m=0}^{M-1} w'(m) y^{(ct)} \left((k-m) \frac{T_{sym}}{O} \right) . \tag{2.8}$$

The approximated symbols are extracted by downsampling by decimating by O:

$$
\begin{aligned}
\hat{x}(n) &= \hat{x}' \left(O(n+1) - 1 \right) , \\
&= \sum_{m=0}^{M-1} w'(m) y^{(ct)} \left((O(n+1) - 1 - m) \frac{T_{sym}}{O} \right) , \\
&= \sum_{m=0}^{M-1} w'(m) y^{(ct)} \left(n T_{sym} + \frac{(O-1)T_{sym}}{O} - \frac{m T_{sym}}{O} \right) .
\end{aligned} \tag{2.9}
$$

The multichannel model can be extracted from (2.9) by restructuring as O summations of decimated series $w'(m)$ and $y'(k)$:

$$
\begin{aligned}
\hat{x}(n) &= \sum_{m=0}^{(M/O)-1} w'(Om) y^{(ct)} \left((n-m) T_{sym} + \frac{(O-1)T_{sym}}{O} \right) \\
&\quad + \sum_{m=0}^{(M/O)-1} w'(Om+1) y^{(ct)} \left((n-m) T_{sym} + \frac{(O-2)T_{sym}}{O} \right) \\
&\quad \vdots \\
&\quad + \sum_{m=0}^{(M/O)-1} w'(Om+O-1) y^{(ct)} \left((n-m) T_{sym} \right) , \\
&= \sum_{m=0}^{(M/O)-1} w'(Om) y \left((n-m)O + O - 1 \right) \\
&\quad + \sum_{m=0}^{(M/O)-1} w'(Om+1) y \left((n-m)O + O - 2 \right) \\
&\quad \vdots \\
&\quad + \sum_{m=0}^{(M/O)-1} w'(Om+O-1) y \left((n-m)O \right) .
\end{aligned} \tag{2.10}
$$

2-7

Defining sample spaced subchannel variables in terms of the oversampled single channel variables (2.12) allows the estimated symbols to be written as O discrete convolutions:

$$\hat{x}(n) = \left(w^{(1)}(n) \star y^{(O)}(n)\right) + \left(w^{(2)}(n) \star y^{(O-1)}(n)\right) + \ldots + \left(w^{(O)}(n) \star y^{(1)}(n)\right) \ . \quad (2.11)$$

$$b^{(i)}(n) = b' \left(nO + i - 1\right)$$
$$y^{(i)}(n) = y' \left(nO + i - 1\right)$$
$$h^{(i)}(n) = h \left(nO + i - 1\right) \quad (2.12)$$

Finally, the subchannel siganls $y^{(i)}(n)$ are derived in terms of the subchannel impulse responses:

$$
\begin{aligned}
y^{(i)}(m) &= \sum_{n=0}^{N-1} x(n) h_{eff}^{(ct)} \left(\frac{(Om + i - 1)T_{sym}}{O} - nT_{sym} - t_o \right) + b^{(i)}(m) \ , \\
&= \sum_{n=0}^{N-1} x(n) h_{eff}^{(ct)} \left((m - n)T_{sym} + \frac{(i - 1)T_{sym}}{O} - t_o \right) + b^{(i)}(m) \ , \\
&= x(m) * h^{(i)}(m) + b^{(i)}(m) \ . \quad (2.13)
\end{aligned}
$$

So $\mathbf{h}^{(i)}$, $b^{(i)}(n)$, $y^{(i)}(n)$, and $\mathbf{w}^{(i)}$ are now defined in terms of their single channel analogs. With these definitions, (2.11) and (2.13) map the system input $x(n)$ to the output $\hat{x}(n)$ and the multichannel model is described completely.

2.3.2   Convolution Matrix.   The discrete linear convolution operation can be expressed in matrix form. In general, recasting the convolution as a matrix operation allows for faster convolution computations. In the context of communications

channel modeling and equalization filtering, properties of the convolution matrix corresponding to the effective channel impulse response provide insight into equalization performance (see Section 2.4.3). The following block notation is derived from [5] and [11].

To begin, define the subchannel impulse response $h^{(i)}(n)$ and equalization filters $w^{(i)}(n)$ sequences as vectors. Each impulse response vector has length L and each equalization filter has length M/O.

$$\mathbf{h}^{(i)} = [h^{(i)}(0), \ h^{(i)}(1), \ ... \ h^{(i)}(L-1)]^T \tag{2.14}$$

$$\mathbf{w}^{(i)} = [w^{(i)}(0), \ w^{(i)}(1), \ ... \ w^{(i)}(M/O-1)]^T \tag{2.15}$$

The subchannel equalization filters can be stacked columnwise to make a single vector $\mathbf{w}(n)$ according to (2.16), which should not be confused with the oversampled filter tap vector $\mathbf{w}'$ in Figure 2.1.

$$\mathbf{w}(n) = \begin{bmatrix} \mathbf{w}^{(O)}(n) \\ \vdots \\ \mathbf{w}^{(1)}(n) \end{bmatrix} \tag{2.16}$$

The subchannel matched filter output $y^{(i)}(n)$ can be expressed as a vector by recasting all of the discrete sequences in terms of vectors or convolution matrices. To proceed, let $\mathbf{y}^{(i)}(n)$ be a vector of N matched filter samples such that

$$\mathbf{y}^{(i)}(n) = [y^{(i)}(n), \ y^{(i)}(n-1), \ y^{(i)}(n-2), \ ... \ y^{(i)}(n-N+1)]^T \ . \tag{2.17}$$

Similarly, $\mathbf{x}(n)$ and $\mathbf{b}^{(i)}(n)$ are defined according to

$$\mathbf{x}(n) = [x(n), \ x(n-1), \ x(n-2), \ ... \ x(n-N-L+2)]^T \ , \tag{2.18}$$

$$\mathbf{b}^{(i)}(n) = [b^{(i)}(n), \ b^{(i)}(n-1), \ b^{(i)}(n-2), \ ... \ b^{(i)}(n-N+1)]^T \ . \tag{2.19}$$

The subchannel convolution matrix $\mathbf{H}_N^{(i)}$ for the ith subchannel acts on $(N + L - 1)$ transmitted symbols in $\mathbf{x}^{(i)}(n)$ to give N samples in $\mathbf{y}^{(i)}(n)$ (2.20). The length of the effective channel impulse response as an integer number of symbol periods is L. $\mathbf{H}_N^{(i)}$ is a block diagonal matrix with $\mathbf{h}^{(i)}$ on the diagonal (2.21).

$$\mathbf{y}^{(i)}(n) = \mathbf{H}_N^{(i)}\mathbf{x}(n) + \mathbf{b}^{(i)}(n) \tag{2.20}$$

$$\mathbf{H}_N^{(i)} = \overbrace{\left[\begin{array}{ccccccc} h^{(i)}(0) & \cdots & h^{(i)}(L-1) & 0 & \cdots & \cdots & 0 \\ 0 & h^{(i)}(0) & \cdots & h^{(i)}(L-1) & 0 & \cdots & 0 \\ \vdots & & & & & & \vdots \\ 0 & \cdots & \cdots & 0 & h^{(i)}(0) & \cdots & h^{(i)}(L-1) \end{array}\right]}^{N+L} \Big\} N \tag{2.21}$$

Stacking all of the subchannels columnwise, the entire multichannel matched filter output $\mathbf{y}(n)$ can be expressed in terms of the block convolution matrix containing the effective channel impulse response of each subchannel:

$$\begin{aligned} \mathbf{y}(n) &= \begin{bmatrix} \mathbf{y}^{(1)}(n) \\ \vdots \\ \mathbf{y}^{(O)}(n) \end{bmatrix}, \\ &= \begin{bmatrix} \mathbf{H}_N^{(1)} \\ \vdots \\ \mathbf{H}_N^{(O)} \end{bmatrix} \mathbf{x}(n) + \begin{bmatrix} \mathbf{b}^{(1)}(n) \\ \vdots \\ \mathbf{b}^{(O)}(n) \end{bmatrix}, \\ &= \mathbf{H}_N\mathbf{x}(n) + \mathbf{b}(n) . \end{aligned} \tag{2.22}$$

Calculating the estimated symbol vector $\hat{\mathbf{x}}(n)$ of length N requires a matched filter output vector $\mathbf{y}(n)$ of length $O(N + M/O - 1)$. Each subchannel equalization filter $\mathbf{w}^{(i)}$ can be cast as a convolution matrix $\mathbf{W}_N^{(i)}$ with dimensionality $(M/O +$

$N) \times N$. Concatenating these convolution matrices row-wise (2.23) produces the estimated symbol vector solution in (2.24).

$$\mathbf{W}_N = \left[\mathbf{W}_N^{(O)} \cdots \mathbf{W}_N^{(1)}\right] \tag{2.23}$$

$$\hat{\mathbf{x}}(n) = \mathbf{W}_N \mathbf{y}(n) \tag{2.24}$$

2.4 Equalization Techniques

To better understand the major equalization algorithm families, a classification structure is desired. The equalization algorithms discussed in this section are shown in Figure 2.3, organized according to the hierarchy presented in Haykin's *Adaptive Filter Theory* [4]. This survey contrasts several key algorithm characteristics relevant to non-cooperative receiver operation as discussed in Section 2.4.1. After defining these algorithm traits, the algorithms of interest are summarized. Because the behavior of blind equalization algorithms is often described relative to least mean square (LMS) adaptive filtering based on a known training signal, an overview of LMS is presented first [4:231]. The constant modulus and Sato algorithms, which share a similar structure with the LMS algorithm, are presented next. A block subspace decomposition algorithm based on eigenvalue decomposition of the received signal's autocorrelation matrix is described in detail. Finally, spectrum fitting and Shalvi and Weinstein's higher-order cumulants approaches are reviewed. Special attention is given to the statistical assumptions made by each algorithm and the performance under non-ideal conditions for possible LPI signalling techniques.

2.4.1 Equalization Algorithm Key Characteristics. Haykin groups blind algorithms into two broad categories: algorithms based on the estimation of a signal's second order statistics (SOS) vice algorithms requiring higher-order statistics (HOS) to be estimated. Because second order statistics can be estimated accurately with far fewer observations than higher-order statistics, SOS based algorithms typically
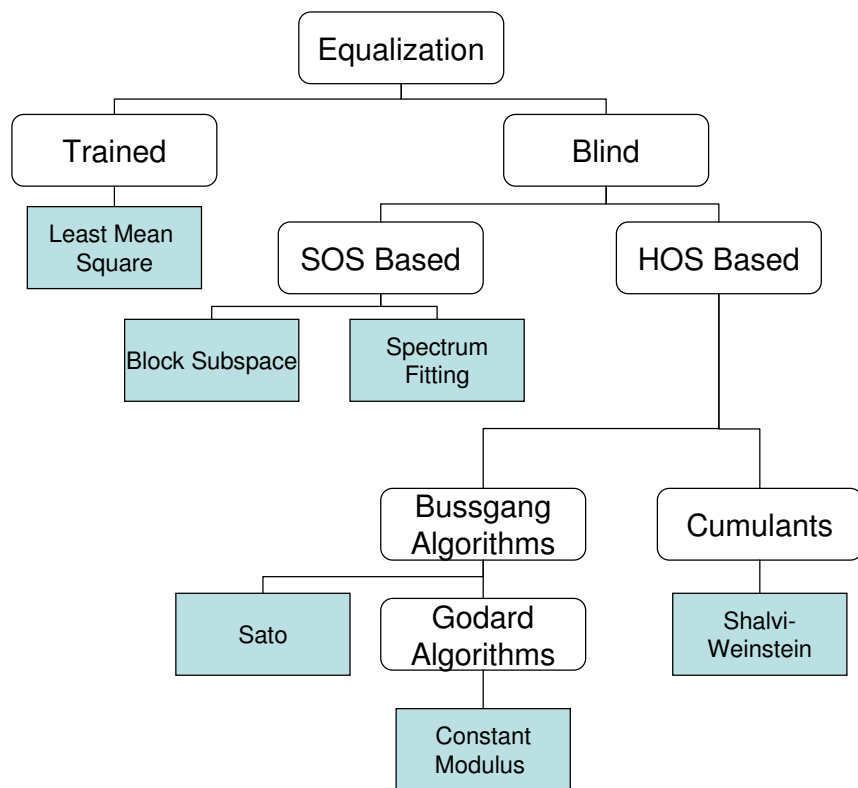
Figure 2.3:   Hierarchy of equalization algorithms

converge significantly faster than those leveraging HOS [4]. Convergence speed can be quite important in a wireless environment with a dynamic channel response. The ability of the receiver to extract meaningful information often hinges on whether the equalizer can track the changing impulse response of the channel and invert the multipath/fading effect [24].

Equalizer sampling rate is another characteristic useful for classification. Generally, an algorithm either uses a single sample from each communications symbol, or multiple samples (note that this assumes the symbol rate is known by the receiver). Algorithms utilizing multiple samples per transmitted symbol are considered fractionally spaced equalizers (FSE), and generally perform better than equivalent sample spaced or baud spaced equalization (BSE) methods [16:161]. Fractional sampling techniques often converge faster and with greater accuracy than their sample spaced analogs [4:727].

The ability of a blind equalization algorithm to adapt in real time is useful to consider, particularly when considering applications in wireless systems which are often subject to time-varying channel behavior. Algorithms that update the equalization filter on a symbol-by-symbol basis are considered to be continuously adaptive. Algorithms which process a block of observed symbols transmitted under a single channel condition to identify an equalization filter are labeled periodically adaptive for the purposes of this thesis.

An equalization method is considered direct if the output of the algorithm is the tap weights of the linear equalization filter $\mathbf{w}$. For example, the equalization filter is estimated many times in some iterative algorithms. The indirect equalization approach first estimates the channel impulse response $\mathbf{h}$ before solving for the equalization filter taps.

2.4.2 Least Mean Square (LMS) Algorithm. The LMS algorithm applied to equalization is an adaptive method of updating the tap weights of a transverse filter based on the difference between the filter output and the known source signal originally
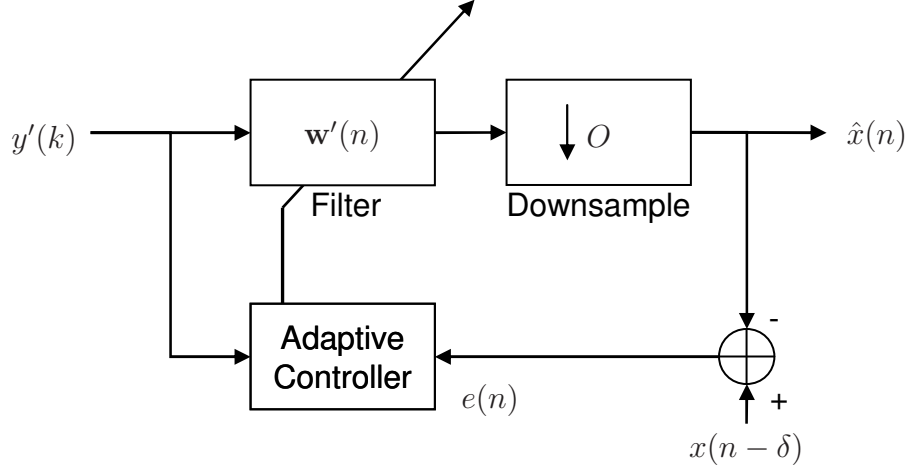
Figure 2.4:   Block diagram of the least mean square algorithm

transmitted. The process is a stochastic extension of deterministic steepest descent algorithms that use the gradient of an error term to determine how the tap weights should be updated to decrease the error term. Instead of explicitly computing the gradient, the LMS algorithm estimates the gradient based on the known transmitted signal, received signal, and current filter tap weights. Figure 2.4 depicts a receiver implementation of the LMS algorithm [4:231]. The equalization filter is updated after processing each received symbol, giving a new set of tap coefficients for $\mathbf{w}$ at each symbol index n.

Both the method of steepest descent and LMS algorithms use a cost function defined by the expectation of the square of the error term $e(n)$. The resulting cost function can be written in terms of the statistics of the transmitted and received

signals [18:287]. Using the multichannel model notation, the cost function is

$$
\begin{aligned}
J(n) &= \mathrm{E}\left[e^*(n)e(n)\right] \ , \\
&= \mathrm{E}\left[\left(x(n-\delta) - \mathbf{w}^T(n)\mathbf{y}(n)\right)^* \left(x(n-\delta) - \mathbf{w}^T(n)\mathbf{y}(n)\right)\right] \ , \\
&= \mathrm{E}\left[x^*(n-\delta)x(n-\delta)\right] - 2\mathrm{Re}\left\{\underbrace{\mathrm{E}\left[x(n-\delta)\mathbf{y}^H(n)\right]}_{\mathbf{p}_{xy}^T} \mathbf{w}^*(n)\right\} \\
&\quad + \mathbf{w}^T(n)\underbrace{\mathrm{E}\left[\mathbf{y}(n)\mathbf{y}^H(n)\right]}_{\mathbf{R}_y} \mathbf{w}^*(n) \ , \\
&= \mathrm{E}\left[x^*(n-\delta)x(n-\delta)\right] - 2\mathrm{Re}\left\{\mathbf{p}_{xy}^T\mathbf{w}^*(n)\right\} + \mathbf{w}^T(n)\mathbf{R}_y\mathbf{w}^*(n) \ . \quad (2.25)
\end{aligned}
$$

Taking the gradient of the cost function with respect to the filter $\mathbf{w}$ gives

$$
\nabla_{\mathbf{w}}J(n) = -2\mathbf{p}_{xy}^T + 2\mathbf{w}^T(n)\mathbf{R}_y \ . \qquad (2.26)
$$

Note that the expectations have been rewritten as the correlation matrix $\mathbf{R}_y$ of the received signal vector $\mathbf{y}(n)$ and the cross correlation vector $\mathbf{p}_{xy}$ of the received signal $\mathbf{y}(n)$ with the current symbol from the known training signal [18:287]. Convergence of the steepest descent method depends on the autocorrelation matrix and cross-correlation vector remaining constant at all time steps n, thus the transmitted symbol sequence $x(n)$ is assumed to be wide-sense stationary (WSS) and the received signal after sampling is either WSS if $y'(k)$ is sample spaced or cyclostationary if $y'(k)$ is fractionally spaced. In practice, LMS can be effective for time-varying channels if the convergence speed is fast relative to the changing channel response, even though this violates the stationary assumption for $y(n)$ [4:203-205].

In LMS, the gradient of the cost function is no longer a deterministic function of filter coefficients. Instead, the gradient at each time step is estimated stochastically using a different estimate of the autocorrelation and cross-correlation matrices at each

time step according to

$$\hat{\nabla}_{\mathbf{w}} J(n) = -2\hat{\mathbf{p}}^T(n) + 2\mathbf{w}(n)^T \hat{\mathbf{R}}_y(n) \ , \tag{2.27}$$

where

$$\hat{\mathbf{R}}_y(n) = \mathbf{y}(n)\mathbf{y}^H(n) \ ,$$

$$\hat{\mathbf{p}}_{xy}(n) = \mathbf{y}^*(n)x(n-\delta) \ .$$

Note that the length of the received vector must match the length of the filter. The filter length, in turn, needs to be large enough to approximate the inverse channel response. Using three times the length of the finite channel impulse response model to determine the filter length is typical [4:236].

The estimated gradient of the cost function produces the filter update function given by

$$
\begin{aligned}
\mathbf{w}(n+1) &= \mathbf{w}(n) - \mu \left(\hat{\nabla} J(n) \right)^T \ , \\
&= \mathbf{w}(n) + \mu \mathbf{y}^*(n) \left(x(n) - \mathbf{y}^T(n)\mathbf{w}(n) \right) \ , \\
&= \mathbf{w}(n) + \mu \mathbf{y}^*(n)e(n) \ . \tag{2.28}
\end{aligned}
$$

As implied by the function, the adaptive controller in the LMS algorithm updates the filter after each received symbol [4:236]. The parameter μ is the step size that controls how much the filter weights are updated in the direction indicated by $\hat{\nabla} J(n)$. The step size must be small enough to prevent the filter coefficients from jumping too far past the error minima with each iteration and diverging. For values of μ that converge, however, smaller step sizes result in slower convergence. Although the step size is somewhat arbitrary, the general convergence criteria calls for μ to be small relative to the inverse of the largest eigenvalue of $\mathbf{R}_y$ [4:288].

Because the symbol-by-symbol update of the filter coefficients is based on an estimate of the gradient that varies with every iteration, the filter never converges to the exact equalization solution that inverts the channel effects completely. Instead, the estimate will continue to fluctuate around the optimal solution after convergence. The average residual mean square error, or misadjustment, after convergence is directly proportional to the step size. Thus, step size selection must balance convergence speed and steady state error. This has driven investigation of LMS algorithms with variable step sizes [7].

2.4.3 Constant Modulus Algorithm (CMA). The constant modulus algorithm (CMA) is one of the most common blind equalization techniques [5]. The algorithm is functionally similar to the LMS algorithm, sharing the same adaptive update method and modest processing requirements for implementation. Both symbol spaced and fractionally spaced versions have been studied extensively. CMA is a part of a larger class of Bussgang blind adaptive algorithms that directly equalize the channel based on higher-order statistics [4]. The fractionally spaced version has the advantage of converging to the same equalization solution as the trained LMS algorithm (perfect equalization) under noiseless conditions for most channels [5]. The criteria for convergence to the LMS solution are presented below. Sample spaced CMA, on the other hand, has been shown to require impractical constraints such as infinite filter length in order to achieve perfect equalization [2].

Intuitively, CMA works by minimizing an error term based on the difference between the expected symbol amplitude and the sampled magnitude of the symbol:

$$e(n) = \frac{\mathrm{E}\left[|x(n)|^4\right]}{\mathrm{E}\left[|x(n)|^2\right]} - |\hat{x}(n)|^2 \ . \tag{2.29}$$

The error term can be minimized using the same update strategy as the LMS error minimization technique described in Section 2.4.2. Error minimization operates on the square of the error term, which itself contains the symbol estimate squared $|x(n)|^2$,

so convergence relies implicitly on the estimation of fourth order statistics via time averaging. This HOS dependence dictates the low convergence speed of the CMA algorithm relative to SOS based methods [4:730].

Clearly, if the source signal is of constant modulus, the error term approaches zero as the filter approaches convergence. Although not obvious, CMA converges even when the source signal does not have a constant modulus. In this case, however, the minima of the cost surface no longer correspond to zero cost. The non-zero steady state cost of the minima have the effect of "flattening" the shape of the cost surface, resulting in slower convergence. This "flattening" phenomena becomes more pronounced as the kurtosis of the source signal increases [5:1935].

As with the LMS algorithm, the step size μ must strike a balance between convergence speed and steady state mean square error, making variable step size strategies desirable [23]. For example, one such method performs a second cost minimization with respect to the step size at each iteration, searching the cost surface in the direction of steepest descent as calculated by the gradient estimation. This minimization determines the "optimal" step size for the current iteration. This approach has the additional advantage of reducing the likelihood of converging to local minima for multimodal cost surfaces [26].

Like LMS, CMA assumes a wide-sense stationary or cyclostationary received signal (depending on the sampling rate of the receiver). Under time-varying channel conditions, the received signal statistics will fluctuate, violating the WSS assumption. However, given sufficiently slow channel variation, the signal statistics may still be stable enough for the time-averaging implicit in CMA to equalize the channel and track the variation in cost surface minima [4:688].

In the case of fractionally spaced CMA, the following four conditions guarantee that the cost surface minima correspond to filter coefficients that perfectly equalize the channel response. First, the channel must be noiseless. Second, the (possibly complex) source signal must be composed of a series of independent, identical symbols from a

circularly symmetric constellation. Third, the kurtosis of the symbol distribution must be less than the kurtosis of a Gaussian distribution [4:727]. Lastly, the channel convolution matrix as defined by Tong *et al.* must be full column rank [20]. The combined channel-filter impulse response for an FSE is presented in terms of the effective channel convolution matrix in Section 2.3.2. Notably, the second and third requirements for perfect equalization are properties of the source signal, suggesting that these features may be exploitable in the design of LPI communications systems, although these assumptions are not exploited in this thesis.

The full column rank requirement of the channel convolution matrix leads to a minimum number of filter taps required for perfect equalization. For a matrix to be full column rank, it must have at least as many rows as columns. The number of required taps is a function of the length of the channel response and the number of samples during each symbol period according to (2.30), where M is the total number of filter tapes, either arranged in a single, fractionally spaced vector in the single receiver model, or as O symbol spaced vectors of length M/O in the multichannel model. L is the number of symbol periods over which the channel impulse response is non-zero, and O is the number of samples taken during each symbol period in the single channel model, or the number of antennas in the multichannel model [5:1930].

$$M \geq L + \frac{M}{O} - 1$$
$$\therefore M \geq \frac{O(L-1)}{O-1} \approx L \tag{2.30}$$

Another extension of the full column rank condition is the requirement that the impulse response of each channel (in the multichannel system model) be linearly independent of other channel impulse responses. In other words, the z-transform of the channel responses must share no common zeros [4:693].

Many variations of CMA have been developed, typically with the goal of addressing specific CMA shortcomings. Vector CMA [25] is of particular interest in relation to the LPI strategy proposed in Chapter III. Vector CMA suggests a means of equalizing source signals with high kurtosis such as QAM constellations produced by shell mapping. Vector CMA defines an error term based on a vector of successive symbols in an attempt to create a statistic with sub-Gaussian kurtosis. In the case of shell mapping, the encoding structure is such that a properly chosen symbol block length produces uniformly distributed error statistics that can be minimized via the cost surface gradient descent [22, 25]. This process is similar to the bank of LMS equalizers discussed as a cooperative receiver structure for the LPI signal design.

2.4.4 Sato Algorithm. Like the constant modulus algorithm, Sato's algorithm is an adaptive algorithm based on LMS. As in LMS and CMA, the Sato algorithm directly equalizes the received signal by iteratively adjusting the equalization filter coefficients. As originally proposed in [13], the Sato algorithm is developed in the context of multilevel pulse amplitude modulation (PAM). The algorithm simplifies equalization by dividing the PAM detection space into two equally likely regions, and then modelling the signal as binary with the remaining levels considered as additive noise. In a zero-mean PAM signal, this is equivalent to considering only the sign of the signal [13]. The resulting error term for a received symbol is given by

$$e(n) = \hat{x}(n) - [\text{sgn } \hat{x}(n)] \cdot E\left[|x(n)|\right] \ . \tag{2.31}$$

The Sato algorithm is subject to the same channel impulse response constraints as CMA. Local minima in the cost surface are also a difficulty, particularly in noisy environments. With no particular advantages over CMA and an infinite equalizer length requirement for perfect equalization [4:722], the Sato algorithm is not pursued as a non-cooperative receiver architecture in this thesis.

2.4.5 Block Subspace Decomposition Algorithm. Subspace decomposition is a channel identification algorithm (indirect equalization) for oversampled signals with cyclostationary statistics. The primary advantage of the subspace decomposition method over CMA is that it relies on second-order statistics, which can be estimated well with relatively few samples compared to higher-order statistics. The algorithm is not continually adaptive in the sense that the channel is not estimate is not iteratively refined on a symbol by symbol basis. Instead, a block of consecutive samples must be collected. Conceivably, a sufficiently slow time-varying channel could be repeatedly estimated using a sliding block of samples, making it a candidate for a periodically adaptive implementation. The significant complexity of subspace decomposition is a limiting factor. Also, as a fractionally spaced algorithm, subspace decomposition is subject to the same full column rank requirement on the channel convolution matrix as CMA as discussed in Section 2.4.3 [4:689-701].

The subspace decomposition method considers the correlation matrices of the transmitted signal and the received signal. Interestingly, the theoretical development of the subspace method includes an additive noise source which is restricted to be bandlimited, stationary, and independent from the transmitted signal without disturbing the ability of the algorithm to approach perfect equalization [11, 20]. Specifically, the correlation matrix of the received signal in terms of the correlations of the transmitted and noise vectors is derived in (2.32), where $\mathbf{H}$ is the channel convolution matrix as derived in Section 2.3.2 [4:694]. Note that the final line assumes that the noise vector is composed of independent, identically distributed random variables with variance σ^2.

$$
\begin{aligned}
\mathbf{R}_y &= E\left[\mathbf{y}\mathbf{y}^H\right] \\
&= E\left[(\mathbf{H}\mathbf{x} + \boldsymbol{\nu})(\mathbf{H}\mathbf{x} + \boldsymbol{\nu})^H\right] \\
&= E\left[\mathbf{H}\mathbf{x}\mathbf{x}^H\mathbf{H}^H\right] + E\left[\boldsymbol{\nu}\boldsymbol{\nu}^H\right] \\
&= \mathbf{H}\mathbf{R}_x\mathbf{H}^H + \mathbf{R}_\nu \\
&= \mathbf{H}\mathbf{R}_x\mathbf{H}^H + \sigma^2\mathbf{I}
\end{aligned}
\tag{2.32}
$$

Rewriting the correlation matrix of the received signal in terms of eigenvalues and eigenvectors using Mercer's theorem (also called the spectral theorem) produces

$$\sum_{k=0}^{ON-1} \lambda_{y,k} \mathbf{q}_{y,k} \mathbf{q}_{y,k}^H = \sum_{k=0}^{ON-1} \lambda_{z,k} \mathbf{q}_{z,k} \mathbf{q}_{z,k}^H + \sigma^2 \mathbf{I} , \tag{2.33}$$

where $\mathbf{q}_{y,k}$ and $\lambda_{y,k}$ are the eigenvectors and eigenvalues of the composite received signal correlation matrix $\mathbf{R}_y$, $\mathbf{q}_{z,k}$ and $\lambda_{z,k}$ are the eigenvectors and eigenvalues of the noiseless transmitted signal's correlation matrix after channel effects, O is the number of received samples per transmitted symbol, and N is the total number of received symbols [4:813]. Because each correlation matrix $\mathbf{R}$ is positive semi-definite, the eigenvalues of each term in (2.33) are all nonnegative. Although each term produces a square correlation matrix of size ON, the correlation matrix of the transmitted signal $\mathbf{H}\mathbf{R}_x\mathbf{H}^H$ has a rank of only $(N + L)$, where L is the channel length in terms of symbol periods (effective channel order). Thus, $\mathbf{H}\mathbf{R}_x\mathbf{H}^H$ has at most $(N+L)$ positive eigenvalues and $ON - (N+L)$ eigenvalues equal to zero. This naturally divides vector space of $\mathbf{R}_y$ into two subspaces: the eigenvectors corresponding to the $(N+L)$ largest eigenvalues span the signal subspace and the eigenvectors corresponding to the rest of the eigenvalues (each with magnitude σ^2) span the noise subspace [11].

Defining the eigenvectors spanning the noise subspace as $\mathbf{g}_k$ leads to (2.34). Substituting $\mathbf{R}_y$ as defined in (2.32) into (2.34) leads to (2.35) [4:695]. This result can also be reached directly by stating that the noise subspace spanned by $\mathbf{g}_k$ is orthogonal to the subspace defined by the columns of the convolution matrix $\mathbf{H}$. Moulines, *et al.* showed that solving (2.35) for $\mathbf{H}$ with the restriction $\mathbf{H} \neq \mathbf{0}$ produces a unique solution (with an arbitrary scale factor) [11].

$$\mathbf{R}_y \mathbf{g}_k = \sigma^2 \mathbf{g}_k, \ k = N + L + 1, \ldots, ON \tag{2.34}$$

$$\mathbf{H}^H \mathbf{g}_k = \ \mathbf{0}, \quad k = N + L + 1, \ldots, ON \tag{2.35}$$

To cleanly extract the channel coefficients $\mathbf{h}$, (2.35) is often restructured. In (2.36), each eigenvector $\mathbf{g}_k$ has been recast into a convolution matrix $\mathbf{G}_k$ following the process in Section 2.3.2.

$$\mathbf{G}_k^H \mathbf{h} = \mathbf{0} \tag{2.36}$$

Furthermore, (2.36) can be expressed as a scalar by setting the square norm of $\mathbf{G}_k^H \mathbf{h}$ to zero:

$$\left\| \mathbf{G}_k^H \mathbf{h} \right\|^2 = \mathbf{h}^H \mathbf{G}_k \mathbf{G}_k^H \mathbf{h} = 0 \ . \tag{2.37}$$

Finally, a cost function can be defined in terms of (2.37). In this cost function (2.38), the eigenvector convolution matrix is replaced by an estimate computed from the block of received samples. The cost function can then be minimized under the constraint that $\mathbf{h} \neq \mathbf{0}$ [4:697].

$$J(\mathbf{h}) = \mathbf{h}^H \left(\sum_{k=0}^{ON-N-L-1} \hat{\mathbf{G}}_k \hat{\mathbf{G}}_k^H \right) \mathbf{h} \tag{2.38}$$

After identifying the channel estimate, the estimated channel convolution matrix $\hat{\mathbf{H}}$ can be constructed directly. An estimate of the transmitted signal can be obtained by taking the pseudoinverse of $\hat{\mathbf{H}}$:

$$\hat{\mathbf{x}} = \hat{\mathbf{H}}^\dagger \mathbf{y} = \left(\hat{\mathbf{H}}^H \hat{\mathbf{H}} \right)^{-1} \hat{\mathbf{H}}^H \mathbf{y} \ . \tag{2.39}$$

Alternatively, using the singular value decomposition of $\mathbf{R}_y$ to extract the eigenvalues leads to a transmitted signal estimation method that does not require the additional pseudoinverse computation [20].

In the channel identification development above, several assumptions have been made. As mentioned previously, the received signal must be cyclostationary in order to estimate the correlation matrix from via time-averaging [20]. In addition, the channel noise was assumed to be white (noise samples are uncorrelated). The variance of the noise was assumed to be known, however, this is not necessary if the effective

channel order L is known, which is also a known constant in the above subspace channel identification derivation [4:697]. Accurate channel length estimation is also critical to extracting the equalizer tap coefficients from the channel estimate, with a poor estimate leading to an unstable solution. Channel order estimation is preferred over noise power estimation since numerical methods exist for estimating the effective channel order without knowledge of the noise variance [8]. Finally, like CMA, the subspace algorithm relies on the linear independence of the virtual channels [20].

2.4.6   Spectrum Fitting Algorithms.   Spectrum fitting channel identification algorithms based on second order statistics are a frequency domain parallel to the time domain block subspace algorithms. As an SOS-based algorithm, spectrum fitting has the potential to accurately identify the channel filtering coefficients in relatively few symbol periods as compared to HOS-based algorithms. Like the block subspace method, spectrum fitting performs matrix operations on a collected set of fractionally sampled symbols, making it periodically adaptive. The channel properties that ensure a unique identification solution are the same as those for the block subspace algorithm. The frequency domain approach provides an alternative formulation of the conditions under which SOS-based channel identification succeeds [3, 19]. Of note, Ding and Li point out that this method is is not affected by the kurtosis of the input signal, unlike most CMA algorithms which break down for near-Gaussian sources [3].

The general strategy of spectrum fitting algorithms relies on an estimate of the power spectral density of the received signal. In the multichannel model, the data sequence in each branch (or antenna) is stationary, so autocorrelation can be estimated via time averaging. Taking the Fourier transform of each antenna produces O power spectral density functions, referred to as "cyclic spectra" [19]. The coefficients of the cyclic spectra can be used to construct a block convolution matrix similar in spirit to G in the subspace decomposition algorithm. This leads to an error minimization solution involving a singular value decomposition of the block convolution matrix. Because

2-24

spectrum fitting is a frequency domain analog of block subspace decomposition, it is not investigated further in this thesis.

2.4.7 Cumulants Method. Shalvi and Weinstein have proposed a direct blind equalization method based on matching selected second and fourth order statistics of the channel input and equalization filter output. The result is an adaptive gradient descent algorithm similar in spirit to CMA, with the advantage that source signal distributions with kurtosis exceeding the kurtosis of the Gaussian distribution (super-Gaussian) are allowable. Specifically, the Shalvi-Weinstein method assumes the source distribution consists of zero-mean, identically distributed independent symbols and that the first through fourth moments of the source distribution exist. Additionally, the excess kurtosis of the source distribution cannot equal zero, so Gaussian distributions are not equalized by this method. The channel constraints for the Shalvi-Weinstein algorithm are the same as those for CMA [14].

The mathematical foundation developed in [14] upon which this algorithm is based is the following theorem:

$$\text{If } E\left[|\hat{x}(n)|^2\right] = E\left[|x(n)|^2\right] ,$$
$$\text{then } |K\left(\hat{x}(n)\right)| \leq |K\left(x(n)\right)| , \tag{2.40}$$

where
$$K\left(x(n)\right) = E\left[|x(n)|^4\right] - E^2\left[|x(n)|^2\right] - \left|E\left[x^2(n)\right]\right|^2 . \tag{2.41}$$

$K\left(x(n)\right)$ is kurtosis as defined in [14]. The kurtosis magnitude of the input and output symbols in (2.40) are equal when the combined channel/filter response is a discrete unit impulse. In other words, when the output sequence of the equalizing filter is identical to the input sequence with some delay, then the kurtosis of the two sequences is equal (assuming the sequences have equal power) [14].

This leads to the adaptive equalization strategy of selecting filter coefficients to maximize the kurtosis of the output sequence under the equal power constraint

$E\left[|x(n)|^2\right] = E\left[|\hat{x}(n)|^2\right]$. The constrained maximization problem leads to a gradient ascent formulation. This gradient ascent form, in turn, can be transformed into a symbol-by-symbol iterative approximation:

$$\hat{\mathbf{w}}(n+1) = \hat{\mathbf{w}}(n) + \mu \cdot [\text{sgn } K(\hat{x}(n))] \, |\hat{x}(n)|^2 \, \hat{x}(n)\tilde{\mathbf{y}}^*(n) \; . \tag{2.42}$$

where $\tilde{\mathbf{y}}^*(n)$ is the received symbol stream passed through a whitening filter. For source signals with sub-Gaussian kurtosis, the tap update algorithm proposed in [14] simplifies to gradient descent using the CMA error term (2.29). Because the DPSK constellations used in this thesis are sub-Gaussian, the cumulants method is not studied as a potential non-cooperative receiver.

III. LPI Signal Design

The goal of this thesis is to investigate a communications signal structure that resists equalization by blind methods, leveraging non-cooperative receivers' reliance on blind equalization to create an LPI signal. In designing such a scheme, the impact to the cooperative communications link must also be considered, both in terms of transmission accuracy and system complexity. This chapter proposes a strategy of introducing a time dither into the symbol synchronization of the transmitter. This dither creates dynamic ISI at the receiver input which hinders blind equalization. A cooperative receiver, however, can successfully deconvolve the symbol sequence if the timing dither of the symbol transmissions is known. The signaling scheme is developed in detail in Section 3.1. Section 3.2 presents cooperative receiver designs for this communications signal and Section 3.3 discusses the behavior of notional non-cooperative receivers with blind algorithms with respect to the symbol dither signal.

3.1 Signal Design

All equalization techniques discussed in Chapter II rely on a sufficiently slow time variation in the effective channel impulse response. This thesis investigates the feasibility of achieving LPI characteristics in a communications signal by injecting time-varying ISI into the waveform via dither in the symbol transmission synchronization. To prevent signal interception, the resulting ISI must be severe enough to prevent meaningful demodulation and vary in time in a manner that prohibits effective blind equalization.

More explicit discussion of synchronization dither requires additional notation. In most traditional transmitters, communications symbols are transmitted at a constant rate with the leading edge of each symbol exactly T_{sym} seconds apart. To create ISI in the LPI waveform, let the leading edge of each symbol be delayed up to an entire additional symbol period. In other words, the LPI waveform is composed of a series of time blocks of duration T_{sym}, each block containing the leading edge of exactly one communications symbol somewhere within the block. This dithering method pre-
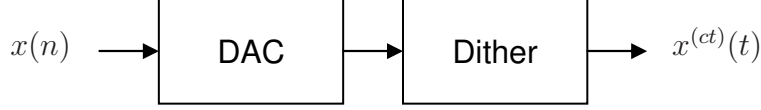
Figure 3.1:   A dither block in the transmitter creates ISI.

serves symbol order and fixes the average symbol transmission rate to a constant rate of $1/T_{sym}$, simplifying the cooperative receiver demodulation process.

The delay of the nth symbol relative to the leading edge of the nth symbol period is $d(n)$. This delay is applied after the DAC in the single channel communications model in Figure 2.1, as shown in Figure 3.1. This delay implementation of dither requires a new expression for $x^{(ct)}(t)$:

$$x^{(ct)}(t) = \sum_{n=0}^{N-1} x(n)\delta\left(t - nT_{sym} - d(n)\right) , \qquad (3.1)$$

where $d(n)$ is a sample of random variable D with a probability density function $p_D^{(ct)}(t)$ and ct denotes a *continuous time* waveform. This thesis considers uniform density functions, although more exotic density functions are possible, so long as the function is zero for $t < 0$ and $t \geq T_{sym}$. The uniform dither distribution is completely defined by the dither range, which is $0 \leq d(n) < T_{max}$. The probability density function can be written in terms of T_{max} according to

$$p_D^{(ct)}(t) = \begin{cases} 1/T_{max}, & 0 \leq t < T_{max} \\ 0, & t < 0 \text{ or } t \geq T_{max} . \end{cases} \qquad (3.2)$$

Clearly, for $p_D^{(ct)}(t)$ to satisfy the restrictions above, the dither range T_{max} is restricted to $[0, T_{sym}]$.

In practice, the sequence of symbol delays is a pseudorandom sequence with terms selected from a discrete set of possible delays. In this discrete case, the symbol period is subdivided into P evenly-spaced possible dither values. The probability

density function for a discrete uniform random variable D is given by

$$p_D^{(ct)}(t) = \frac{1}{p_{max}+1} \sum_{p=0}^{p_{max}} \delta\left(t - \frac{pT_{sym}}{P}\right) , \qquad (3.3)$$

where p_{max} must be from the set of integers ranging over $[0, P)$. The parameter p_{max} in the discrete distribution is related to the dither range T_{max} according to

$$p_{max} = \left\lfloor \frac{PT_{max}}{T_{sym}} \right\rfloor , \qquad (3.4)$$

where $\lfloor x \rfloor$ is the largest integer not exceeding x.

As a pseudorandom sequence, the delay code $d(n)$ will have some finite period N_d. In most cases, this thesis considers long delay codes with periods N_d larger than the number of transmitted symbols. The cooperative receiver described in Section 3.2.1, however, requires short period relative to the number of symbols available for training the equalization filter(s).

The severity of ISI in this waveform is a function of the pulse shape and the symbol delay probability density function. Conceivably, symbol-to-symbol variation in the pulse shape of the communications waveform could be used as an alternative or in addition to symbol synchronization dither to inject ISI. Pulse shape variation, however, introduces additional complexity on matched filtering in the cooperative receiver. For this reason, the LPI benefits due to intentional ISI are characterized using a fixed pulse shape and varying symbol dither according a pseudorandom sequence.

3.2 *Cooperative Receiver Strategies*

This thesis develops cooperative receiver designs by applying signal processing techniques on the sampled matched filter output. To effectively demodulate a pseudorandom dither waveform (PDW), a cooperative receiver uses some knowledge of the delay sequence used to generate the waveform in the transmitter. Two methods are suggested here. In the first, the periodic nature of the symbol delay sequence is uti-
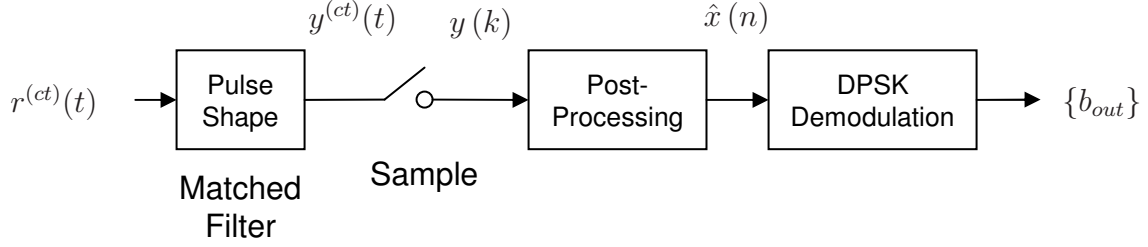
Figure 3.2: Generic structure for the cooperative and non-cooperative receivers described in this chapter.

lized. In the second cooperative receiver design, full knowledge of the delay sequence is assumed to construct an equalization filter according to the MSE algorithm (in a line-of-sight environment).

Both the cooperative and non-cooperative receivers discussed in the remainder of this chapter use the structure shown in Figure 3.2. The signal at the receiver input $r^{(ct)}(t)$ is passed through a matched filter based on the communication signal pulse shape. For non-cooperative receivers, it is assumed that the pulse shape can be estimated using the power spectral density of the received waveform. The rate at which the matched filter output is sampled and the Post-Processing block are specific to the different receiver structures. The resulting estimate of the source symbol sequence $\hat{x}(n)$ is demodulated to produce the output bit stream.

3.2.1 Bank of Equalizers. This equalization structure takes advantage of the periodicity of the symbol delays in the delay code sequence. Assuming the physical channel is static, all samples at the matched filter ouptut spaced $(N_d T_{sym})$ seconds apart are subject to the same effective channel. Thus each collection of these samples is WSS. A cooperative receiver with knowledge of the delay sequence period can cycle through a bank N_d equalization filters, one for each effective channel. Thus, this multiple filter approach is only feasible for dither codes with small periods due to convergence and coefficient storage considerations. The impact of short period codes is discussed in greater detail below. The receiver structure for a fractionally spaced equalizer with oversampling rate 2 and delay code period N_d is depicted in Figure 3.3.

3-4
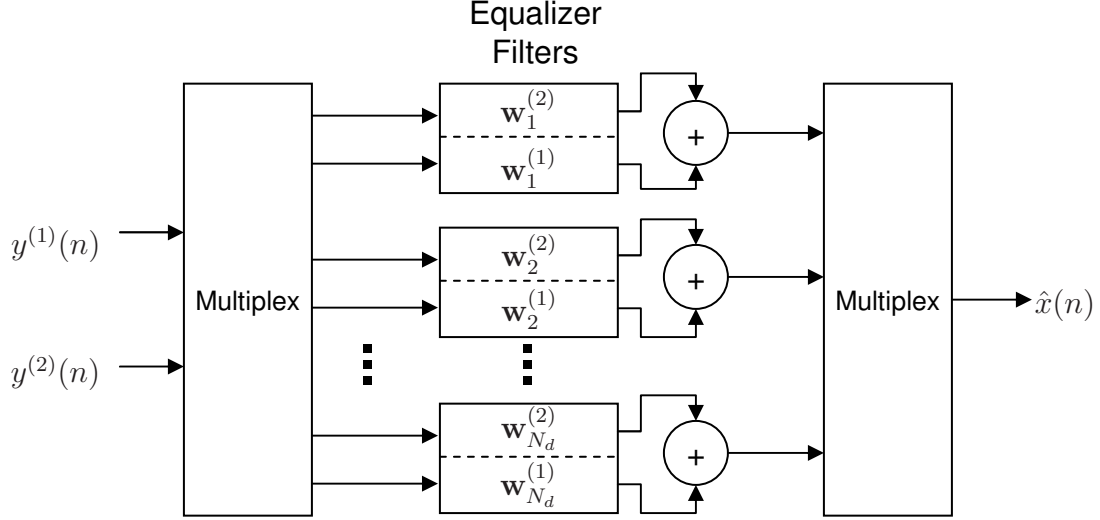
Figure 3.3: By applying a different equalizer $\mathbf{w}_j^{(i)}$ for each pseudorandom dither entry in the dither code, the effective channel at each equalizer input is static, allowing the filters to converge.

The remaining task is to find the equalizer filter taps such that the output of each filter is an estimate of a unique decimation of the original symbol sequence $x(n-\delta)$. In other words, to produce a complete estimate $\hat{x}(n)$, each filter must estimate $x(n-\delta)$ decimated by N_d, but with different phases. In addition, the phase of each must be known so that filter outputs can be recombined in the correct order. Because the number of (fractionally spaced) equalizer filters matches the dither sequence period, the sample statistics at each filter input are stationary and many classical equalization algorithms are applicable.

Of the equalization algorithms described in Chapter II, the trained approach of adaptive LMS is the best candidate. The adaptive LMS algorithm can be directly applied in each filter branch to train each equalizer without introducing any increase in algorithm complexity. The simplest method to ensure that each estimated symbol sequence at the equalizer outputs represent unique subsets of the transmitted symbol sequence $x(n)$ is to use the same δ parameter for each filter. With this approach, the demultiplexer can recombine the filter outputs using the same order of parsing used in the multiplexer.

The CMA method does not extrapolate to a multiplexed approach quite as easily. The difficulty arises from the indeterminate nature of the delay δ between the source sequence and the estimated sequence at the equalizer output in the classical CMA implementation. This algorithm approximates the sequence $x(n - \delta)$, but δ is not specified explicitly. In the equalizer bank approach proposed here, each equalizer is computed independently and may result in different integer values of δ. If this happens, the parallel equalizers may produce estimates of the same decimation of the original symbol sequence, while other subsequences are not estimated at all. Notionally, it should be possible to force each equalizer to produce a symbol sequence uncorrelated with the output of each other equalizer, but this requires increased complexity. Furthermore, even if the symbol subsequence in each branch is independent, the proper order for recombining the equalizer outputs into a single sequence is not known.

The subspace algorithm first computes a channel estimate which is used to find an equalization filter, so the relative delay δ between the input and output symbol sequences can be controlled explicitly. The robustness of the equalizer with respect to noise, however, is highly dependent on the value of δ, so only a subset of possible delays are reasonable candidates for a particular effective channel impulse response [11]. It is conceivable that the effective channels seen at the equalizer inputs will be similar enough to have a common δ value that is near-optimal for each filter branch, although not guaranteed.

In addition to only minor additional complexity in the receiver architecture, advantages of the LMS bank of equalizers scheme include intrinsic multipath mitigation and modest a-priori knowledge of the delay sequence in the transmitter. The only knowledge of the pseudorandom delay sequence used to create the waveform in the transmitter is the period N_d. Any change in the delay code or the physical channel merely requires the equalization filters to be retrained. Typically, a communications system using LMS equalization will retransmit the training sequence periodically. If

the sequence is sufficiently long for the filters in the receiver to converge, the dither code could be changed in the transmitter every time the training sequence is resent.

A major limitation of this method is slow filter convergence and increased memory requirements to store coefficients for N_d filters. The number of training symbols for convergence is increased by a factor of N_d over a standard transmitter/receiver configuration because each equalizer must be trained independently and only sees one symbol for every N_d symbols transmitted. For long delay codes (with large periods), equalization filter convergence time may be prohibitively large. Similarly, the coefficients for each of the N_d filters must be stored within the receiver, limiting the code period. Certainly, any decrease in the dither code length may facilitate code estimation by a non-cooperative receiver. In addition, a short code uses few samples of the random variable D, and may not be a good representation of the governing distribution. As a result, a particular (short period) code may have unique ISI severity corresponding to widely disparate degrees of LPI protection.

3.2.2 MSE Minimization Using Known Delay Sequence.   If the pulse shape and the delay code sequence of the PDW are known by the receiver, the ISI at the matched filter output due to overlapping symbol shapes can be expressed as a known time-varying impulse response. In a line-of-sight, lossless environment, each sample of the matched filter output can be written in terms of a discrete impulse response that describes the contribution of input symbols to the output sample in question. For a completely known channel, MSE minimization is a common approach for computing a discrete FIR filter to deconvolve the channel effects. Typically, the MSE minimization algorithm assumes a constant channel impulse response and produces a single filter. In the PDW equalization problem, a unique MSE minimization solution must be found for each of the N_d elements in the delay code sequence.

The theoretical foundation of the MSE algorithm presented in [18:287] is similar to the adaptive LMS development discussed in Section 2.4.2. Instead of using stochastic methods to estimate the expected value of the correlation matrices in the

cost function (3.5), however, the matrix coefficients of $\mathbf{R}_y$ and $\mathbf{p}_{xy}$ are known.

$$
\begin{aligned}
J(n) &= \mathrm{E}\left[x^*(n-\delta)x(n-\delta)\right] - 2\mathrm{Re}\left\{\mathrm{E}\left[x(n-\delta)\mathbf{y}^H(n)\right]\mathbf{w}^*\right\} \\
&\quad + \mathbf{w}^T\mathrm{E}\left[\mathbf{y}(n)\mathbf{y}^H(n)\right]\mathbf{w}^* \\
&= \mathrm{E}\left[x^*(n-\delta)x(n-\delta)\right] - 2\mathrm{Re}\left\{\mathbf{p}_{xy}^T\mathbf{w}^*\right\} + \mathbf{w}^T\mathbf{R}_y\mathbf{w}^*
\end{aligned}
\tag{3.5}
$$

By setting the cost function gradient (3.6) to zero, the optimal equalization filter in the mean-square error sense can be found explicitly (3.7).

$$
\nabla_{\mathbf{w}}J(n) = -2\mathbf{p}_{xy}^T + 2\mathbf{w}^T\mathbf{R}_y
\tag{3.6}
$$

$$
\mathbf{w}_{opt} = \left(\mathbf{R}_y^T\right)^{-1}\mathbf{p}_{xy}
\tag{3.7}
$$

In adapting the MSE algorithm for the pseudorandom delay waveform, a fractionally spaced implementation is considered. The vectorized matched filter output $\mathbf{y}(n)$ is a columnwise stack of the sampled subchannels at the matched filter output (see (2.17) and (2.22) in Section 2.3.2). Similarly, the subchannel equalization filters are stacked in a column:

$$
\mathbf{w}(n) = \begin{bmatrix} \mathbf{w}^{(O)}(n) \\ \vdots \\ \mathbf{w}^{(1)}(n) \end{bmatrix}.
\tag{3.8}
$$

In traditional MSE, the effective channel impulse response is static and the source sequence $x(n)$ is uncorrelated, so the received sequence within each subchannel $y^{(i)}(n)$ is stationary and the autocorrelation $E\left[y^{(i)}(n_1)y^{(i)*}(n_2)\right]$ is dependent only on the difference $\delta = n_2 - n_1$ and reduces to $E\left[y^{(i)}(n)y^{(i)*}(n-\delta)\right]$. In the pseudorandom delay waveform, ISI due to pulse shape dither creates N_d different effective channels. To signify this, let $\mathbf{H}_N(n)$ denote the convolution matrix that maps the transmitted symbols in vector $\mathbf{x}(n)$ to the output sample vector $\mathbf{y}(n)$. Note that the convolution matrix must now be indexed by n to account for the potentially unique delay applied to each symbol. The autocorrelation matrix, then, is also dependent on n according

to

$$\begin{aligned}
\mathbf{R}_y(n) &= E\left[\mathbf{y}(n)\mathbf{y}^H(n)\right] \ , \\
&= E\left[\left(\mathbf{H}_N(n)\mathbf{x}(n) + \mathbf{b}(n)\right)\left(\mathbf{H}_N(n)\mathbf{x}(n) + \mathbf{b}(n)\right)^H\right] \ , \\
&= E\left[\mathbf{H}_N(n)\mathbf{x}(n)\mathbf{x}^H(n)\mathbf{H}_N^H(n)\right] + E\left[\mathbf{b}(n)\mathbf{b}^H(n)\right] \ , \\
&= \mathbf{H}_N(n)\mathbf{R}_x\mathbf{H}_N^H(n) + \mathbf{R}_b \ .
\end{aligned} \tag{3.9}$$

In a similar manner, the cross-correlation vector $\mathbf{p}_{xy}(n)$ is dependent on the symbol index n:

$$\begin{aligned}
\mathbf{p}_{xy}(n) &= E\left[\mathbf{y}^*(n)x(n-\delta)\right] \ , \\
&= E\left[\left(\mathbf{H}_N(n)\mathbf{x}(n) + \mathbf{b}(n)\right)^* x(n-\delta)\right] \ , \\
&= \mathbf{H}_N^*(n)E\left[\mathbf{x}^*(n)x(n-\delta)\right] \ .
\end{aligned} \tag{3.10}$$

Finally, the MSE optimal filter is now indexed by symbol as well:

$$\mathbf{w}_{opt}(n) = \left(\mathbf{R}_y^T(n)\right)^{-1}\mathbf{p}_{xy}(n) \ . \tag{3.11}$$

The remaining task is to find the parameters that define $\mathbf{R}_y(n)$ and $\mathbf{p}_{xy}(n)$. Specifically, $\mathbf{H}_N(n)$, $\mathbf{R}_x$, $\mathbf{R}_b$, and $E\left[\mathbf{x}^*(n)x(n-\delta)\right]$ must all be assigned numeric values.

If the source sequence $x(n)$ is zero-mean iid, then $\mathbf{R}_x$ is simply the identity matrix scaled by $E\left[x^*(n)x(n)\right]$ and $E\left[\mathbf{x}^*(n)x(n-\delta)\right]$ has only one non-zero term with value $E\left[x^*(n)x(n)\right]$ at the $(\delta+1)$th element.

The elements within noise autocorrelation matrix $\mathbf{R}_b$ can be expressed analytically in terms of the white Gaussian noise power spectral density in the physical channel N_o and the matched filter $f(t)$. Each element of

$$\mathbf{R}_b = E\left[\mathbf{b}(n)\mathbf{b}^H(n)\right] \tag{3.12}$$

can be expressed as $E\left[b'(k_1)b'^*(k_2)\right]$. Substituting for the definition of $b'(k)$ from (2.7) in Section 2.3.1 gives

$$E\left[b'(k_1)b'^*(k_2)\right] =$$
$$E\left[\int_{-\infty}^{\infty} f^{(ct)}(\tau_1)\,\nu^{(ct)}(T_1 - \tau_1)\,d\tau_1 \int_{-\infty}^{\infty} f^{(ct)*}(\tau_2)\,\nu^{(ct)*}(T_2 - \tau_2)\,d\tau_2\right] , \qquad (3.13)$$

where

$$T_1 = \frac{k_1 T_{sym}}{O} ,$$
$$T_2 = \frac{k_2 T_{sym}}{O} .$$

The whiteness property of the AWGN signal $\nu^{(ct)}(t)$ implies that the autocorrelation is

$$E\left[\nu^{(ct)}(t_1)\nu^{(ct)}(t_2)\right] = \begin{cases} N_o, & t_1 = t_2 \\ 0, & t_1 \neq t_2 . \end{cases} \qquad (3.14)$$

Applying this to (3.13), the two-dimensional integration over area $d\tau_1 d\tau_2$ is only non-zero when $T_1 - \tau_1 = T_2 - \tau_2$. As a result, (3.13) reduces to a line-integral of the form

$$E\left[b'(k_1)b'^*(k_2)\right] = N_o \int_{-\infty}^{\infty} f^{(ct)}(\tau_1)\,f^{(ct)*}(T_2 - T_1 + \tau_1)\,d\tau_1 . \qquad (3.15)$$

The integrand of (3.15) is simply the convolution of pulse shape $f^{(ct)}(t)$ and the matched filter $f^{(ct)*}(-t)$. Thus, the elements of $\mathbf{R}_b$ are samples of the convolution (3.16), scaled by the noise power spectral density N_o (3.17).

$$g^{(ct)}(t) = f^{(ct)}(t) * f^{(ct)*}(-t)$$
$$= \int_{-\infty}^{\infty} f^{(ct)}(\tau)\,f^{(ct)*}(t + \tau)\,d\tau \qquad (3.16)$$

$$E\left[b'(k_1)b'^*(k_2)\right] = N_o g^{(ct)}\left[(n_2 - n_1)T_{sym} + (i_2 - i_1)T_{sym}/O\right] \qquad (3.17)$$

As an alternative to analytically solving for the elements of $\mathbf{R}_b$ as shown above, the filtered noise correlations can be estimated by time-averaging the samples of the matched filter output when the communications waveform is not present, taking advantage of the WSS nature of the filtered noise.

Finally, the convolution matrix $\mathbf{H}_N(n)$ must be found. As mentioned above, $\mathbf{H}_N(n)$ is indexed by symbol n because of the unique timing delay of each symbol. In a convolution matrix, each column represents the sampled lattice of the continuous time effective channel impulse response that models the amplitude scale factor of a particular symbol at future points in time. In the PDW model described in this thesis, the continuous time effective impulse response $h_{eff}^{(ct)}(t)$ is the same for each transmitted symbol. The pseudorandom timing delay of each symbol, however, impacts the synchronization of the sampling lattice relative to $h_{eff}^{(ct)}(t)$ that models the influence of a symbol at each sample of the matched filter output. In other words, each column of $\mathbf{H}_N(n)$ contains the a sampled lattice of the effective channel impulse response, but with potentially differing sampling phases as determined by the delay of each particular symbol. Taking the sampling lattice phase offset due to a symbol's delay $d(n)$, the ith subchannel impulse response defined in (2.14) is now written as

$$\begin{aligned}
\mathbf{h}^{(i)}(n) = [&h_{eff}^{(ct)}\left((i-1)T_{sym}/O - t_0 - d(n)\right),\ h_{eff}^{(ct)}\left((O+i-1)T_{sym}/O - t_0 - d(n)\right), \\
&h_{eff}^{(ct)}\left((2O+i-1)T_{sym}/O - t_0 - d(n)\right),\ ..., \\
&h_{eff}^{(ct)}\left(((L-1)O+i-1)T_{sym}/O - t_0 - d(n)\right)]^T, \\
= [&h_n^{(i)}(0),\ h_n^{(i)}(1),\ h_n^{(i)}(2),\ ...\ h_n^{(i)}(L-1)]^T. \qquad (3.18)
\end{aligned}$$

Consequently, the subchannel convolution matrix for the pseudorandom delay waveform is

$$\mathbf{H}_N^{(i)}(n) =$$

$$
\overbrace{\begin{bmatrix}
h_n^{(i)}(0) & \cdots & h_{n-L+1}^{(i)}(L-1) & 0 & \cdots & \cdots & 0 \\
0 & h_{n-1}^{(i)}(0) & \cdots & h_{n-L}^{(i)}(L-1) & 0 & \cdots & 0 \\
\vdots & & & & & & \vdots \\
0 & \cdots & \cdots & 0 & h_{n-N+1}^{(i)}(0) & \cdots & h_{n-N-L+2}^{(i)}(L-1)
\end{bmatrix}}^{N+L} \Bigg\} N
$$

$$(3.19)$$

and the composite convolution matrix $\mathbf{H}_N(n)$ is constructed by stacking the subchannel convolution matrices column-wise as in (2.22). With these definitions, $\mathbf{w}_{opt}(n)$ can now be calculated from (3.11).

Because the equalization filters are deterministic, this modified MSE cooperative receiver design has no need to estimate signal statistics like the algorithms presented in Chapter II. Instead, the equalization filter taps are computed analytically. For a static physical channel and a particular delay code sequence, N_d filters must be calculated. Thus, the initial computational complexity for a new effective channel $h_{eff}^{(ct)}(t)$ involves computing N_d matrix inverses, which only need to be computed once.

The symbol estimation of the modified MSE receiver is optimal in the mean-squared error sense with respect to the available samples. Because the matched filter output is sampled at a constant rate and samples are not synchronized to the symbol dithers, some symbol energy loss is expected due to non-optimal sampling. Oversampling helps compensate for this suboptimal sampling strategy.

Computation of the effective channel impulse response is not directly addressed in the receiver design. Under line-of-sight conditions, knowledge of the pulse shape (which is assumed to allow the receiver to use a matched filter) and the transmission delay is sufficient. In the case of a multipath physical channel, the channel model must be estimated, possibly via transmission of a known training waveform.
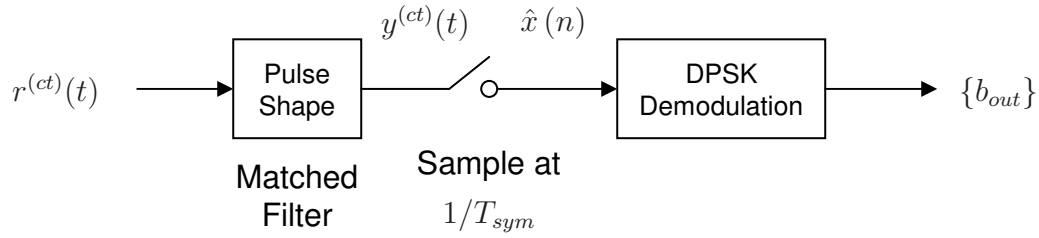
Figure 3.4: Generic structure for the cooperative and non-cooperative receivers described in this chapter.

The calculation of each equalization filter $\mathbf{w}_{opt}(n)$ requires that the cooperative receiver have full knowledge of the pseudorandom symbol delay sequence used in the transmitter. Also, the receiver must be fully synchronous in the sense that the symbol estimate $\hat{x}(n - \delta)$ relies on the application of the corresponding filter $\mathbf{w}_{opt}(n)$.

3.3 Non-cooperative Receivers

Several non-cooperative receiver structures are considered here with respect to their ability to exploit an intercepted PDW. Each notional non-cooperative receiver is assumed to have knowledge of the symbol period, pulse shape, and symbol constellation, but no knowledge of the symbol dither constants $d(n)$. A basic receiver that makes no attempt to account for the symbol timing dither is be considered first. Next, a receiver with blind multipath equalization processing is considered. A third possible non-cooperative receiver strategy involves estimating the symbol delays to sample the matched filter output asynchronously.

3.3.1 Basic Receiver. This section considers the receiver shown in Figure 3.4. Note that the matched filter output is sampled at a rate of $1/T_{sym}$, with constant time T_{sym} between successive samples. No post-processing is performed. The sampling phase is synchronized to the optimum time for a symbol with delay $d(n)$ equal to the mean of the probability density function associated with D.

Assuming a line-of-sight physical channel and a traditionally modulated waveform (with no symbol timing dither), if the matched filter output samples are synchronized to the received waveform, intersymbol interference is not present. For the

PDW in a line-of-sight channel, the ISI is now solely due to pulse shape overlap caused by symbol dither. Thus, any statistically significant deviation from the bit error rate without symbol timing dither can be attributed to the ISI induced by the PDW.

3.3.2 Blind Equalizer Receiver.   Because the structure of multipath interference is similar to the ISI caused by symbol timing dither in the PDW, a non-cooperative receiver using blind equalization techniques is considered here. Equalization to mitigate the ISI within the PDW is attempted using equalizer filters determined by the Constant Modulus Algorithm and the subspace decomposition algorithm. Fractionally-spaced versions of both equalization algorithms are implemented, with the matched filter output in Figure 3.2 sampled at a rate of $2/T_{sym}$. As in the basic receiver architecture described in the previous section, the sampling is synchronized to the mean symbol dither.

Equalization using CMA and subspace decomposition is described in Section 2.4.3 and Section 2.4.5, respectively. Both of these methods rely on the cyclostationarity of the oversampled matched filter output, which is clearly violated by the dynamic ISI within the PDW. However, it is conceivable that the average interference between symbols based on their relative indexes could lead to some benefit from an equalization filter. Any potential BER improvement from such a strategy would depend on the particular pulse shape and the distribution of the delay terms $d(n)$.

3.3.3 Symbol Dither Estimation Receiver.   In the previous two non-cooperative receivers, standard techniques are considered with respect to the PDW. The architecture considered here specifically targets interception of a PDW (in a line-of-sight environment or known physical channel impulse response). Assuming knowledge of the pulse shape, signal power, and the symbol constellation, a symbol can be assigned to each symbol period that best fits the received waveform in a sum (or mean) squared error sense. Within each symbol period, the receiver searches for the symbol and delay pair that minimizes the sum squared difference between the received waveform and the estimated symbols. This is accomplished by creating an estimated waveform

in the receiver via modulation of the estimated symbol sequence and application of the estimated time dither to each symbol.

Symbol and delay estimation proceeds as follows. Using the known effective channel impulse response and signal power at the receiver input, the continuous time signal representing each symbol in the constellation can be created within the receiver. Using complex baseband symbols, let

$$s_i^{(ct)}(t) = s_i h_{eff}^{(ct)}(t) \tag{3.20}$$

be the continuous time shape for complex symbol s_i at the receiver (see (4.2)). The receiver must assume some finite set of $\hat{Q}$ possible symbol dither values for each of N symbols. The initial estimated waveform is $\hat{y}_0^{(ct)}(t) = 0$. Symbols are estimated by taking N iterations of the three steps below.

$$
\begin{aligned}
&(1): z_j^{(ct)}(t,i,q,n) = \hat{y}_{j-1}^{(ct)}(t) + s_i^{(ct)}\left(t - qT_{sym}/\hat{Q} - nT_{sym}\right) \\
&(2): i_j, q_j, n_j = \arg\min_{i,q,n}\left\{\int_{t_0}^{t_0+NT_{sym}}\left[y^{(ct)}(t) - z_j^{(ct)}(t,i,q,n)\right]^2 dt\right\} \\
&(3): \hat{y}_j^{(ct)}(t) = \hat{y}_{j-1}^{(ct)}(t) + s_{i_j}^{(ct)}\left(t - q_jT_{sym}/\hat{Q} - n_jT_{sym}\right)
\end{aligned} \tag{3.21}
$$

In step (1), all valid combinations of symbol and symbol are used to create temporary signal estimates by adding the potential symbols to the previous iteration's estimate. Step (2) selects the symbol i, symbol index n, and symbol dither q set that results in the smallest sum error term. Finally, the new signal estimate is created in step (3).

The ranges of i and q are the same for each iteration. All symbols in the $M-$ary constellation are considered for i and the dither estimate ranges over the set of all possible integer steps: $q \in \left[0...\hat{Q} - 1\right]$. The search range of n begins as the integers from 0 to $N - 1$, inclusive, but shrinks with each iteration. After each iteration, one symbol is estimated and no future iterations can assign a symbol to that symbol period, so n_j is removed from the search range. After N iterations, one symbol has been estimated per each symbol period. Note that this process assumes that

the receiver is able to synchronize to the symbol period boundaries of the received waveform.

The computational complexity of this approach is not trivial. The search space of the first iteration alone requires computing $\left(M\hat{Q}N\right)$ error terms, where N will often be quite large. To be feasible, only a fraction of the received symbols is considered at a time.

Optimization of this symbol estimation technique is beyond the scope of this thesis. The iterative method described here could be replaced by a Viterbi-like technique the considers $\left(M\hat{Q}\right)$ branches at each node. Sparse channel identification techniques may also apply to this problem by considering the series of symbols (modeled as complex impulses in the PDW) as the impulse response of a sparse multipath channel. Symbol estimation is then the equivalent to the sparse channel identification problem, with the additional restrictions that each channel ray must be one of the complex symbols in the communications constellation s_i and only one impulse is allowed in each symbol period. In the sparse channel identification method proposed by [1], estimation of the ray locations is performed prior to estimation of ray magnitude. The ray location estimation is analogous to estimating the symbol dither and could be used in the cooperative receiver MSE approach from Section 3.2.2.

IV. Numerical Simulation Design

In this chapter, a numerical simulation is developed to investigate the LPI signal design from Chapter III. The model includes a transmitter, dispersive noisy channels, and receivers employing several equalization techniques. The simulation calculates the experimental bit error rate for a transmitter, channel, receiver set.

The $\texttt{Matlab}^{\circledR}$ model is described in Section 4.1 and the associated parameters are outlined in Section 4.2. Modeling limitations and assumptions of the simulation are discussed in Section 4.3. The remainder of the chapter validates the components of the model by comparing the model outputs under input conditions for which the result is predictable.

4.1 Model Overview

The end-to-end communications system depicted in Figure 4.1 is modeled by a discrete numerical $\texttt{Matlab}^{\circledR}$ simulation. The transmitter block converts the input bit stream into a baseband waveform representing a series of DPSK symbols. The waveform is a discrete sampling of the analog waveform leaving the transmitter. The channel injects white Gaussian noise and any multipath effects into the system. Finally, the receiver module estimates the transmitted symbols from the received signal (which now includes channel effects) and produces the output bit sequence.

4.1.1 *Transmitter.* The transmitter (Figure 4.2) produces the sampled transmit waveform $u(p)$ from the input bit sequence. The bit sequence is a pseudo-random binary sequence generated by the Marsaglia subtract and borrow algorithm as implemented in $\texttt{Matlab}^{\circledR}$.

$\{b_{in}\} \longrightarrow$ | Transmitter | $\longrightarrow$ | Channel | $\longrightarrow$ | Receiver | $\longrightarrow \{b_{out}\}$
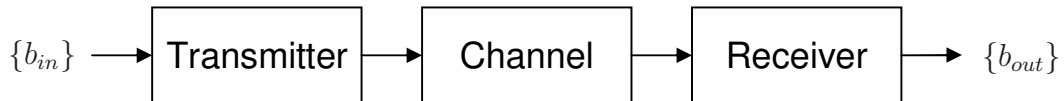
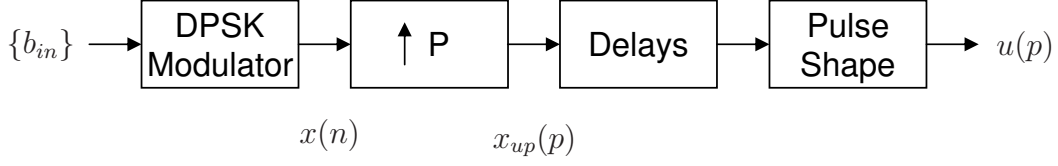Figure 4.1:   Numerical simulation block diagram

Figure 4.2:   Simulated transmitter block diagram

This simulation uses Differential Phase Shift Key (DPSK) modulation to encode the input bit sequence into a series of complex symbols. In this baseband model, the in-phase and quadrature components of the PSK signal are represented by the real and imaginary parts of the symbol, respectively. In the complex symbol space, DPSK constellations are circularly symmetric about the origin, with equal magnitude symbols and constant phase difference between adjacent symbols. In a constellation with M symbols, the input bit stream is segmented into words of length $l = log_2(M)$ bits. Each l-bit word is mapped to a phase offset using Gray coding. Per (4.1), the corresponding symbol is found by adding the phase offset to the phase of the previous symbol in the series [16:195].

$$x(n) = \begin{cases} s_1, & n = 1 \\ \cos\left(\theta_n\right) + j\sin\left(\theta_n\right), & n > 1 \end{cases} \tag{4.1}$$
$$\theta_n = \theta_{n-1} + \Delta\theta_n$$

Figure 4.3 shows a 4-ary DPSK constellation with the associated phase shift mapping in Table 4.1. In this example, the input bit stream 110001 results in the symbol sequence

$$[x(1), x(2), x(3), x(4)] = [s_1, s_3, s_3, s_4] \; , \tag{4.2}$$

where

$$s_i = \cos\left(\theta_i\right) + j\sin\left(\theta_i\right) \; ,$$
$$\theta_i = \frac{\pi}{4} + \frac{(i-1)\pi}{2} \; .$$

4-2
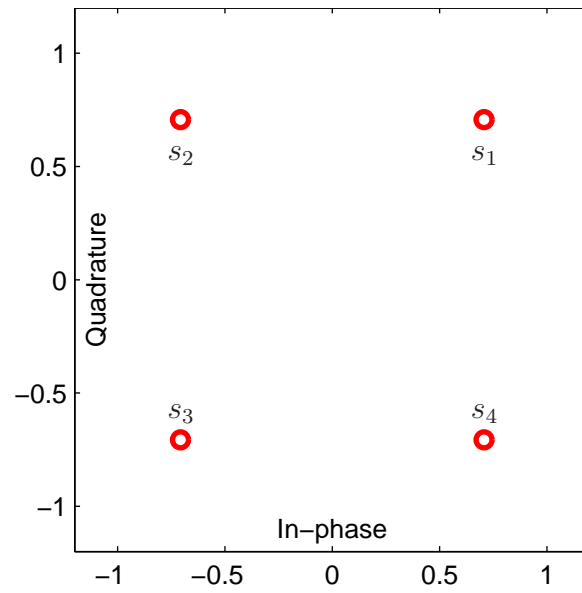
Figure 4.3:   4-ary DPSK Constellation

Table 4.1:   4-ary DPSK Gray code mapping

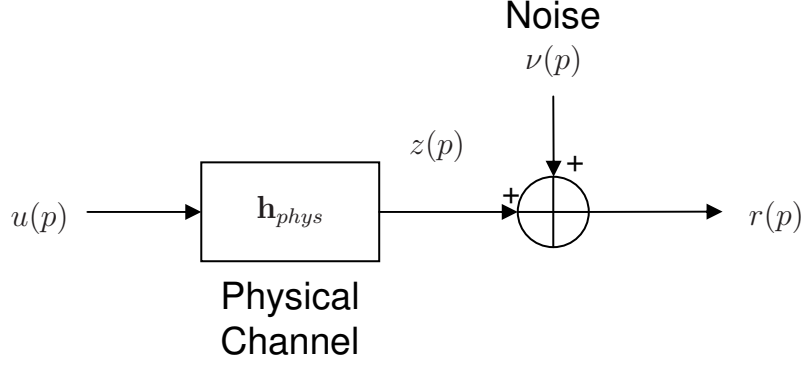| Word	Phase Shift, $\Delta\theta$
00	0
01	$\frac{\pi}{2}$
11	π
10	$\frac{3\pi}{2}$

Figure 4.4:   Simulated channel block diagram

The Upsampling Block increases the sampling frequency by inserting an integer number of zero-valued samples between each symbol. After upsampling, the symbols are now complex impulses spaced P samples apart (so the sampling rate is P/T_{sym} samples per second). Discrete representations of continuous time signals in the numerical simulation are indexed by p.

Symbol timing dither to create ISI is implemented by the Delay Block. The dither is realized by moving each impulse some integer number samples according to the delay code.

Finally, the data signal consisting of complex impulses is convolved with the pulse shape signal $f(p)$ to produce the transmitted waveform.

4.1.2 Channel.   The simulated physical channel is a combination of dispersion ($\mathbf{h}_{phys}$) and AWGN ($\nu(p)$) as seen in Figure 4.4. Dispersion (or multipath) effects are included by convolving the transmitted waveform with the impulse response of the physical channel. All physical channel models in the simulation are static. Because this is a baseband simulation, the phase distortion that could be caused by multipath carrier signal interference is not directly included in this model. To indirectly include phase distortion, the coefficients of the physical channel impulse response are allowed to be complex.

4-4

r(p) → | Pulse Shape | → | ↓ (2/P) | → | Post-processing | → | DPSK Demod | → {b_{out}}
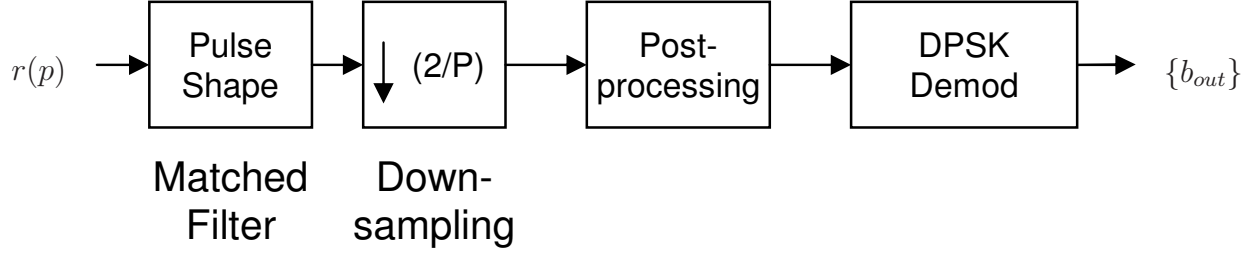
Matched Filter   Down-sampling

Figure 4.5:   Simulated receiver block diagram

After applying the multipath effects, AWGN is added to the signal. The discrete noise samples are complex, with both the real and imaginary parts of each noise samples following an independent Gaussian distribution. The Marsaglia ziggurat algorithm in Matlab® is used to produce pseudorandom Gaussian samples. The variance of both the real and imaginary Gaussian distributions is scaled to achieve a desired SNR at the channel output (equivalent to the input of the receiver).

4.1.3 Receiver.   The simulated receiver model performs matched filtering, downsampling, post-processing, and demodulation (Figure 4.5). The matched filter convolves the received signal with the same pulse shape used in the transmitter. Downsampling of the filtered signal to a sampling period of $T_{sym}/2$ results in two samples per symbol period. Although the simulation is expandable to downsample at higher rates, fractionally spaced equalization algorithms are restricted to two sub-channels in this thesis. Receiver models using symbol spaced data use only the first subchannel $y^{(1)}(n)$. Note that for symbol spaced receiver structures, downsampling synchronization significantly impacts the SNR at the downsampler output. This simulation synchronizes the first subchannel to the point where the impulse response of the effective channel (including the effects of the pulse shape, physical channel, and matched filtering) has maximum magnitude. This strategy maximizes the SNR for the standard transmitter (no pseudorandom symbol delay) under line-of-sight conditions. When the pseudorandom dither transmitter is used, the first subchannel synchronizes to the average location of the maximum effective channel impulse response within the symbol period.

Both continuously adaptive and periodically adaptive equalization algorithms are modeled in this thesis. To directly compare the bit error rates of continuously and periodically adaptive methods, the equalizer coefficients are held constant during data collection. The coefficients are determined by training the equalizer prior to each experiment using an independent series of bits.

The DPSK demodulator uses the phase difference between the current complex estimated symbol and the previous estimated symbol to map to a bit string. Because the bit estimation is based only on the phase difference between successive symbols, this DPSK demodulation technique is not affected by rotation of the constellation caused by phase ambiguity. Sklar calls this differentially coherent detection of differentially encoded PSK modulation [16:218]. For binary DPSK, the probability of bit error is

$$P_b = \frac{1}{2} e^{\frac{-E_b}{N_o}} , \tag{4.3}$$

where E_b is the information signal average energy per bit and N_o is the noise power spectral density. E_b is derived from the average energy per symbol E_s and the number of symbols in the constellation M:

$$E_b = \frac{E_s}{\log_2(M)}. \tag{4.4}$$

Because DPSK demodulation considers both the current symbol and the previous symbol, E_s includes the energy of both.

For differentially coherent detection of M-ary DPSK, the approximate probability of symbol error is [16:230]

$$P_E(M) \approx 2Q \left(\sqrt{\frac{2E_s}{N_o}} \sin \frac{\pi}{\sqrt{2M}} \right) . \tag{4.5}$$

This approximation is valid only for large E_s/N_o ratios. The large E_s/N_o approximation leads to the assumption that most symbol errors result in misidentification as an adjacent symbol, producing only one bit error per symbol error due to Gray coding.

In this manner, the probability of bit error for M-ary DPSK is estimated by [16:230]

$$P_b(M) \approx \frac{P_E(M)}{\log_2(M)} \; . \tag{4.6}$$

The simulation produces an output bit sequence that is a truncated estimate of the input bit sequence. This truncation is due to the convolution operation used to apply the effective channel and the equalization filter. The linear convolution output is restricted to the terms for which both signals in the convolution overlap completely. In this manner, the convolution of signals with M and N samples produces a signal with $|N - M| + 1$ samples. The net effect is an estimated symbol series $\hat{x}(n)$ that is shorter than the transmitted symbol sequence $x(n)$. All observed bit error rates in the simulation only consider the bits estimated at the output of the receiver, ignoring the leading and trailing truncated bits.

4.2 Model Parameters

Many transmitter, channel, and receiver parameters are variable in the simulation. The large number of parameters creates a need to be explicit when describing a particular simulation result. This section discusses the implementation of each module (transmitter, channel, and receiver) and defines the relevant parameters. The simulation parameters are summarized in Table 4.2.

4.2.1 Global Parameters.   In numerical modeling, all analog signals are approximated by discrete signals. The fidelity of the discrete approximation in this simulation is determined by the number of samples per symbol period, P. All experiments presented herein used 64 samples per symbol period unless otherwise noted.

4.2.2 Transmitter.   Within the Transmitter module, the signal constellation, pulse shape, and symbol delay parameters must be defined. For the purposes of this simulation, the signal constellation and pulse shape are always assumed to be known by the receiver.

Table 4.2:   Simulation parameters

P	Number of samples per symbol period used to model analog signals
M	Number of symbols in the DPSK constellation
Pulse Shape	Pulse shape in the transmitter and the corresponding matched filter in the receiver
$\mathbf{d}$	Delay code sequence used to determine the number of samples to delay each symbol in the transmitter
p_{max}	Maximum allowable delay in the sequence $\mathbf{d}$
$\mathbf{h}_{phys}$	Physical channel model
SNR	Signal-to-noise ratio as measured the receiver input
Equalization Parameters	Equalization algorithm and associated parameters
O	Number of samples per symbol period after receiver downsampling (Equivalent to the number of subchannels in the multiple output model)

Table 4.3:   DPSK Gray code mapping

Binary		4-ary		8-ary	
Word	Phase Shift, $\Delta\theta$	Word	Phase Shift, $\Delta\theta$	Word	Phase Shift, $\Delta\theta$
0	0	00	0	000	0
1	π	01	$\frac{\pi}{2}$	001	$\frac{\pi}{4}$
		10	$\frac{3\pi}{2}$	010	$\frac{3\pi}{4}$
		11	π	011	$\frac{\pi}{2}$
				100	$\frac{7\pi}{4}$
				101	$\frac{3\pi}{2}$
				110	π
				111	$\frac{5\pi}{4}$

Binary, 4-ary, and 8-ary DPSK Gray coded constellations are supported by the simulation (Figure 4.6). Each constellation is circularly symmetric with equal-magnitude symbols, satisfying the *apriori* assumptions of all the equalization techniques discussed in Chapter II. Table 4.3 gives the Gray code phase shift assignments for each DPSK constellation.

The pulse shapes modeled are impulse, square, and square root raised cosine (SRRC), plotted in Figure 4.7. The impulse pulse shape is a single discrete impulse with unity magnitude. The square pulse shape is a rectangular function with width equal to the symbol period T_{sym}. To conserve energy through the Pulse Shape block in the transmitter, the amplitude of the square pulse shape is $1/T_{sym}$.

For the SRRC pulse shape, the roll-off factor β determines the "spread" of the shape according to (4.7) [6:225]. Because the SRRC is unbounded in time, the pulse must be truncated in any physical system. When the SRRC is used in this simulation, the default pulse window is ten symbol periods wide, centered at $t = 0$ in the SRRC
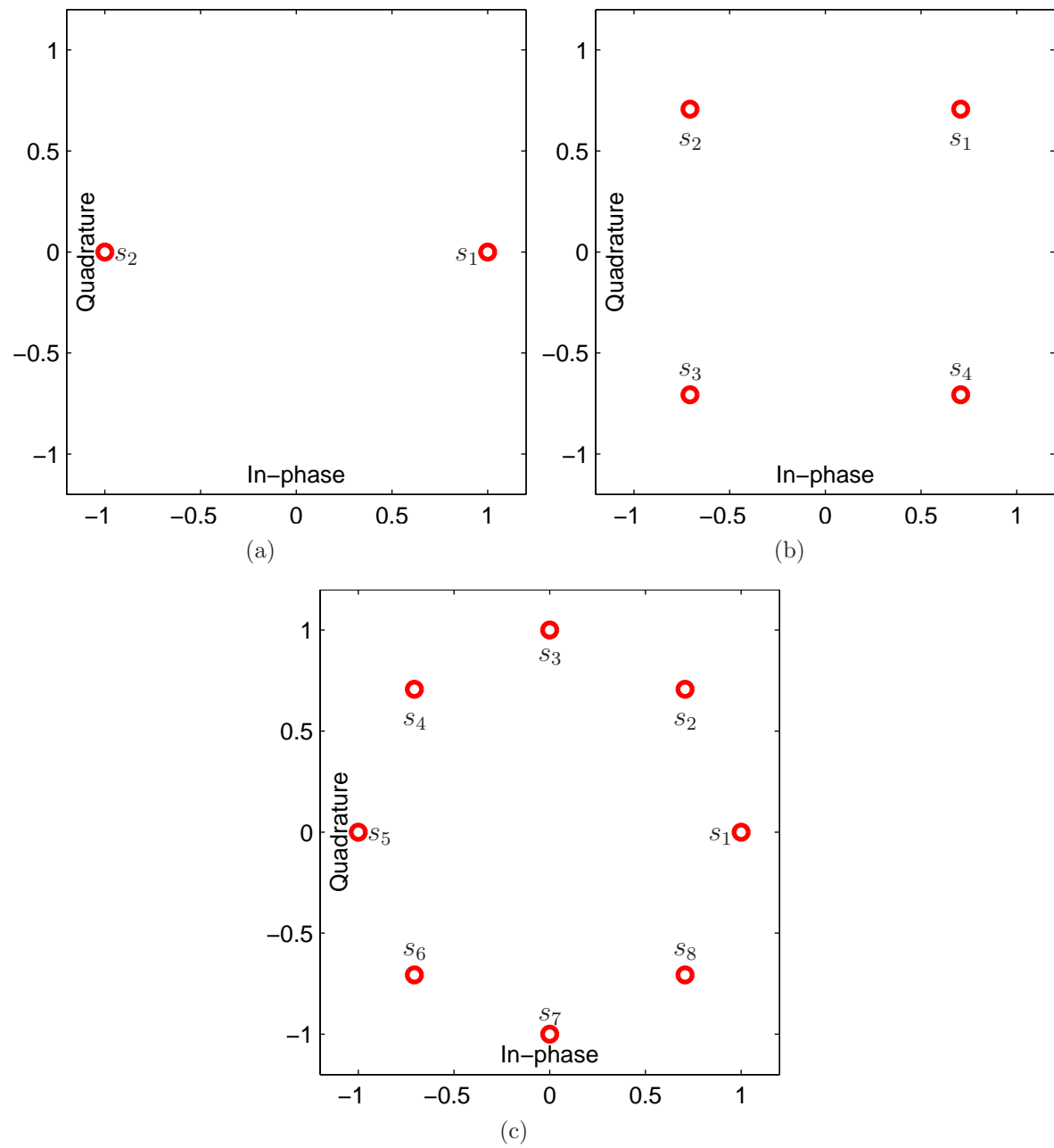
Figure 4.6: (a) Binary DPSK Constellation (b) 4-ary DPSK Constellation (c) 8-ary DPSK Constellation

pulse shape equation:

$$f(t) = \begin{cases} \frac{1}{\sqrt{T_{sym}}} \frac{\sin[\pi(1-\beta)t/T_{sym}]+(4\beta t/T_{sym})\cos[\pi(1+\beta)t/T_{sym}]}{(\pi t/T_{sym})\left[1-(4\beta t/T_{sym})^2\right]}, & t \neq 0, t \neq \pm\frac{T_{sym}}{4\beta} \\ \frac{1}{\sqrt{T_{sym}}}\left[1-\beta+(4\beta/\pi)\right], & t = 0 \\ \frac{\beta}{\sqrt{2T_{sym}}}\left[\left(1+\frac{2}{\pi}\right)\sin\left(\frac{\pi}{4\beta}\right)+\left(1-\frac{2}{\pi}\right)\cos\left(\frac{\pi}{4\beta}\right)\right], & t = \pm\frac{T_{sym}}{4\beta} \end{cases} \quad (4.7)$$

To implement the symbol timing dither, the Delay Block delays each symbol impulse up to $P-1$ samples. The delay code $\mathbf{d}$ is a pseudorandom series of integers that defines the particular delay of each symbol (4.8). Being a finite pseudorandom series, the pattern of delays repeats every N_d symbols, where N_d is the length of the delay code. The maximum allowable delay must be set to less than $P-1$ samples to prevent adjacent symbols from being transmitted in the wrong order (4.9). The distribution of integer delays in the random delay sequence is always uniform in this simulation. To model a standard transmitter, the maximum allowable delay is simply restricted to zero samples.

$$\mathbf{d} \triangleq \{d(1), d(2), ..., d(N_d)\} \quad (4.8)$$

$$d(n) \in \mathbb{I}[0, p_{max}], \, 0 \leqslant p_{max} \leqslant P-1 \quad (4.9)$$

4.2.3   Channel.   The simulated physical channel is a combination of dispersion and AWGN. The dispersion is applied via convolution with the physical channel impulse response per Section 4.1. Although any discretized impulse response can be inserted into the simulation, this thesis characterizes receiver performance using a line-of-sight, lossless channel with a delay of ten samples.

AWGN is added to the signal after applying the physical channel impulse response. The variance of the noise samples can be specified either by SNR or E_b/N_o at the receiver input. The actual simulated SNR is then estimated by taking the ratio
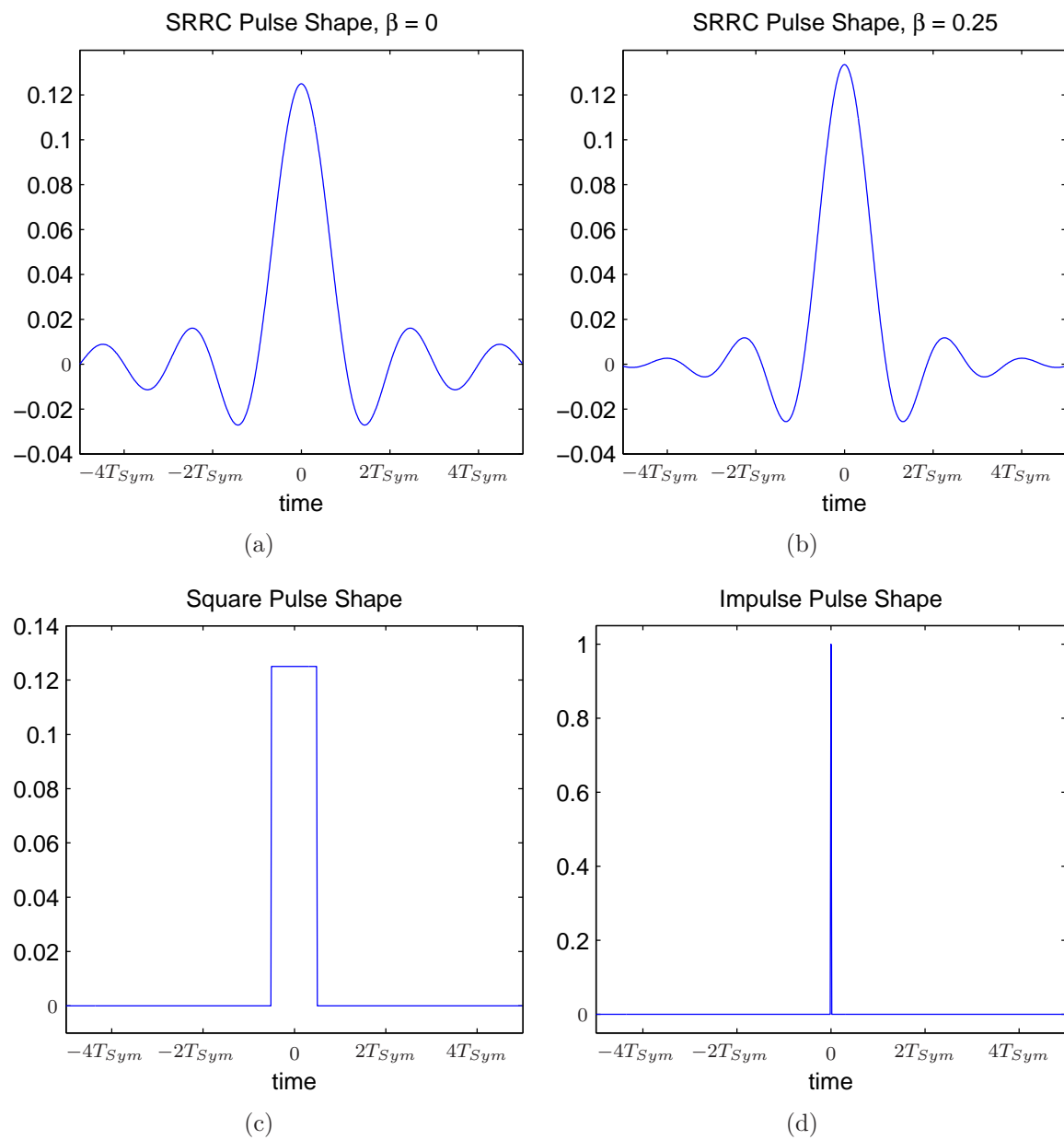
Figure 4.7: (a) SRRC pulse shape, $\beta = 0$ (b) SRRC pulse shape, $\beta = 0.25$ (c) Square pulse shape (d) Impulse pulse shape

of mean squares of the information signal $z(p)$ and noise signal $\nu(p)$ according to

$$SNR \approx \frac{\sum |z(p)|^2}{\sum |\nu(p)|^2} \ . \tag{4.10}$$

In the line-of-sight case with no multipath effects and no symbol dither, the inter-symbol interference is negligible (at least for the pulse shapes used in this thesis), so the signal power in the SNR calculation can be estimated directly from the simulation just prior to adding the noise in Figure 4.4. When ISI is present in the signal, some clarification is necessary. For the purposes of this document, the signal power is still measured directly from the simulated signal prior to adding noise (after applying multipath effects) and noise power is still measured from the AWGN signal $\nu(p)$. In practice, however, the ISI due to multipath, symbol dither, and/or non-ideal pulse shapes can be treated as an additional noise source. The contribution of ISI to bit errors is dependent on the quality of equalization, with perfect equalization eliminating ISI completely. Hence, all SNR calculations in this thesis do not consider ISI as a source of noise power unless explicitly stated.

4.2.4 Receiver. The receiver parameters are different for each receiver structure modeled in the simulation. Table 4.4 lists the algorithms and parameters associated with each. The optimal set of parameters for each receiver model is highly dependent on the transmitter and channel parameters. Optimization of a receiver parameter set is not trivial due to the number of permutations of parameter combinations. In lieu of exhausting all possible receiver configurations, the parameters for each experiment are chosen by making reasonable assumptions about the receivers knowledge of the transmitter and the channel.

For algorithms using statistical averaging, N is the number of symbols output by the transmitter for the purpose of estimating the equalization filter(s). The actual number of symbols available to the algorithm in the receiver is somewhat less than N due to truncation of the leading and trailing samples. This truncation omits the received samples that reflect initiation and termination transients. For most results

Table 4.4:   Equalization algorithm parameters

Basic	N/A	No parameters necessary
FS CMA	μ	Gradient descent step size
	M	Number of taps in the equalizer (equalizer length)
	N	Number of symbols used to train the equalizer
Subspace	$\hat{L}$	Estimate of the length of the effective channel (in symbol periods)
	M	Number of taps in the equalizer (equalizer length)
	N	Number of symbols used to train the equalizer
FS LMS Bank	μ	Gradient descent step size
	M	Number of taps in the equalizer (equalizer length)
	δ	Impulse response delay to which the equalizer converges (in symbol periods)
	N	Number of symbols available for equalizer estimation
Modified MSE	δ	Impulse response delay to which the equalizer converges (in symbol periods)
	$\hat{L}$	Estimate of the length of the effective channel (in symbol periods)

presented in this thesis, $N = 5,000$ symbols which is be large enough for algorithms based on higher-order statistics to reach steady-state. This is required to reflect the "best case" bit error performance. It should be acknowledged that this approach renders the superior convergence speed of the subspace decomposition algorithm a moot point in this simulation.

The gradient descent algorithms, fractionally spaced CMA and the bank of fractionally spaced LMS equalizers, require an iteration step size μ. The magnitude of the step size must strike a balance between maximizing convergence speed and minimizing steady-state error (see Section 2.4.2). For this simulation, μ has been tuned for each set of transmitter/channel parameters using emperical simulation.

The number of taps in the equalization filter, M, must be defined for the trained algorithms. For the FS CMA and FS LMS bank receivers, the number of taps is chosen to satisfy the minimum length condition in (2.30) for (potentially) perfect equalization, (see Section 2.4.3). The maximum effective channel length is $L = 20$ symbol periods, so $M = 40$ unless otherwise noted for these two receivers.

The subspace decomposition algorithm equalization solution is unstable when the effective channel length estimate $\hat{L}$ and equalizer length M are overestimated. To prevent the potential noise amplification that occurs when this happens, these two parameters are tuned empirically by observing the output bit error rate for a range of parameter sets for each transmitter/channel configuration.

For the FS LMS bank and modified MSE algorithms, the δ parameter establishes the difference between the indexing of the input bit stream and the estimated output bit stream. For an unknown channel, δ is often determined by minimizing bit error rate over a range of δ values. In simulation, pulse shape duration, physical channel impulse response, and the matched filter are known and combined to calculate the effective channel impulse response length L. With this information, each matched

filter sample $y^{(i)}(n)$ is known to be a function of the previous L symbols according to

$$y^{(i)}(n) = F\left[x(n - L + 1), x(n - L + 2), ..., x(n)\right] . \quad (4.11)$$

In a similar manner, the estimated symbol $\hat{x}(n)$ is a function of previous M/O matched filter samples in each subchannel $y^{(i)}(n)$. Combining the effective channel impulse response length and number of equalization filter taps allows an estimated symbol to be a function of a specific set of transmitted symbols:

$$\hat{x}(n) = F\left[x\left(n - \frac{M}{O} - L + 2\right), x\left(n - \frac{M}{O} - L + 1\right), ..., x(n)\right] . \quad (4.12)$$

Combining (4.11) and (4.12) provides the natural bounds on δ:

$$\delta_{opt} \in \left\{0, 1, ..., L + \frac{M}{O} - 2\right\} . \quad (4.13)$$

This thesis studies line-of-sight channels with a known transmission delay. For an ideal line-of-sight channel, the effective channel impulse response is the convolution of the pulse shape and the matched filter with some delay, which is symmetric about the impulse response maximum. In the particular line-of-sight channel used in this thesis, the transmission delay is ten samples, or 17% of a symbol period, so a good estimate for δ_{opt} is

$$\delta_{opt} \approx \frac{1}{2}\left(L + \frac{M}{O} - 2\right) \quad (4.14)$$

Unless otherwise stated, this is the value of δ used in this thesis.

For the modified MSE receiver, the number of equalizer filter taps M is a function of the estimated channel length $\hat{L}$ according to

$$M = O\hat{L} \quad (4.15)$$

For the line-of-sight channel used in this thesis, the actual channel length L is used as the estimated channel length parameter for the modified MSE receiver.

4.3 Assumptions

The simulation described in this chapter makes several assumptions and simplifications in the communications system model. These limitations are detailed below.

By using a baseband simulation, the effects of carrier waveform phase interference between multipath reflections is not captured explicitly in the multipath model. Instead, the potential phase interference effects of the carrier waveform are accounted for by the baseband multipath channel coefficients in the simulation. These coefficients are allowed to be complex to model the impact of the reflection on the phase of the carrier signal.

Doppler effects are not modeled in this baseband simulation. The frequency of the notional carrier waveform is assumed to be equal for each multipath reflection at the receiver input.

The receiver knows the time when the impulse response of the combined channel/pulse shape is at a maximum and synchronizes the primary channel to sample at this point. This synchronization is critical for symbol spaced receivers. Conceivably, a blind detector could estimate this sampling synchronization via energy detection and averaging over many symbols. When the transmitter applies pseudorandom delays to each symbol, the point within each symbol period for which the effective channel impulse response is at a maximum in the receiver is no longer the same for each symbol. In this case, the receiver synchronizes to the average time at which the impulse response is at a maximum. Again, this synchronization is deterministic within the simulation, so the receiver synchronization is assumed to be perfect and stable.

The modified MSE receiver requires knowledge of the additive channel noise power. This simulation uses sample mean and variance of the noise signal to directly determine the noise power. In reality, the noise signal is not available independent from the information signal at the receiver input, so another noise estimation technique would be required. This could be as simple as measuring the power at the receiver input when the transmitter is not present.
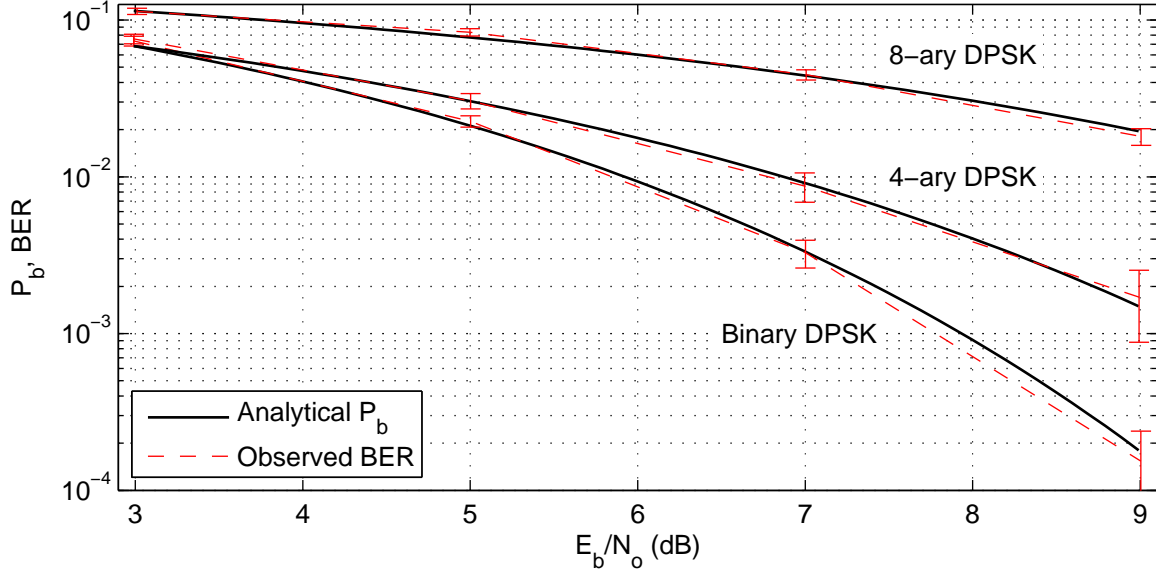
Figure 4.8: Simulated bit error rates for DPSK in a LOS channel compared to the analytical probability of bit error.

4.4 Simulation Verification

This section presents incremental simulation results to validate the simulation components. To demonstrate the modulator and demodulator models, the bit error rates produced via simulation under line-of-sight conditions are compared to theoretical DPSK performance. The effects of multipath models are demonstrated by analyzing the impact on bit error rate and examining the received symbols in the signal space. The equalizers are then inserted into the receiver model to demonstrate their multipath mitigation capabilities.

4.4.1 DPSK Simulation Validation. Figure 4.8 compares the analytical probability of bit error for DPSK constellations in the presence of AWGN to the bit error rates observed in simulation using an ideal line-of-sight physical channel. Over the E_b/N_o range considered here, the difference between analytical bit error probability and the simulated result is not statistically significant. All error bars on plots in this thesis represent 95% confidence intervals produced by Monte Carlo simulation [10:266]. An ideal square pulse shape is used in the transmitter to prevent ISI.
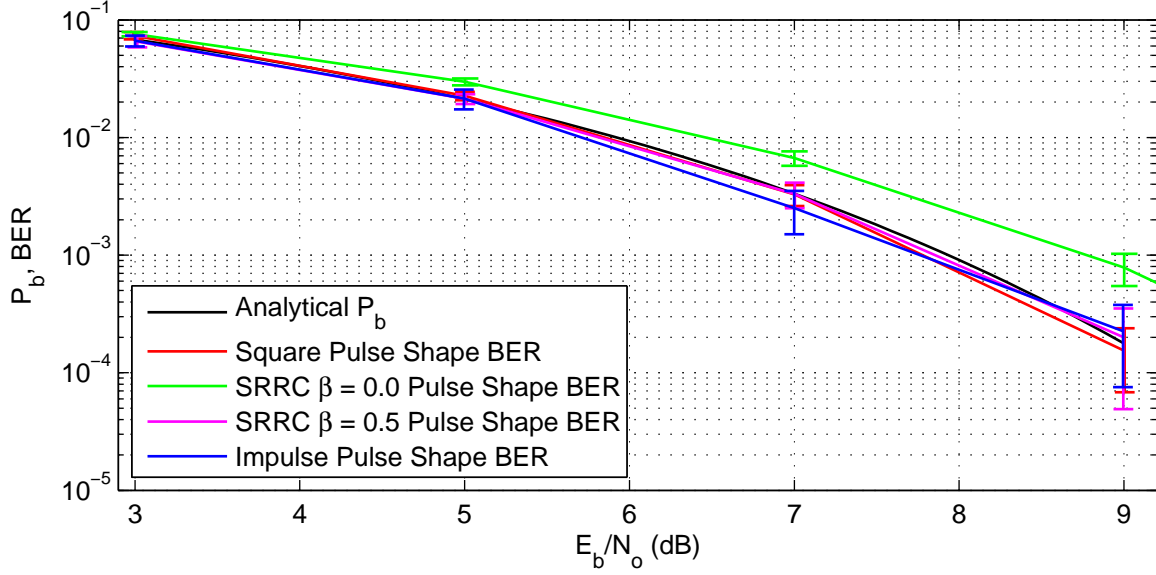
Figure 4.9: Simulated bit error rates for binary DPSK in a LOS channel. The truncated SRRC shape introduces ISI that degrades the receiver performance.

In practice, the SRRC pulse shape is more practical than an ideal square wave because of bandwidth considerations. An infinite length SRRC pulse shape and matched filter pair results in no ISI, like the square wave pulse shape. When the SRRC pulse shape is (necessarily) truncated, typically to a total width of $10T_{sym}$ in this simulation, the symbol-spaced samples at the matched filter output are subject to ISI, degrading the bit error rate. Figure 4.9 demonstrates the effect of ISI due to SRRC windowing. Note that for equal size pulse shape windows, the bit error rate degradation is most severe for small β (wide SRRC shape). Figure 4.10 shows that small β results in large sidelobes in the effective channel impulse response with zero crossings that do not synchronize to the rate $1/P$ downsampling.

4.4.2 Multipath Interference Validation. A simple sparse physical channel model shown in Figure 4.11(a) is used to demonstrate multipath modeling in the simulation. The effect of the channel on the location of received symbols in the signal space of a QPSK modulated waveform (at $E_b/No = 9$ dB measured at the matched filter input) is given in Figure 4.11(b). An SRRC, $\beta = 0.25$ pulse shape and matched filter are in use here. After differentially coherent demodulation, the observed BER is
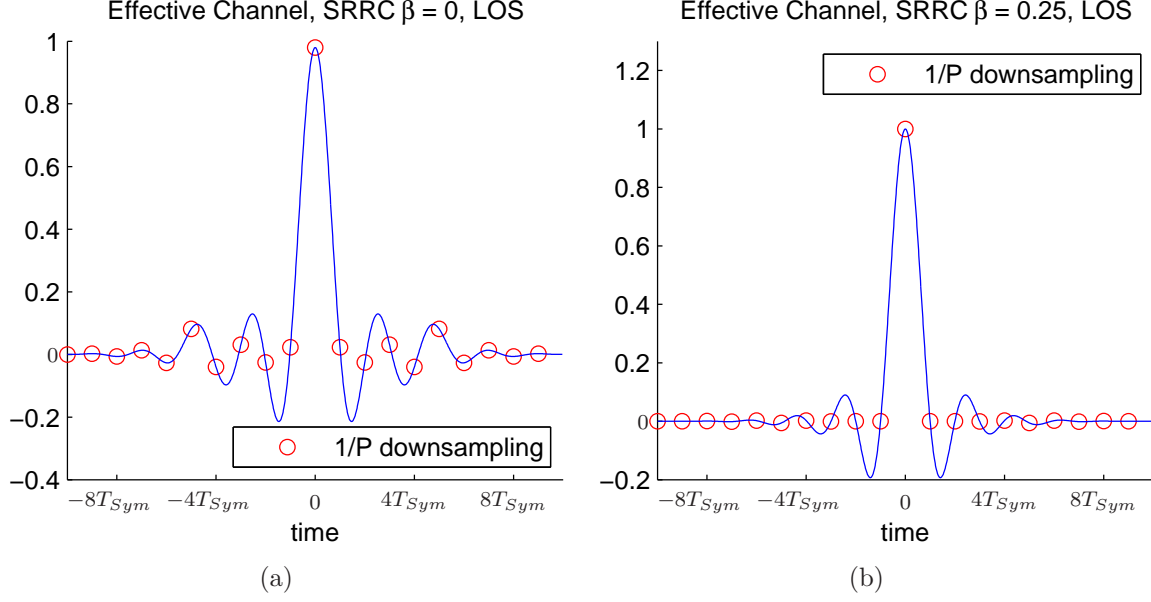
Figure 4.10: Effective channel impulse responses (pulse shape and matched filter). The receiver synchronizes the first symbol spaced subchannel to the impulse response maximum. (a) $\beta = 0$. (b) $\beta = 0.25$

0.24 vice the BER of 0.0088 observed in simulation for the line-of-sight channel at this bit energy to noise ratio. Note that the imaginary component of the physical channel impulse response produces a rotation of the constellation in the symbol space. The BER degradation due to this multipath channel is summarized over a range of E_b/N_o ratios in Figure 4.12. Over this range, the severe ISI caused by the multipath channel dominates the accuracy of the demodulator bit estimation; the 8 dB gain in E_b/N_o only improves the BER from 0.28 to 0.23.

4.4.3 Equalizer Validation. To demonstrate the ISI mitigation capability of fractionally spaced CMA, fractionally spaced LMS, and subspace decomposition, each equalizer is applied transmitter and channel described in the previous section. Each equalizer uses $N = 5,000$ transmitted symbols for training before the equalizer output symbols are demodulated for BER calculations. After demodulating 5,000 symbols, the equalizers are reset and trained again, analogous to periodically adaptive equalization. For fractionally spaced CMA and LMS, the step size μ is selected

4-20
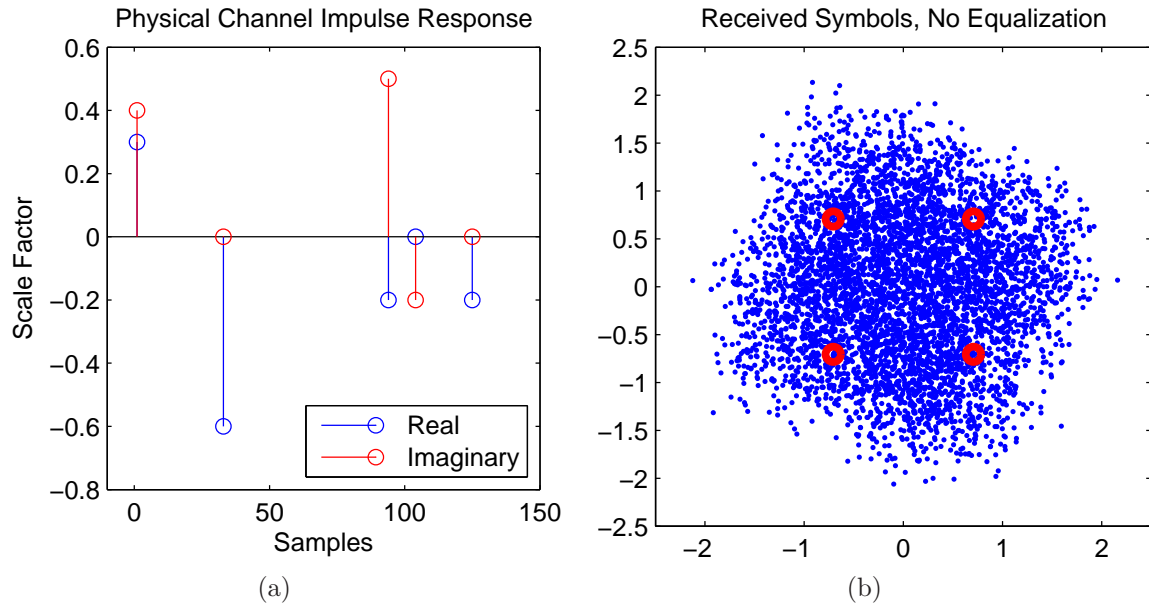
Figure 4.11: (a) Impulse response of a sparse multipath channel. (b) Received samples in the signal space for QPSK modulation using an SRRC $\beta = 0.25$ pulse shape at $E_b/N_o = 9$ db.
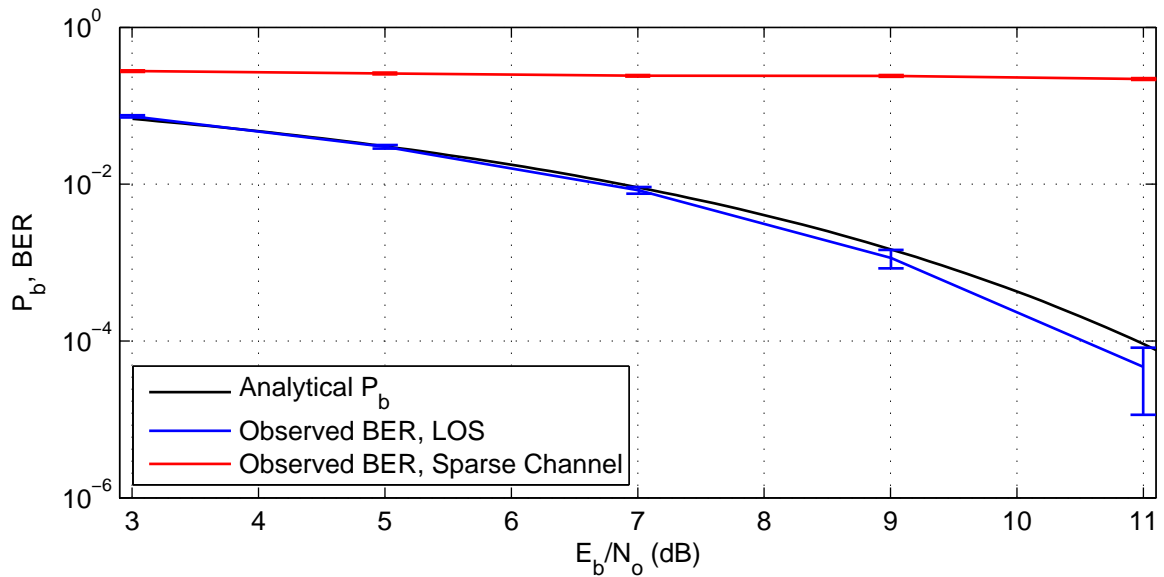
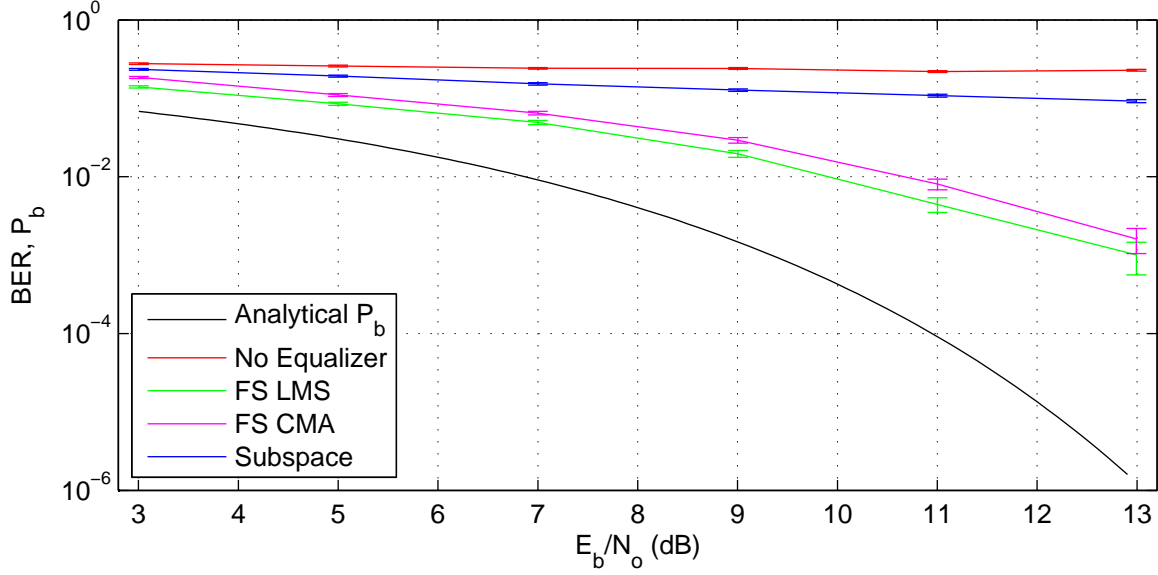Figure 4.12: ISI due to the sparse multipath channel model dominates the observed BER.

Figure 4.13: Applying equalizer filters at the matched filter output improves BER performance for the multipath channel. The 4-ary PSK communications system is using an SRRC, $\beta = 0.25$ pulse shape and matched filtering.

experimentally to produce near-optimal convergence over the E_b/N_o range of interest in the sparse channel environment with the 5,000 symbols transmitted for training. The effective channel length $\hat{L}$ and the number of equalizer filter taps M are also determined empirically.

Figure 4.13 compares the bit accuracies achieved by CMA, LMS, and subspace decomposition equalization algorithms to the BER observed without equalization. CMA and LMS error rates behave similarly across the E_b/N_o range shown here. None of the equalizer outputs approach the analytical probability of bit error achievable in the absence of multipath interference. The subspace method shows only a slight improvement over the unequalized case for this multipath channel.

V. Simulation Results

This chapter presents numerical simulation results demonstrating the LPI characteristics of the pseudorandom dither communications signal described in Chapter III. The performance of both cooperative receivers and non-cooperative receivers are quantified by the observed bit error rate after signal demodulation. Section 5.1 characterizes the behavior of the cooperative receivers (modified MSE and LMS bank). The non-cooperative receiver simulation results are presented in Section 5.2. The cooperative and non-cooperative receivers are compared in Section 5.3 in an attempt to select a set of operating parameters that yields LPI characteristics with little penalty to the cooperative receiver link. Finally, the bandwidth impact of the dither strategy on DPSK modulation is considered in Section 5.4.

5.1 Cooperative Receiver Performance

Results for the modified MSE deconvolution and adaptive LMS equalizer bank receiver structures are presented below. The performance of each cooperative receiver structure is demonstrated using the same set of analyses. First, the bit error rates (BER) oberved for each cooperative receiver using traditional binary, 4-ary, and 8-ary DPSK signalling schemes are presented (using a line-of-sight (LOS), AWGN channel). This result is compared to the analytical probability of bit error (P_b) for each particular signalling scheme to identify any potential BER penalty associated with the receiver structure for standard DPSK modulated signals. Note that standard M-ary DPSK modulation is equivalent to using the PDW with the symbol dither set to zero seconds for each symbol. Next, the BER behavior of each receiver is examined with respect to the pseudorandom dither waveform (PDW) dither range. BER results for varying SRRC pulse shape roll-off factor (β) and symbol dither range are contrasted with the goal of selecting a set of waveform parameters for each cooperative receiver structure that allows for accurate detection of the PDW signal and significant detection degradation in non-cooperative receivers. This set of parameters for the PDW is used to study BER behavior for a range of E_b/N_o.
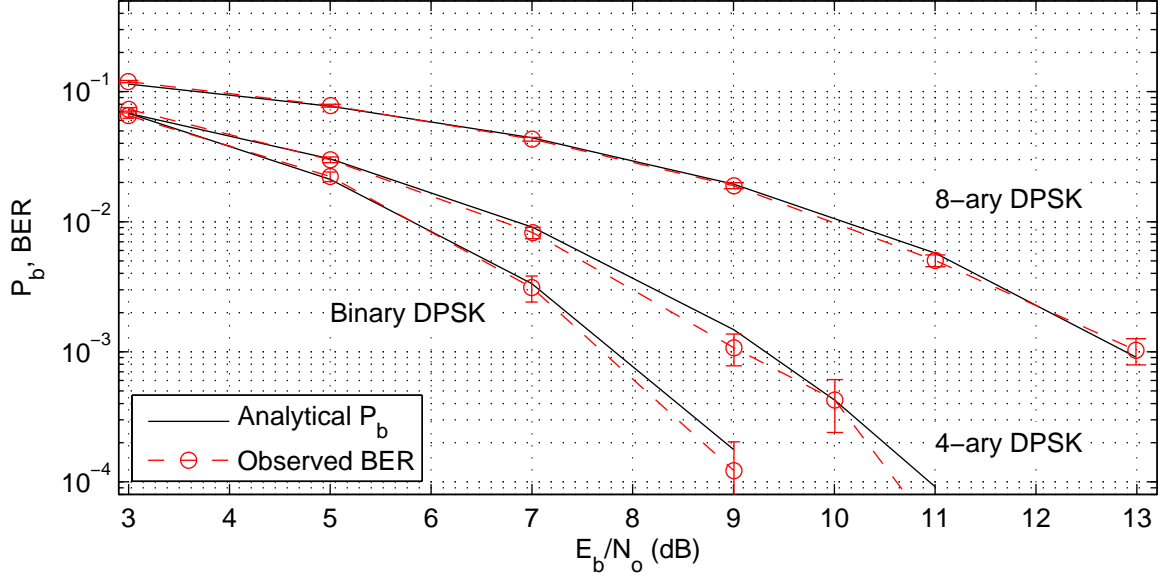
Figure 5.1: The modified MSE cooperative receiver accuracy is statistically similar to the analytical probability of bit error.

5.1.1 Modified MSE Deconvolution. For a LOS channel, the observed BER using the modified MSE deconvolution receiver structure matches the analytical bit error probability predicted by (4.3), (4.5), and (4.6) for input E_b/N_o ratios shown in Figure 5.1. The error bars on the observed BER data points in this plot and all others in this chapter represent 95% confidence intervals produced by Monte Carlo simulation [10:266]. In addition, the complexity of the modified MSE receiver is significantly reduced when the symbol dither is restricted to zero because only a single convolution matrix is required, and the inverse need only be calculated a single time. Thus, equalization using the modified MSE receiver in a LOS, AWGN channel is essentially equivalent to a simple matched-filter receiver without post-processing.

Figure 5.2 shows the modified MSE receiver error rate behavior for varying symbol dither ranges. The results reflect a simulated LOS, AWGN channel and $E_b/N_o = 9$ dB at the receiver input. As the symbol dither range increases to a full symbol period, the severity of the ISI increases, causing the observed BER to degrade. The dither threshold at which the BER diverges from the zero dither level is dependent on the pulse shape. Specifically, the more narrow the pulse shape (corresponding to
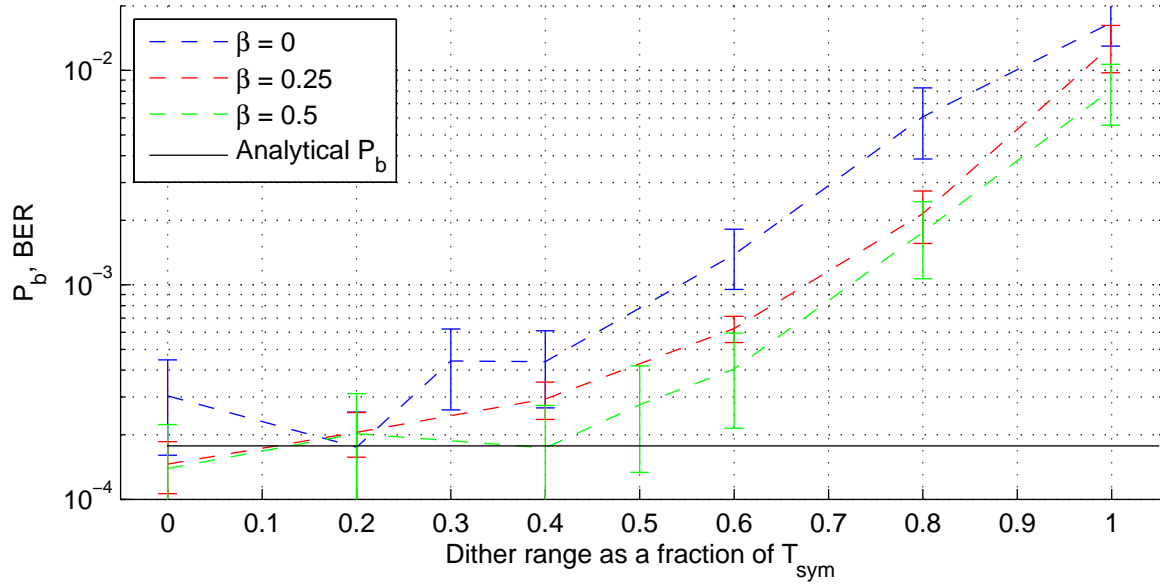
(a)
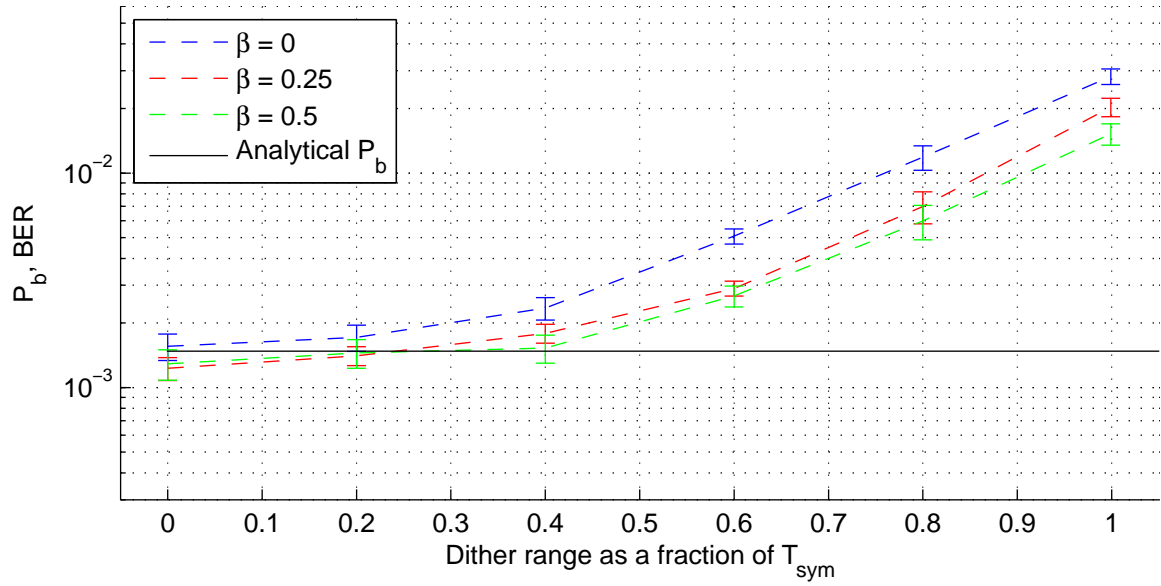
(b)

Figure 5.2: Modified MSE receiver performance as a function of the dither range using a LOS channel at $E_b/N_o = 9$ db. (a) Binary DPSK modulation (b) 4-ary DPSK modulation
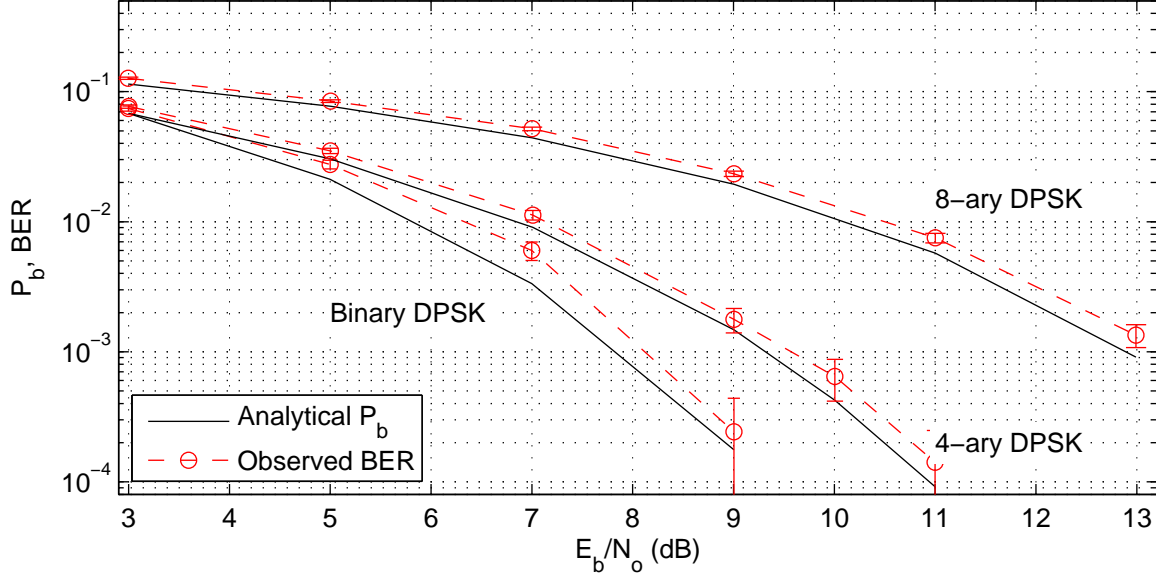
Figure 5.3: Applying the bank of LMS equalizers in a LOS environment increases the BER with respect to the demodulation of the unequalized matched filter output due to misadjustment.

larger β), the larger the dither that can be tolerated before demodulation accuracy is degraded significantly. This directly follows from the lower ISI contribution due to neighboring symbols for narrow pulse shapes.

5.1.2 *Adaptive LMS Equalizer Bank.* Unlike the modified MSE receiver, the LMS bank of equalizers receiver structure produces a BER slightly worse than the analytical probability of bit error for standard DPSK modulation schemes, as seen in Figure 5.3. As discussed in Section 2.4.2, the step size μ and noise prevent the LMS equalizers in the receiver from converging to an exact solution. This effect can be mitigated by adaptively adjusting the LMS filter lengths via channel length estimation and decreasing the step size as the filter converges, which are beyond the scope of this thesis.

The correlation between symbol dither range and observed BER is shown in Figure 5.4. The distinction between the SRRC β parameters is less pronounced than for the modified MSE receiver because misadjustment dominates the minor ISI variation due to SRRC β. As with the modified MSE receiver, ISI due to symbol
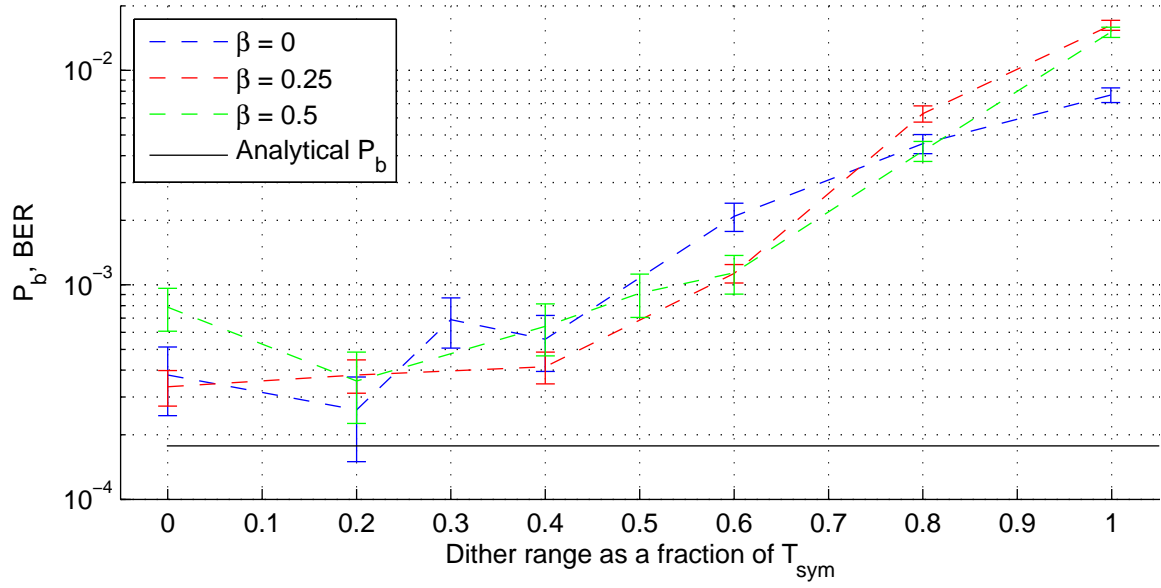
(a)
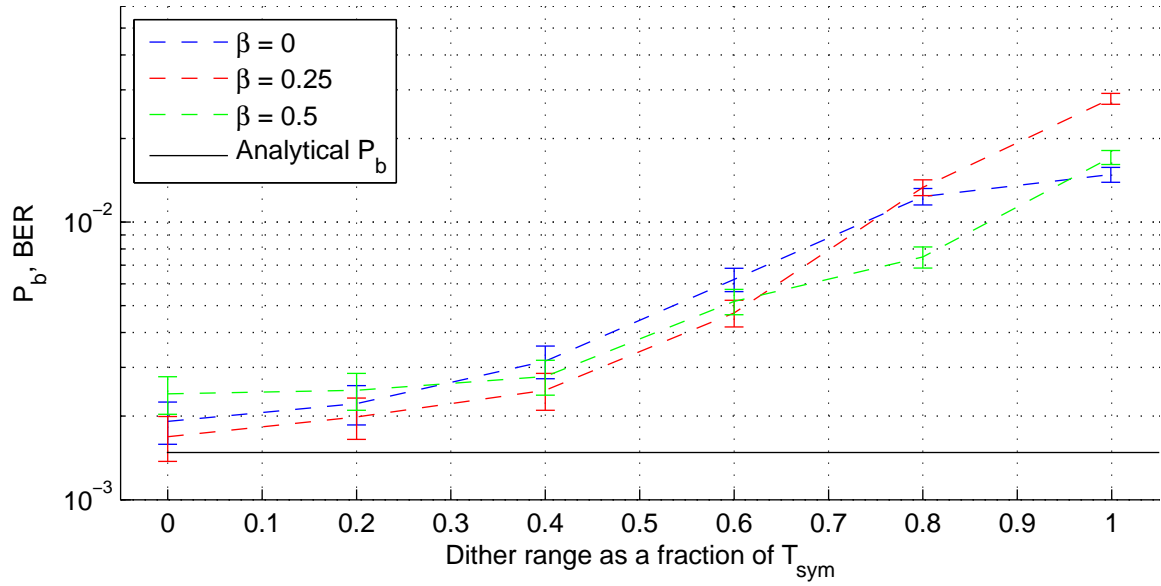
(b)

Figure 5.4: LMS bank receiver performance as a function of the dither range using a LOS channel at $E_b/N_o = 9$ db. (a) Binary DPSK modulation (b) 4-ary DPSK modulation

5-5

dither dominates the BER result as the dither range increases to an entire symbol period.

## 5.2 Non-Cooperative Receiver Performance

This section characterizes the performance of the non-cooperative receivers described in Section 3.3. The observed error rates of each receiver are analyzed in a simulated LOS, AWGN channel.

5.2.1 Basic Receiver.   The basic receiver does not perform any ISI mitigation, simply demodulating the samples of the matched filter output. This architecture produces the observed BER in Figure 5.5. For both binary and 4-ary DPSK modulation, the BER diverges from the the analytical P_b at a uniform dither range of $0.2T_{sym}$. The BER appears to be approaching an upper limit at as dither range increases. Also, the impact of SRRC pulse shape truncation is more pronounced in this receiver structure than in either cooperative receiver, indicating that the two cooperative receivers are mitigating this ISI source as well as the symbol dither ISI.

5.2.2 Blind Equalizer Receiver.   The observed BER for the receiver employing FS-CMA equalization in a LOS environment, shown in Figure 5.6, is not significantly improved relative to the basic receiver error rates in Figure 5.5. In fact, for many parameter combinations, FS-CMA equalization increases the bit error rate due to misadjustment in the FS-CMA steady-state. It should also be noted that the particular sampling synchronization technique employed in this simulation minimizes the benefit of fractionally spaced equalization techniques over the symbol spaced sampling in the basic receiver. Interestingly, the ISI due to SRRC truncation, which is most severe for small β, is not distinctive in the error rates for low dither ranges, another symptom of misadjustment. The same phenomenon can be seen to a lesser degree in the LMS equalizer bank result. In both cases, the $\beta = 0$ error curve is lower than that of the basic receiver, indicating that some equalization of the ISI due to pulse shape truncation is occurring when ISI due to symbol dither is minimal.
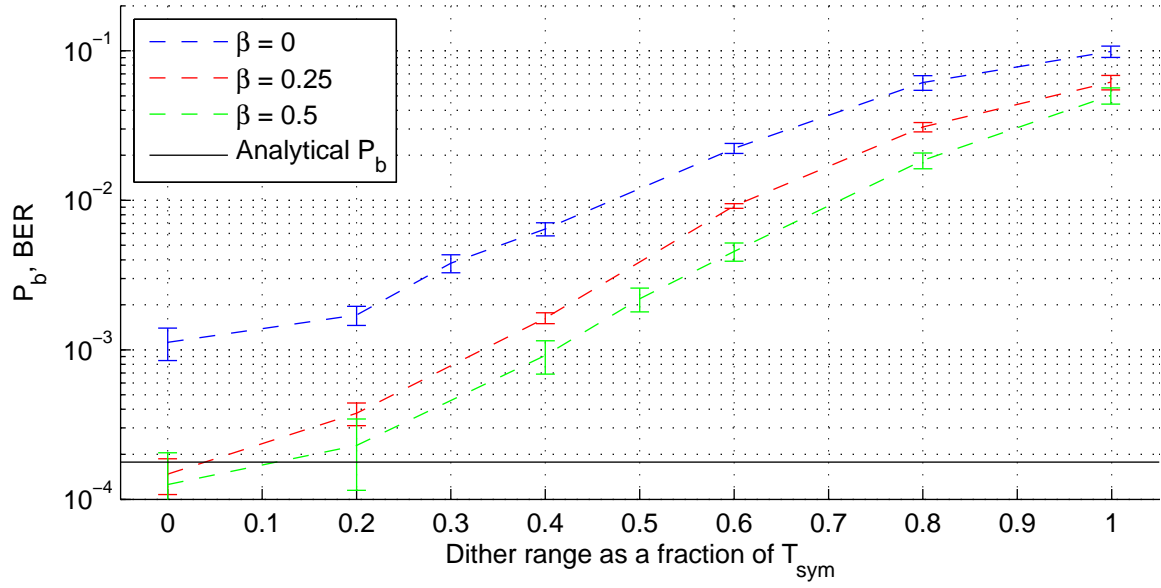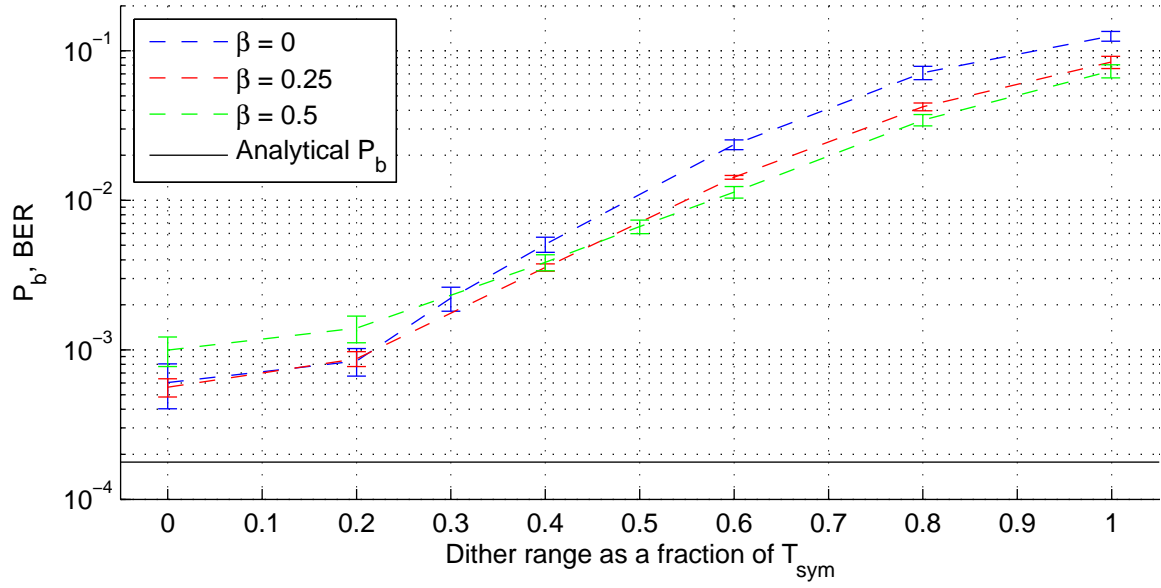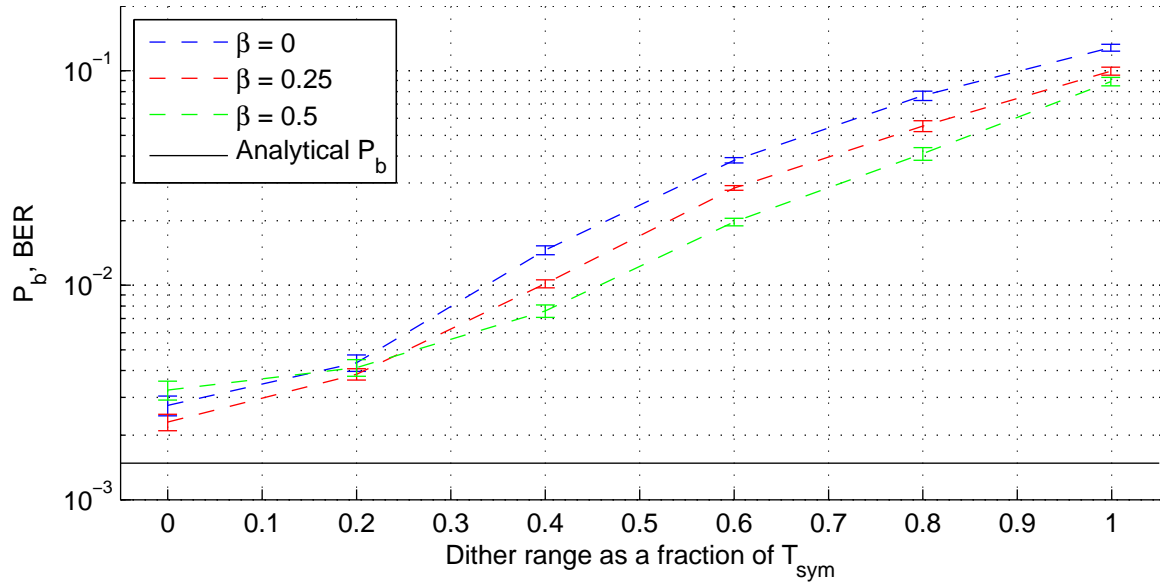
(a)
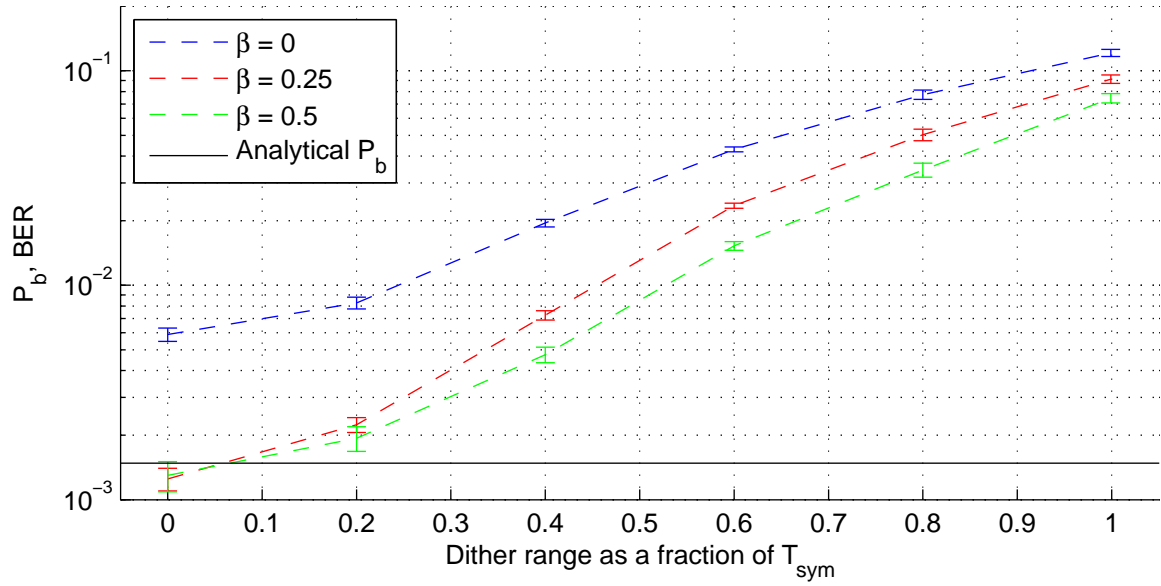
(b)

Figure 5.5: Basic receiver performance as a function of the dither range using a LOS channel at $E_b/N_o = 9$ db. (a) Binary DPSK modulation (b) 4-ary DPSK modulation
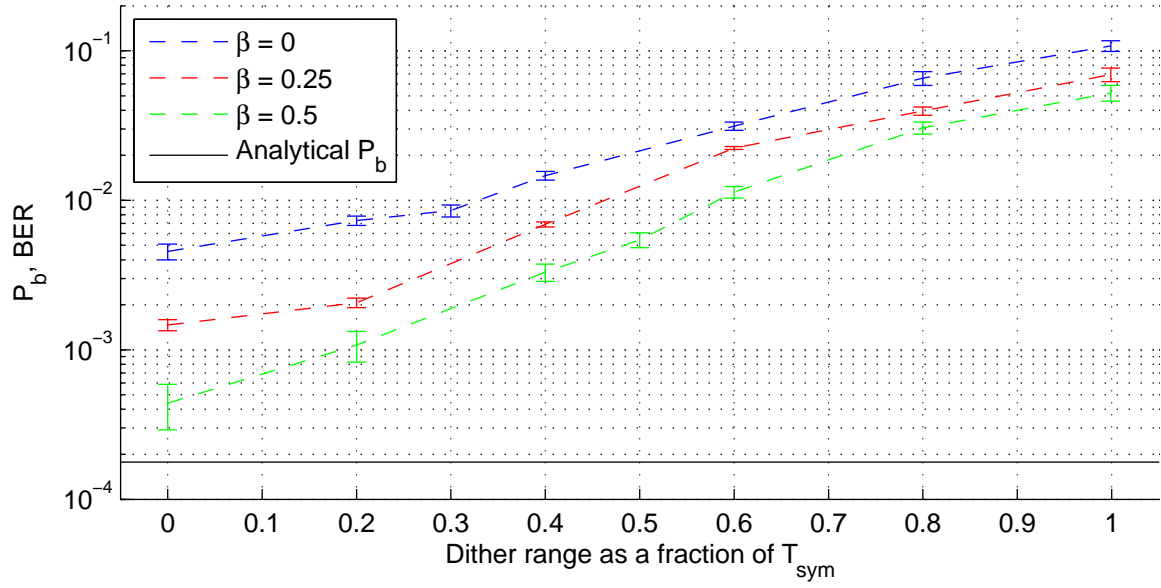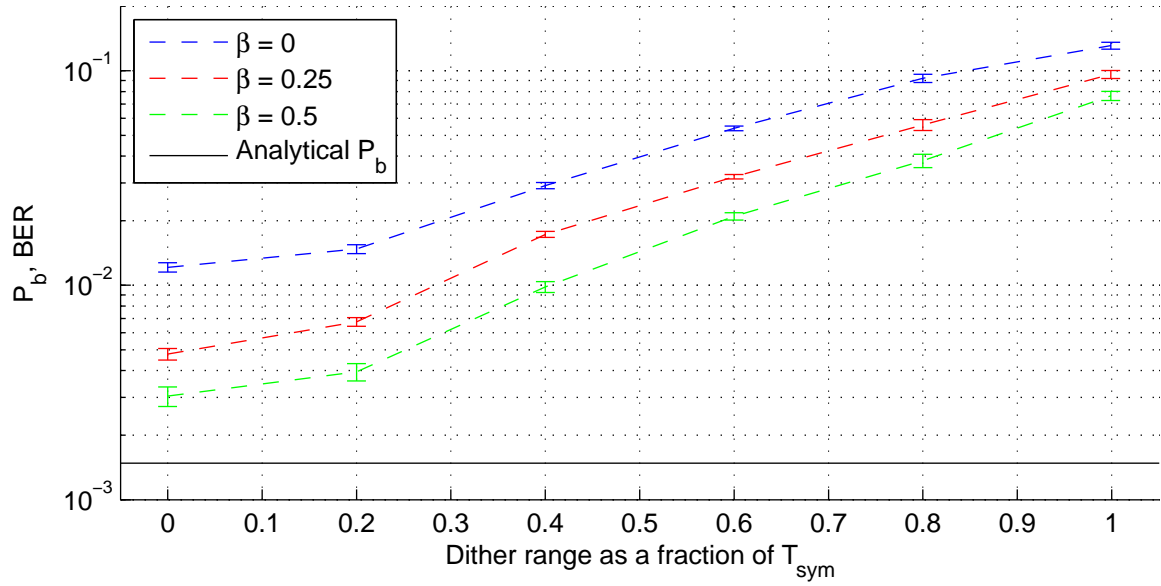
(a)

(b)

Figure 5.6:   FS-CMA equalizer receiver performance as a function of the dither range using a LOS channel at $E_b/N_o = 9$ db. (a) Binary DPSK modulation (b) 4-ary DPSK modulation

The error rates observed in simulation of the subspace equalization receiver (Figure 5.7) indicate that subspace equalization is not suited for mitigation of ISI due to symbol dither in a LOS channel. All of the BER curves are higher than their equivalents in the basic receiver. Even when the dither is removed, the inversion of the correlation matrix within the subspace channel identification algorithm is poorly conditioned, producing the observations in Figure 5.7.

5.2.3   Symbol Dither Estimation Receiver.   The symbol location estimation algorithm described in Section 3.3.3 produces poor symbol identification estimates, as seen in Figure 5.8. All bit error rates shown here fall between 7.9% and 29%. Differentiation between SRRC β values is only apparent when the symbol dither is allowed to vary over $0.5T_{sym}$ or greater. The improvement in BER for increasing symbol dither is contrary to intuition and the behavior of all other receivers. This anomaly is most likely an artifact of the symbol boundary definition within the receiver simulation which biases the error in the estimated symbol locations produced by the algorithm for small dither ranges. Clearly, a more rigorous estimation algorithm is required to make this receiver structure viable.

(a)

(b)

Figure 5.7: Subspace equalizer receiver performance as a function of the dither range using a LOS channel at $E_b/N_o = 9$ db. (a) Binary DPSK modulation (b) 4-ary DPSK modulation
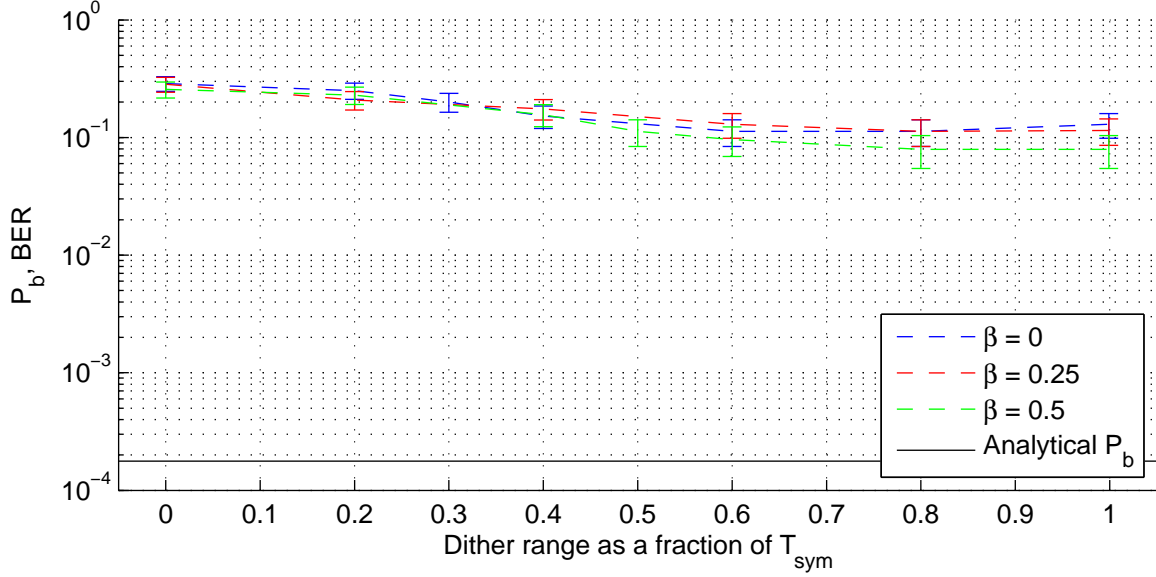
5-10

Figure 5.8:   Dither estimation receiver performance as a function of the dither range for binary DPSK modulation using a LOS channel at $E_b/N_o = 9$ db.

5.3   LPI Signal Parameter Selection

This section explores the potential suitability of applying the pseudorandom dither strategy with DPSK modulation as an LPI signalling scheme. The goal is to find a transmitter/cooperative receiver pair that 1) yields a BER near optimal DPSK performance and 2) results in poor BER for the non-cooperative receivers. Several promising parameter sets are selected using the cooperative and non-cooperative performance curves presented earlier in this chapter. The relative observed BER among the cooperative and non-cooperative receivers suggests that symbol dither can successfully be employed to impede exploitation of the signal information by non-cooperative receivers while preserving the cooperative communication link.

To select a set of signal parameters, the performance curves are grouped by modulation type and pulse shape in Figure 5.9 through Figure 5.14. In these figures, cooperative receivers BER are denoted by solid lines while non-cooperative receiver results are represented by dashed lines. The greatest bit error difference (in a logarithmic sense) between a cooperative receiver and the most accurate non-cooperative receiver occurs for the binary DPSK modulated signal using an SRRC pulse shape
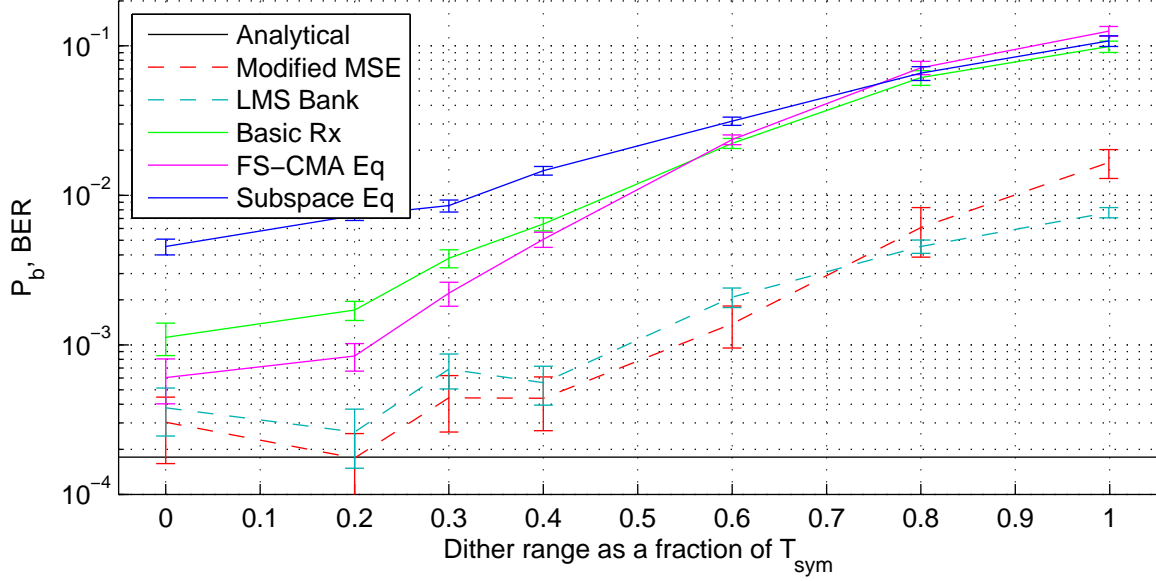
Figure 5.9:   Receiver performance comparison for binary DPSK, SRRC $\beta = 0$ at $E_b/N_o = 9$ db.

with $\beta = 0.25$ and a dither distribution range of $0.6T_{sym}$. At this operating point, found in Figure 5.10, the modified MSE cooperative receiver yields BER $= 5.4 \cdot 10^{-4}$ versus the best non-cooperative receiver at BER $= 8.9 \cdot 10^{-3}$. Bit errors occur 16.4 times as frequently in the non-cooperative receiver than in the cooperative receiver at $E_b/N_o = 9$ dB.

The BER improvement between cooperative and non-cooperative receivers is not as high for 4-ary DPSK modulation at $E_b/N_o = 9$ dB, largely because the analytical 4-ary DPSK BER at $E_b/N_o = 9$ dB is higher than the binary DPSK BER. Thus, the observed BER for the different receivers is dominated by AWGN vice receiver efficiency. For 4-ary DPSK modulation with SRRC pulse shape $\beta = 0.25$ and symbol dither range of $0.6T_{sym}$, the non-cooperative BER is only 7.4 times worse than the modified MSE cooperative receiver BER, as seen in Figure 5.13.

Fixing the symbol dither range at $0.6T_{sym}$ and varying E_b/N_o for binary and 4-ary constellations produces the performance results shown in Figure 5.15 and Figure 5.16. Between the two constellations, the 4-ary scheme produces greater separation between cooperative and non-cooperative receiver performance. For example, to
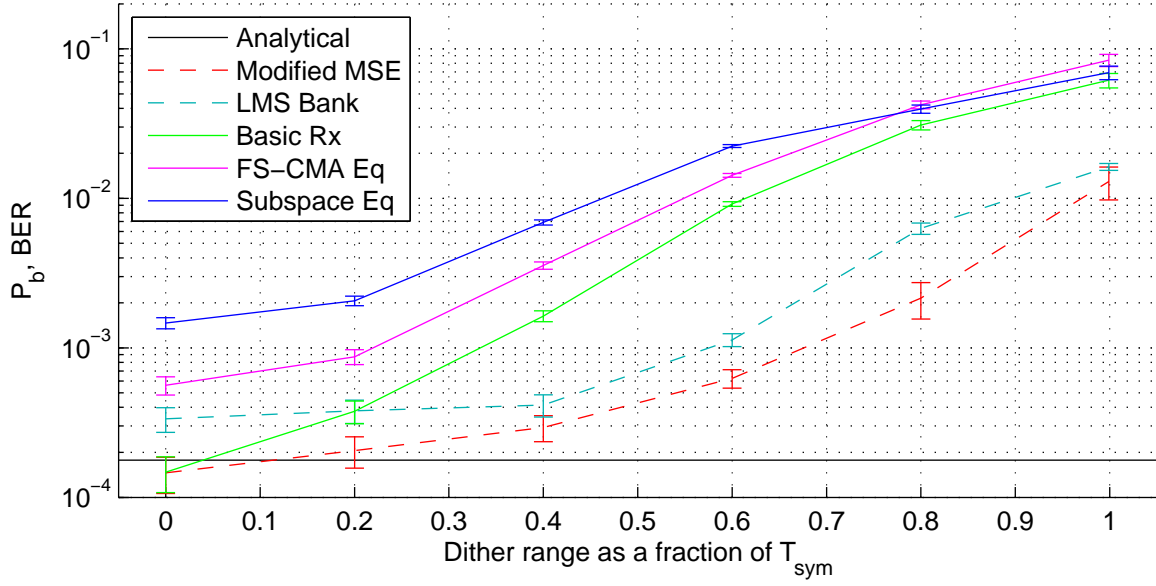
Figure 5.10:   Receiver performance comparison for binary DPSK, SRRC $\beta = 0.25$ at $E_b/N_o = 9$ db.
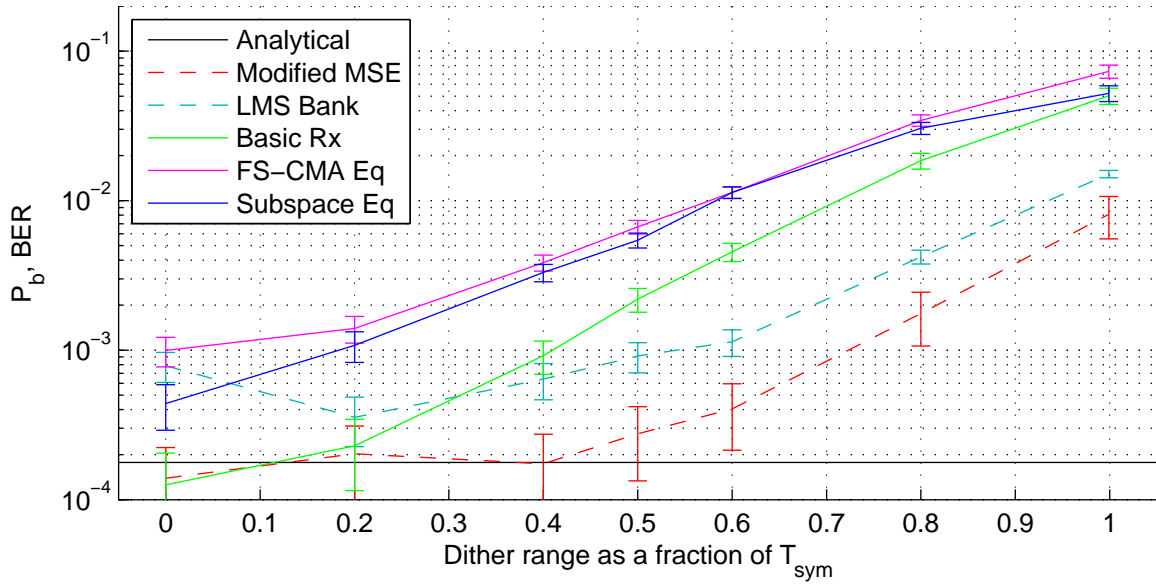

Figure 5.11:   Receiver performance comparison for binary DPSK, SRRC $\beta = 0.50$ at $E_b/N_o = 9$ db.
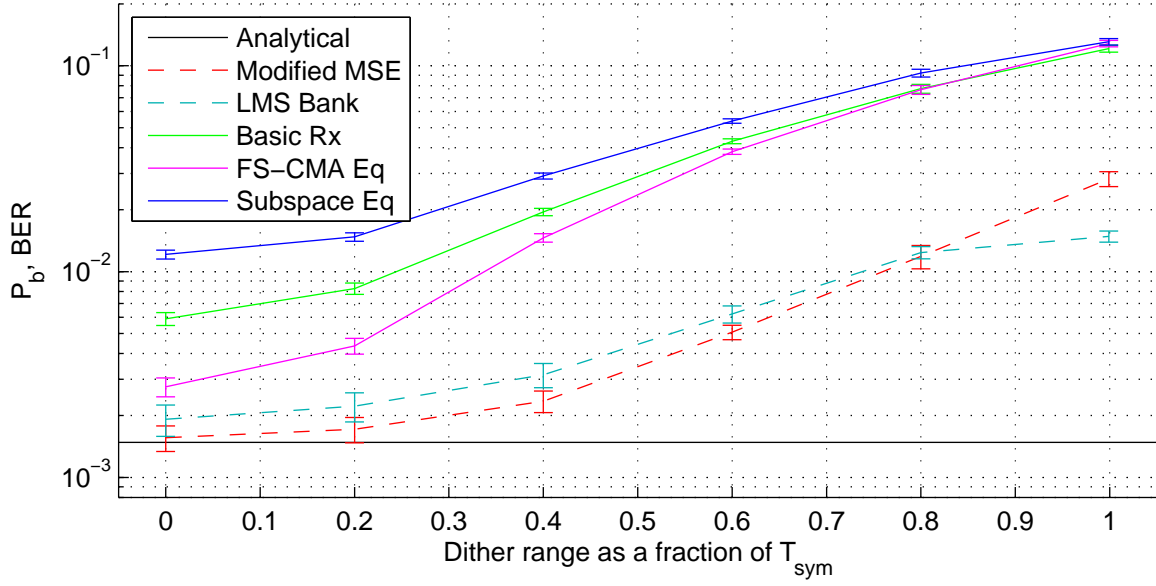
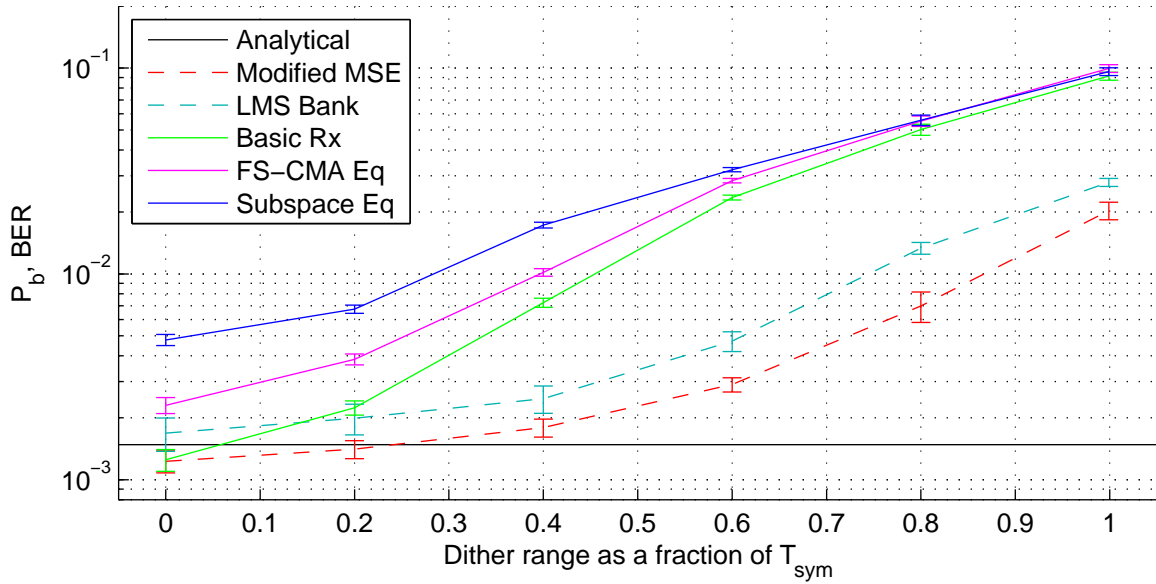Figure 5.12:   Receiver performance comparison for 4-ary DPSK, SRRC $\beta = 0$ at $E_b/N_o = 9$ db.

Figure 5.13:   Receiver performance comparison for 4-ary DPSK, SRRC $\beta = 0.25$ at $E_b/N_o = 9$ db.
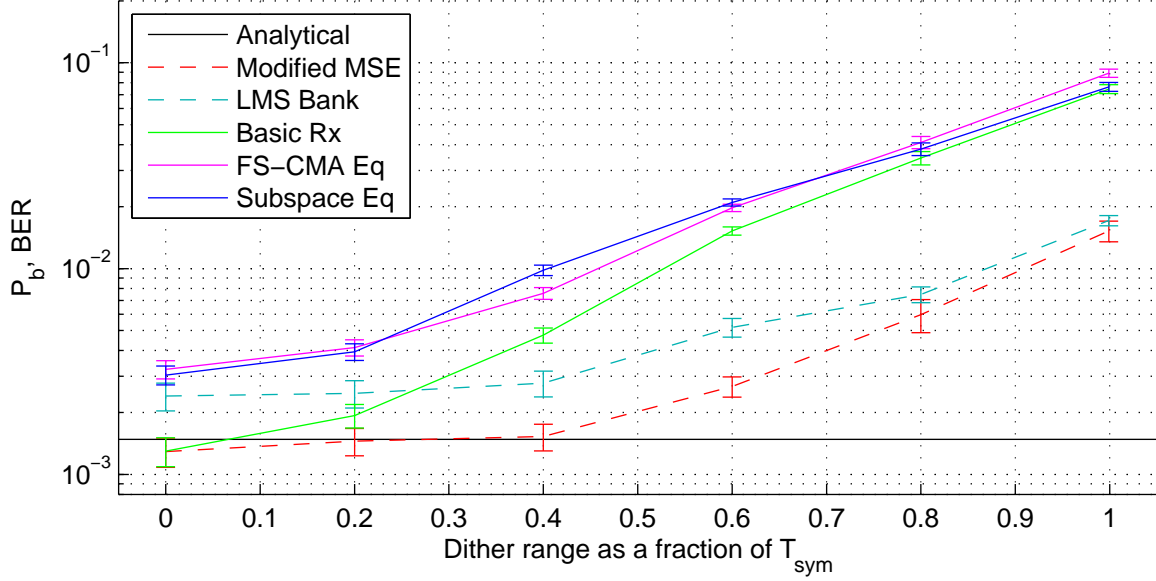
Figure 5.14: Receiver performance comparison for 4-ary DPSK, SRRC $\beta = 0.50$ at $E_b/N_o = 9$ db.

operate at BER $= 1.0 \cdot 10^{-2}$ non-cooperative receivers require ≈ 3 dB more signal power than cooperative receivers in the binary case, while the signal power difference for BER $= 1.0 \cdot 10^{-2}$ is ≈ 6 dB for the 4-ary constellation. In both cases, the BER gap between the cooperative and non-cooperative receivers increases as E_b/N_o grows. In the 4-ary case, the rate of change of non-cooperative BER improvement at high E_b/N_o is near zero, suggesting that the ISI due to symbol dither is dominating the error rate and decreasing the noise power has little effect on BER. Because the basic non-cooperative receiver is outperforming the blind equalization receivers, ISI due to symbol dither does not appear to be mitigated in any of the non-cooperative receivers posited in this thesis. The ISI due to symbol dither, then, sets a lower limit on the non-cooperative receiver BER achievable for each constellation and dither range. This limit can be estimated empirically via simulation by removing the AWGN component in the channel model. This exercise produces a best-case BER $= 5 \cdot 10^{-5}$ for the non-cooperative receivers in Figure 5.15 (not shown on this plot) and BER $= 4.9 \cdot 10^{-3}$ for the non-cooperative receivers in Figure 5.16. This lower limit characterizes the minimum level of security for a particular set of PDW parameters.
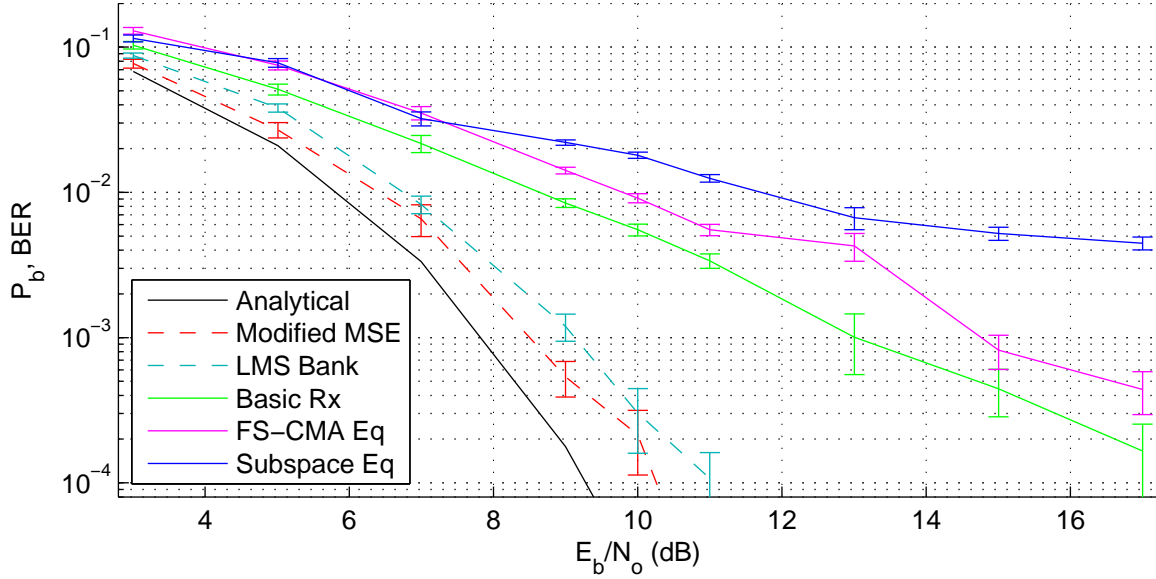
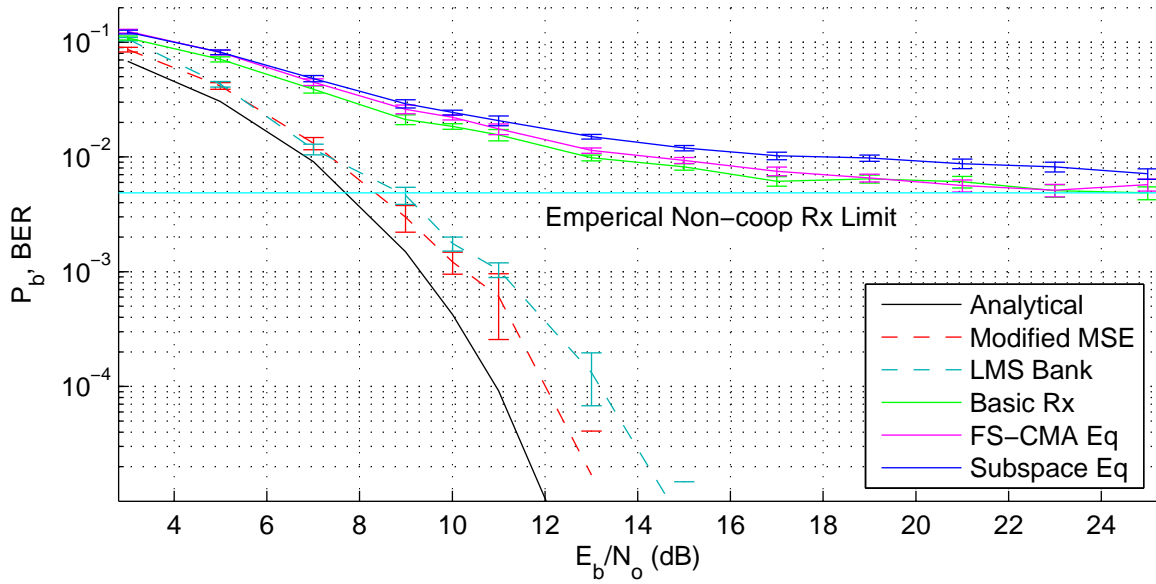Figure 5.15: Receiver performance for binary DPSK, SRRC $\beta = 0.25$, and dither range $0.6T_{sym}$.

Figure 5.16: Receiver performance for 4-ary DPSK, SRRC $\beta = 0.25$, and dither range $0.6T_{sym}$.
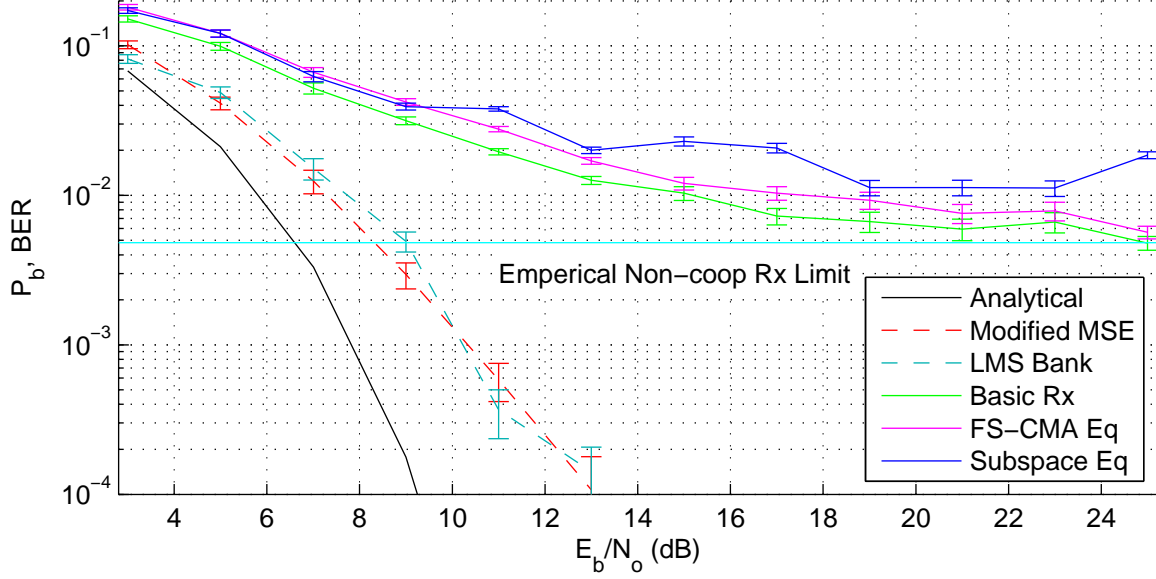
Figure 5.17:   Receiver performance for binary DPSK, SRRC $\beta = 0.25$, and dither range $0.8T_{sym}$.

To degrade the non-cooperative receiver BER lower limit, the symbol dither range can be increased. Setting the symbol dither range to a higher fraction of the symbol period also causes the non-cooperative receivers to approach the BER limit at lower E_b/N_o. In Figure 5.17, non-cooperative receiver demodulation of the binary DPSK signal approaches a lower limit of BER $= 4.8 \cdot 10^{-3}$ at about $E_b/N_o = 17$ dB for a symbol dither range of $0.8T_{sym}$. The E_b/N_o required to achieve BER $= 1.0 \cdot 10^{-2}$ is 9 dB greater for non-cooperative receivers than for cooperative receivers. In the 4-ary constellation, the non-cooperative receiver lower limit is BER $= 2.4 \cdot 10^{-2}$ and is plotted in Figure 5.18.

5.4   Bandwidth Considerations

This section compares the power spectral densities (PSD) of simulated baseband DPSK waveforms with and without symbol timing dither. For standard DPSK modulation, (without symbol dither), the width of the PSD is dependent on the symbol period and the pulse shape. Figure 5.19 shows the effect of β on the null-to-null
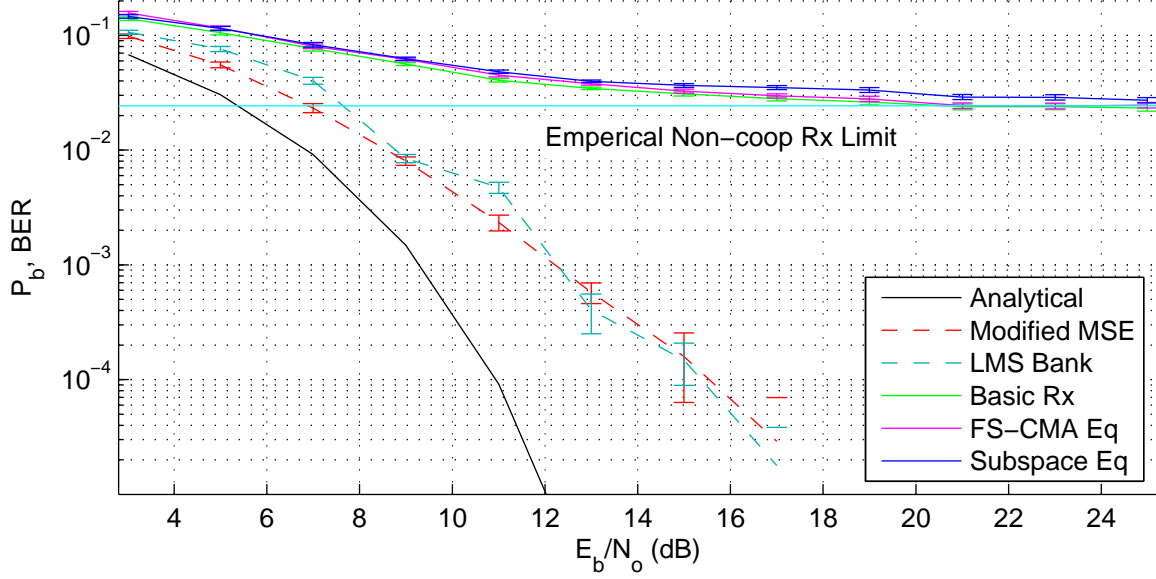
Figure 5.18:   Receiver performance for 4-ary DPSK, SRRC $\beta = 0.25$, and dither range $0.8T_{sym}$.

bandwidth using the SRRC pulse shape. As expected, a narrow SRRC pulse shape in the time domain corresponds to a wide null-to-null bandwidth.

Because the symbol dither strategy does not modify the pulse shape of the transmitted symbols, the spectrum of each symbol is no different between a traditional DPSK waveform and the PDW. The time dither of the PDW induces a phase shift in the symbols in the frequency domain, but the PSD should be consistent with standard DPSK.

In fact, the PSD of the dither waveforms are indistinguishable from standard DPSK signalling. In Figure 5.20, a binary PDW with a dither range of T_{sym} (blue curve) produces a PSD similar to a standard DPSK waveform with dither range of 0 (green curve n Figure 5.19). The PSD invariance with respect to dither range was observed for all SRRC pulse shapes and constellations used in this thesis.
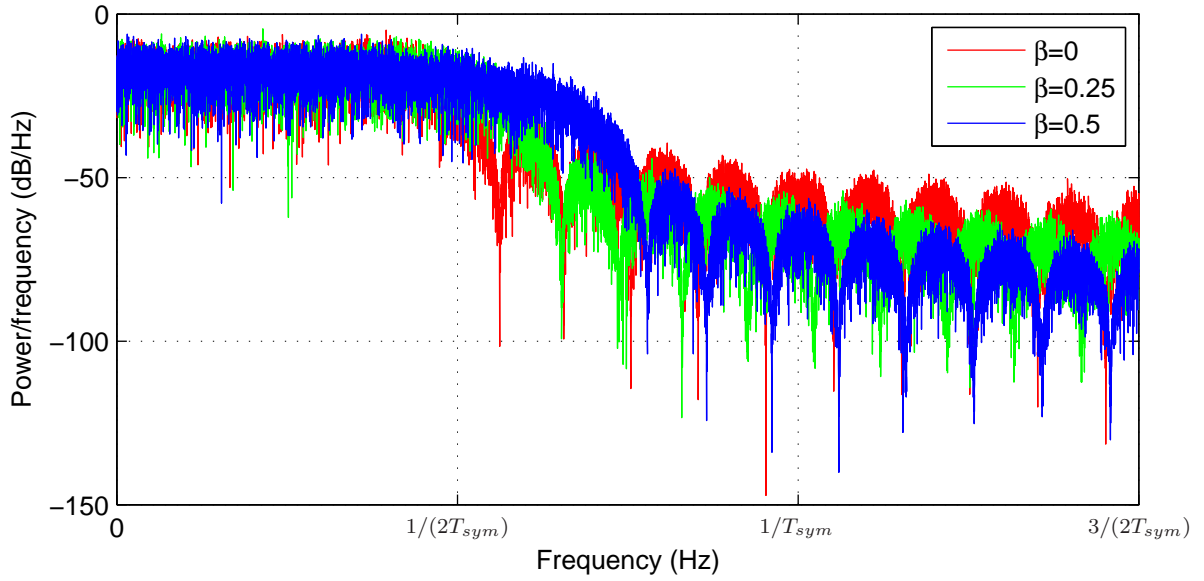
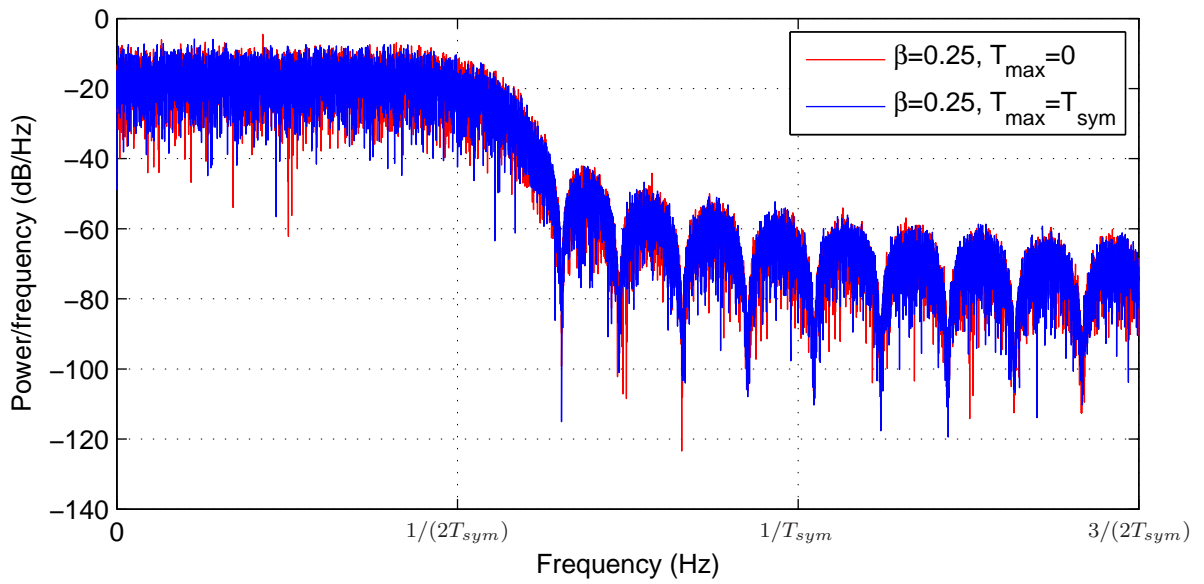Figure 5.19:   PSD for standard binary DPSK using SRRC pulse shapes.

Figure 5.20:   PSD for binary DPSK, SRRC pulse shape with $\beta = 0.25$. Injecting dither into the waveform does not impact the average PSD.

VI. Conclusions and Recommendations

6.1   Conclusions

This thesis demonstrates a communication system that leverages symbol timing dither to hinder interception and exploitation by non-cooperative receivers. Two cooperative receiver structures are shown to reliably recover the digital information with only a slight bit error rate (BER) penalty relative to the optimum performance for the DPSK modulated waveform. The timing dither in DPSK transmitted symbols causes ISI which is not mitigated in the notional non-cooperative receivers simulated in this thesis. The pulse shape of the DPSK waveform and the symbol dither range determine the severity of ISI and set a lower bound on BER of the non-cooperative receivers. For the signal parameters proposed in this thesis, non-cooperative receivers required 2-8 dB more signal power than cooperative receivers to achieve a bit error rate of 1.0%. For three of the four waveform parameter sets analyzed in Section 5.3, non-cooperative receivers produced bit error rates in excess of 0.1%, even for arbitrarily large values of E_b/N_o.

Both cooperative receivers use signal processing techniques to recover the signal from evenly-spaced samples of a traditional matched filter receiver. The modified MSE cooperative receiver, which requires full knowledge of and synchronization to the symbol timing dither, yields marginally better bit estimation accuracy than the LMS bank cooperative receiver. The MSE receiver's BER benefit is computationally expensive and requires a matrix inverse operation for each symbol (assuming the symbol timing dither sequence does not repeat). The LMS bank receiver assumes the symbol dither pattern repeats, and requires the period to be short enough that the dither pattern repeats many times (5,000 times in simulations here) for the equalizers to be trained. Thus, the low computational complexity of this approach comes at the cost of significant equalizer training periods.

Of the non-cooperative receivers considered, the basic sample-spaced receiver with best-case synchronization proved to consistently achieve better BER performance than the more complex non-cooperative receiver strategies. In practice, however,

non-cooperative symbol-level synchronization may not be easily achieved and the oversampled non-cooperative receiver models may more accurately reflect expected non-cooperative receiver performance.

6.2   *Recommendations for Further Study*

In completing this thesis, several avenues for further study have been uncovered. These future research opportunities are concisely summarized below for easy reference.

1. Many variations of the dither waveform are possible. For example, the pseudorandom dither applied to each symbol always followed a uniform probability density function in this work. Any number of more exotic distributions could be used. Also, simulation was restricted here to DPSK modulation. The dither strategy proposed here should be applicable to most direct sequence modulation schemes, including Quadrature Amplitude Modulation (QAM) and Pulse Amplitude Modulation (PAM).

2. Simulation results were restricted to line-of-sight (LOS) channels. Further investigation could consider cooperative receiver performance in the presence of multipath interference.

3. The cooperative receiver designs proposed here are restricted to uniform sampling of the matched filter output, with the acknowledgement that some loss of bit energy is expected. A more complex modified MSE architecture could use complete knowledge of the dither sequence to sample the matched filter output more intelligently.

4. Lastly, only a few notional non-cooperative receivers were used in this thesis. Further work could consider many other non-cooperative receiver designs. In particular, the symbol dither estimation algorithm could be improved. Also, the impact of non-synchronous sampling on the non-cooperative receivers could be characterized.

Bibliography

1. Carbonelli, C., S. Vedantam, and U. Mitra. "Sparse Channel Estimation with Zero Tap Detection". *Wireless Communications, IEEE Transactions on*, 6(5):1743–1763, May 2007.

2. Ding, Z., R. A. Kennedy, B. D. O. Anderson, and C. R. Johnson Jr. "Ill-convergence of Godard blind equalizers in data communication systems". *Communications, IEEE Transactions on*, 39(9):1313–1327, September 1991.

3. Ding, Zhi and Y. Li. "On channel identification based on second-order cyclic spectra". *Signal Processing, IEEE Transactions on*, 42(5):1260–1264, May 1994.

4. Haykin, Simon. *Adaptive Filter Theory*. Prentice Hall, Upper Saddle River, New Jersey, 2002.

5. Johnson, Jr., C. R., P. Schniter, T. J. Endres, J. D. Behm, D. R. Brown, and R. A. Casas. "Blind equalization using the constant modulus criterion: a review". *Proceedings of the IEEE*, 86(10):1927–1950, October 1998.

6. Johnson, Jr., C. R. and W. A. Sethares. *Telecommunications Breakdown: Concepts of Communication Transmitted Via Software-Defined Radio*. Pearson Prentice Hall, Upper Saddle River, NJ, 2004.

7. Kwong, R. H. and E. W. Johnston. "A variable step size LMS algorithm". *Signal Processing, IEEE Transactions on*, 40(7):1633–1642, July 1992.

8. Liavas, A. P., P. A. Regalia, and J. P Delmas. "Blind channel approximation: effective channel order determination". *Signal Processing, IEEE Transactions on [see also Acoustics, Speech, and Signal Processing, IEEE Transactions on]*, 47(12):3336–3344, December 1999.

9. McLendon, J. W. *Information Warfare: Impacts and Concerns*, 171–200. Battlefield of the Future: 21st Century Warfare Issues. University Press of the Pacific, Maxwell AFB, 1998.

10. Montgomery, Douglas C. and George C. Runger. *Applied Statistics and Probability for Engineers*. John Wiley and Sons, Inc., New York, 3rd edition, 2003.

11. Moulines, E., P. Duhamel, J. F. Cardoso, and S. Mayrargue. "Subspace methods for the blind identification of multichannel FIR filters". *Signal Processing, IEEE Transactions on*, 43(2):516–525, February 1995.

12. Phister, P. W. and I. G. Plonisch. "Military Applications of Information Technologies". *Air and Space Power Journal*, 77–90, Spring 2004.

13. Sato, Y. "A Method of Self-Recovering Equalization for Multilevel Amplitude-Modulation Systems". *Communications, IEEE Transactions on [legacy, pre - 1988]*, 23(6):679–682, June 1975.

14. Shalvi, O. and E. Weinstein. "New criteria for blind deconvolution of nonminimum phase systems (channels)". *Information Theory, IEEE Transactions on*, 36:312–321, 1990.

15. Shaw, Arnab, M. Jamali, and N. Wilkins. "Toward Bandwidth Invariance of Spatial Processing in the Non-Cooperative Receiver". *Sensor Array and Multichannel Processing, 2006.Fourth IEEE Workshop on*, 556–560. 2006.

16. Sklar, B. *Digital Communications: Fundamentals and Applications*. Prentice Hall, Upper Saddle River, New Jersey, 2001.

17. Stoney, P. R. "Modern Communications: A Wise Investment". *Air University Review*, July-August 1973.

18. Stüber, G. L. *Principles of Mobile Communication*. Kluwer Academic Publishers, Boston, 1996.

19. Tong, Lang, Guanghan Xu, B. Hassibi, and T. Kailath. "Blind channel identification based on second-order statistics: a frequency-domain approach". *Information Theory, IEEE Transactions on*, 41(1):329–334, January 1995.

20. Tong, Lang, Guanghan Xu, and T. Kailath. "Blind identification and equalization based on second-order statistics: a time domain approach". *Information Theory, IEEE Transactions on*, 40(2):340–349, March 1994.

21. Torrieri, D. J. *Principles of Secure Communication Systems*. Artech House, Boston, 1992.

22. Touzni, A., L. Tong, R. A. Casas, and C. R. Johnson Jr. "Vector-CM stable equilibrium analysis". *Signal Processing Letters, IEEE*, 7:31–33, February 2000.

23. Xiong, Z., Z. Dongfeng, J. Zhigang, and W. Anhong. "A modified blind equalization algorithm based on kurtosis of output signal". *Radio Science Conference, 2004.Proceedings.2004 Asia-Pacific*, 228–231. August 2004.

24. Xue, Y. and X. Zhu. "Wireless channel tracking based on self-tuning second-order LMS algorithm". *IEE Proceedings: Communications*, 150(2):115–120, April 2003.

25. Yang, V. Y. and D. L. Jones. "A vector constant modulus algorithm for shaped constellation equalization". *Signal Processing Letters, IEEE*, 5(4):89–91, April 1998.

26. Zarzoso, V. and P. Comon. "Blind Channel Equalization with Algebraic Optimal Step Size". *Proceedings EUSIPCO-2005, XIII European Signal Processing Conference*. September 2005.

Vita

Nathaniel Liefer was born in Melrose, MA in 1981. After graduating as valedictorian from Rampart High School in Colorado Springs in 1999, he attended Worcester Polytechnic Institute in Massachusetts. Nathaniel's undergraduate coursework included on-site projects for the Country Fire Authority in Victoria, Australia and AMT Ireland at the University of Limerick. He graduated with high distinction, earning a Bachelor of Science Degree in Electrical Engineering in 2003 and was commissioned as a second lieutenant in the United States Air Force. Prior to attending the Air Force Institute of Technology, Nathaniel was a spacecraft bus engineer and chief orbital control analyst for the Milstar communications satellite constellation while serving in the 4th Space Operations Squadron, Schriever AFB, CO. Upon graduation, Capt Liefer will be assigned to the National Reconnaissance Organization in Chantilly, VA.

Permanent address: 2950 Hobson Way
                            Air Force Institute of Technology
                            Wright-Patterson AFB, OH 45433

REPORT DOCUMENTATION PAGE

1. REPORT DATE *(DD-MM-YYYY)*	2. REPORT TYPE		3. DATES COVERED *(From - To)*

4. TITLE AND SUBTITLE	5a. CONTRACT NUMBER
	5b. GRANT NUMBER
	5c. PROGRAM ELEMENT NUMBER

6. AUTHOR(S)	5d. PROJECT NUMBER
	5e. TASK NUMBER
	5f. WORK UNIT NUMBER

7. PERFORMING ORGANIZATION NAME(S) AND ADDRESS(ES)	8. PERFORMING ORGANIZATION REPORT NUMBER

9. SPONSORING/MONITORING AGENCY NAME(S) AND ADDRESS(ES)	10. SPONSOR/MONITOR'S ACRONYM(S)
	11. SPONSOR/MONITOR'S REPORT NUMBER(S)

12. DISTRIBUTION/AVAILABILITY STATEMENT

13. SUPPLEMENTARY NOTES

14. ABSTRACT

15. SUBJECT TERMS

16. SECURITY CLASSIFICATION OF:			17. LIMITATION OF ABSTRACT	18. NUMBER OF PAGES	19a. NAME OF RESPONSIBLE PERSON
a. REPORT	b. ABSTRACT	c. THIS PAGE			
					19b. TELEPHONE NUMBER *(Include area code)*